# DEVELOPMENT OF A CFD ASSISTED 3-D MODELING AND ANALYSIS METHODOLOGY FOR GROOVED HEAT PIPE DESIGN AND PERFORMANCE ASSESSMENT

A THESIS SUBMITTED TO
THE GRADUATE SCHOOL OF NATURAL AND APPLIED SCIENCES
OF
MIDDLE EAST TECHNICAL UNIVERSITY

BY

GÖKAY GÖKÇE

IN PARTIAL FULFILLMENT OF THE REQUIREMENTS
FOR
THE DEGREE OF DOCTOR OF PHILOSOPHY
IN
MECHANICAL ENGINEERING

SEPTEMBER 2020

Approval of the thesis:

**DEVELOPMENT OF A CFD ASSISTED 3-D MODELING AND ANALYSIS METHODOLOGY FOR GROOVED HEAT PIPE DESIGN AND PERFORMANCE ASSESSMENT**

submitted by **GÖKAY GÖKÇE** in partial fulfillment of the requirements for the degree of **Doctor of Philosophy in Mechanical Engineering Department, Middle East Technical University** by,

Prof. Dr. Halil Kalıpçılar
Dean, Graduate School of **Natural and Applied Sciences** ______________

Prof. Dr. M. A. Sahir Arıkan
Head of Department, **Mechanical Engineering** ______________

Prof. Dr. Zafer Dursunkaya
Supervisor, **Mechanical Engineering, METU** ______________

**Examining Committee Members:**

Assoc. Prof. Dr. Merve Erdal
Mechanical Engineering Dept. , METU ______________

Prof. Dr. Zafer Dursunkaya
Mechanical Engineering Dept. , METU ______________

Prof. Dr. İsmail Hakkı Tuncer
Aerospace Engineering Dept. , METU ______________

Assoc. Prof. Dr. Barbaros Çetin
Mechanical Engineering Dept. , Bilkent University ______________

Assist. Prof. Dr. Özgür Ekici
Mechanical Engineering Dept. , Hacettepe University ______________

Date:

**I hereby declare that all information in this document has been obtained and presented in accordance with academic rules and ethical conduct. I also declare that, as required by these rules and conduct, I have fully cited and referenced all material and results that are not original to this work.**

Name, Surname: Gökay Gökçe

Signature :

**ABSTRACT**

**DEVELOPMENT OF A CFD ASSISTED 3-D MODELING AND ANALYSIS METHODOLOGY FOR GROOVED HEAT PIPE DESIGN AND PERFORMANCE ASSESSMENT**

Gökçe, Gökay
Ph.D., Department of Mechanical Engineering
Supervisor: Prof. Dr. Zafer Dursunkaya

September 2020, 125 pages

Although the idea of phase change heat transfer has a long history going back to mid $19^{th}$ century, modeling of multi-phase heat transfer still draws interest from the engineers and scientists worldwide due to its complex nature. Taking advantage of phase-change heat transfer, heat pipes have been used effectively in numerous industrial applications for thermal management of electronic components due to their tremendous advantages. However, multi-dimensional modeling of heat pipes is a challenging task, requiring a physically based mathematical model to address evaporation, condensation and free surface flow phenomena. Although several studies about the flat groove heat pipes are available in the literature, these studies do not address complex groove shapes due to the modeling approach, manufacturing limitations and absence of skin friction correlations for a specific geometry. Nowadays, due to the improvements in simulation technology, more engineering questions can be answered realistically with computers in a virtual environment. However, commercial software are not developed to meet the specific needs to simulate individual problems, especially when sophisticated physical phenomena such as phase change with free surface flow inside the channel is involved. Neither commercial nor academic CFD program that can simulate the flow and heat transfer characteristics of a grooved heat pipe in one step is currently available. To address this, an analysis methodology that computes the liquid flow and heat transfer inside a grooved heat pipe is developed which simultaneously uses a commercial CFD program (Fluent®) along with Python® programming language. With the developed methodology, the effect of various groove models on the heat pipe performance are investigated. The results show that it is possible to design heat pipes with increased performance both in terms of higher heat carrying capacity, and lower peak temperatures with a judicious selection of groove geometry.

Keywords: Flat grooved heat pipe, phase-change modeling, automation of CFD, design of heat pipe

# ÖZ

## OLUKLU ISI BORUSU TASARIMI VE PERFORMANS DEĞERLENDİRMESİ İÇİN HAD DESTEKLİ 3 BOYUTLU ANALİZ METODOLOJİSİ GELİŞTİRİLMESİ

Gökçe, Gökay
Doktora, Makina Mühendisliği Bölümü
Tez Yöneticisi: Prof. Dr. Zafer Dursunkaya

Eylül 2020 , 125 sayfa

Faz değişimi yoluyla ısı transferi fikrinin 19. yüzyılın ortalarına kadar uzun bir geçmişi olmasına rağmen, günümüzde hâlâ, karmaşık yapısı sebebiyle global düzeyde bilim insanlarının ilgisini çekmektedir. Faz değişimi ısı transferinden faydalanan ısı boruları, sağladığı avantajlar nedeniyle elektronik bileşenlerin termal yönetimi amacıyla çok sayıda endüstriyel uygulamada etkili bir şekilde kullanılmaktadır. Bununla birlikte ısı borularının çok boyutlu olarak modellenmesi zorlu bir süreç olup buharlaşma, yoğuşma ve serbest yüzey akışı fenomenlerini içeren fiziksel tabanlı bir matematiksel model gerektirmektedir. Literatürde oluklu ısı boruları hakkında çeşitli çalışmalar bulunmasına rağmen, bu çalışmalar genellikle, karmaşık matematiksel model gerekliliği, üretimden gelen sınırlamalar ve literatürde çeşitli geometriler için sürtünme katsayısı korelasyonlarının olmaması nedeniyle karmaşık oluk şekillerine değinmemektedir. Günümüzde, simülasyon teknolojisindeki gelişmeler sayesinde, sanal ortamda daha fazla mühendislik problemi gerçekçi olarak modellenebilmektedir. Fakat, kanal içinde serbest yüzey akışı ve faz değişimi gibi karmaşık fiziksel fenomenler söz konusu olduğunda, bu problemleri ele almak amacıyla ticari yazılımlar geliştirilmemiştir. Oluklu ısı borularının içindeki akış ve ısı transferi fenomenlerini tek adımda simüle edebilen ticari veya akademik bir CFD programı bulunmamaktadır. Bu amaçla, oluklu ısı boruları içindeki sıvı akışını ve ısı transferini hesaplayan bir metodoloji, Python® programlama dili ile birlikte ticari bir CFD programı (Fluent®) kullanılarak geliştirilmiştir. Geliştirilen metodoloji ile çeşitli oluk şekillerinin ısı borusu performansı üzerindeki etkisi belirlenmiştir. Sonuçlar, oluk şekline dayalı, ısı tranfer kapasitesinin arttırılarak, model içindeki sıcaklığın mümkün olduğunca düşük seviyede tutulduğu, yüksek performanslı ısı boruları tasarlamanın mümkün olduğunu göstermektedir.

Anahtar Kelimeler: Oluklu ısı borusu, faz değişimi modellenmesi, CFD otomasyonu, ısı borusu tasarımı

To my mother

## ACKNOWLEDGMENTS

First, I would like to express my sincere gratitude to my advisor Prof. Dr. Zafer Dursunkaya for his continuous support of my Ph.D. study as well as his valuable and constructive suggestions during the planning, development and execution of this research work. His generosity and willingness to provide his most valuable time has been very much appreciated. His dynamism, vision, sincerity and motivation have all deeply inspired me and my work. It was a great privilege and honor to work and study under his guidance. I am also extremely grateful for the support he has provided in overcoming the numerous obstacles I faced throughout my research. Besides the technical studies, I have thoroughly enjoyed our conversations about literature, art and classical music. I could not imagine having a better advisor and mentor for my Ph.D. study.

Besides my advisor, I would also like to thank the rest of my thesis committee: Prof. Dr. İsmail H. Tuncer and Assoc. Prof. Dr. Barbaros Çetin for their encouragement and insightful comments which impelled me to widen the scopes of my research for better understanding from different perspectives.

I would like to pay my special regards to Dr. Ertuğrul A. Başeşme for providing me unfailing support and continuous encouragement throughout this thesis. I am forever indebted to him for his invaluable contributions in building my CFD skills early in my career. He has taught me more than I could ever give him credit for here. I consider myself truly lucky to have had the opportunity to work with him.

Last but not least, I would like to thank my mother for her caring and unwavering support, not only for her support during this study but for everything in my life.

## TABLE OF CONTENTS

## LIST OF TABLES

TABLES

## LIST OF FIGURES

FIGURES

## LIST OF ABBREVIATIONS

| | |
|---|---|
| 1-D | 1 Dimensional |
| 2-D | 2 Dimensional |
| 3-D | 3 Dimensional |
| $A_d$ | Dispersion constant, J |
| $c$ | Accommodation coefficient |
| $g$ | Gravity, m/s$^2$ |
| $h$ | Step size |
| $h_{fg}$ | Latent heat of evaporation, J/kg |
| $h_{pc}$ | Heat transfer coefficient, J/kg |
| $k$ | Thermal conductivity, W/m.K |
| $m$ | Molar mass of liquid, kg/mol |
| $\dot{m}$ | Mass flow rate, kg/s |
| $\dot{m}'$ | Mass flow rate per unit length, kg/m.s |
| $\dot{m}''$ | Mass flow rate per unit area, kg/m$^2$.s |
| $Me$ | Merit number |
| $P_c$ | Capillary pressure, Pa |
| $P_d$ | Dispersion pressure, Pa |
| $P_l$ | Liquid pressure, Pa |
| $P_v$ | Vapor pressure, Pa |
| $q''$ | Heat flux, W/m$^2$ |
| $R$ | Meniscus radius of curvature, m |
| $R_u$ | Universal gas constant, J/mol.K |
| $T$ | Temperature, K |
| $u$ | Velocity in x-direction, m/s |

| | |
|---|---|
| $v$ | Velocity in y-direction, m/s |
| $V$ | Velocity, m/s |
| $w$ | Velocity in z-direction, m/s |

### ***Greek Symbols***

| | |
|---|---|
| $\delta$ | Liquid film thickness, m |
| $\epsilon$ | Convergence criterion |
| $\eta$ | Effectiveness of heat pipe |
| $\theta$ | Liquid/solid contact angle, Radian |
| $\mu$ | Dynamic viscosity, Pa.s |
| $\nu$ | Kinematic viscosity, $m^2/s$ |
| $\rho$ | Density, $kg/m^3$ |
| $\sigma$ | Surface tension, N/m |
| $\varphi$ | Meniscus angle, Radian |

### ***Subscripts***

| | |
|---|---|
| $c$ | Cooler |
| $cond$ | Condensation |
| $evap$ | Evaporation |
| $g$ | Groove |
| $h$ | Heater |
| $int$ | Interface |
| $l$ | Liquid |
| $lv$ | Liquid-vapor |
| $macro$ | Macro |
| $micro$ | Micro |
| $pc$ | Phase-change |

| | |
|---|---|
| $s$ | Solid |
| $v$ | Vapor |
| $x$ | First derivative along the x-axis |
| $xx$ | Second derivative along the x-axis |
| $xxx$ | Third derivative along the x-axis |

# CHAPTER 1

# INTRODUCTION

Recent advances in technology have led advanced power devices and electronic components to decrease in size continuously; however, removal of dissipated heat from the critical areas is still an important issue in the thermal management of electronic components. Traditional heat removal methods such as adding extended surfaces to a system, forced-air/liquid cooling, spray cooling, etc. may require extra space or demand additional electrical power to operate the process. Strategies involving phase change heat transfer that benefits from the latent heat capacity are generally considered more effective as compared to the mentioned traditional cooling methods (Xing et al., 2018).

Taking advantage of the phase change heat transfer, heat pipes have been implemented to various applications and being used effectively in a wide-range of industrial areas for heat transfer and temperature homogenization. Some examples of application areas of heat pipes include thermal management of electronic components (Ling et al., 2020), heating, ventilating, and air conditioning (HVAC) systems (Ghani et al., 2018), solar power plants (Yang et al., 2016), photovoltaic thermal (PV/T) panels (Deng et al., 2015), space applications (Zhang et al., 2017), nuclear applications (Wang et al., 2017), automotive industry (Greco et al., 2014), aircraft anti-icing (Gilchrist et al., 2009), temperature regulation systems for human body (Faghri et al., 1989), oil pipelines to minimize permafrost degradation (Wang et al., 2019), Stirling engines (Poston et al., 2014) and the drilling applications (Jen et al., 2002).

Advantages of heat pipes lie behind their prevalent utilization. First of all, heat pipes are passive devices, no external power is required to operate heat pipes and operating principles allow the design of a specific structure in which no moving parts are included. Besides the explained advantages, heat pipes can transfer significant amounts of heat over relatively long distances with a small temperature gradients since their effective thermal conductivity is several times higher than the material in which they are manufactured (Chen et al., 2016).

A heat pipe — operating based on phase-change heat transfer phenomena — is a vacuumed, sealed tube that consists of a wick structure and a working fluid. Heat pipes are used to transfer significant amounts of heat from a heat source to a heat sink utilizing two-phase heat and mass transfer. Once a thermal load is applied by activating heat source, working fluid releases latent heat, starts to evaporate, and flows to the cooler side. When the vapor reaches a certain point — where wall temperature is below the saturation temperature — condensation occurs, and condensed liquid is sucked to the heater side if the pressure difference created by capillary action is sufficient enough to overcome pressure loss. This circulation of liquid and vapor phases continues as long as a thermal load exists on the heat pipe. The high value of the latent heat of evaporation allows transferring a significant amount of heat through the heat pipe.

An example of a flat grooved heat pipe is depicted in Figure 1.1. The heat pipe consists of the main body (case), a plexiglass cover, O-ring, and wick structure (channels in this case). Plexiglass cover is installed using the button head screws over the main body to obtain a closed environment. The body is sealed from the ambient by an O-ring. Lateral (A–A) and longitudinal (B–B) sections are provided for better illustration. The heat pipe can be divided into two sections according to the way of the phase change. The zone where evaporation occurs called the evaporator. In this zone, the working fluid attaches to the wall and forms a meniscus while in the condenser zone, the working fluid is flooded from channels and forms a thin layer of liquid over the fin top. The region between the heat source and heat sink on the bottom surface is called the adiabatic region.

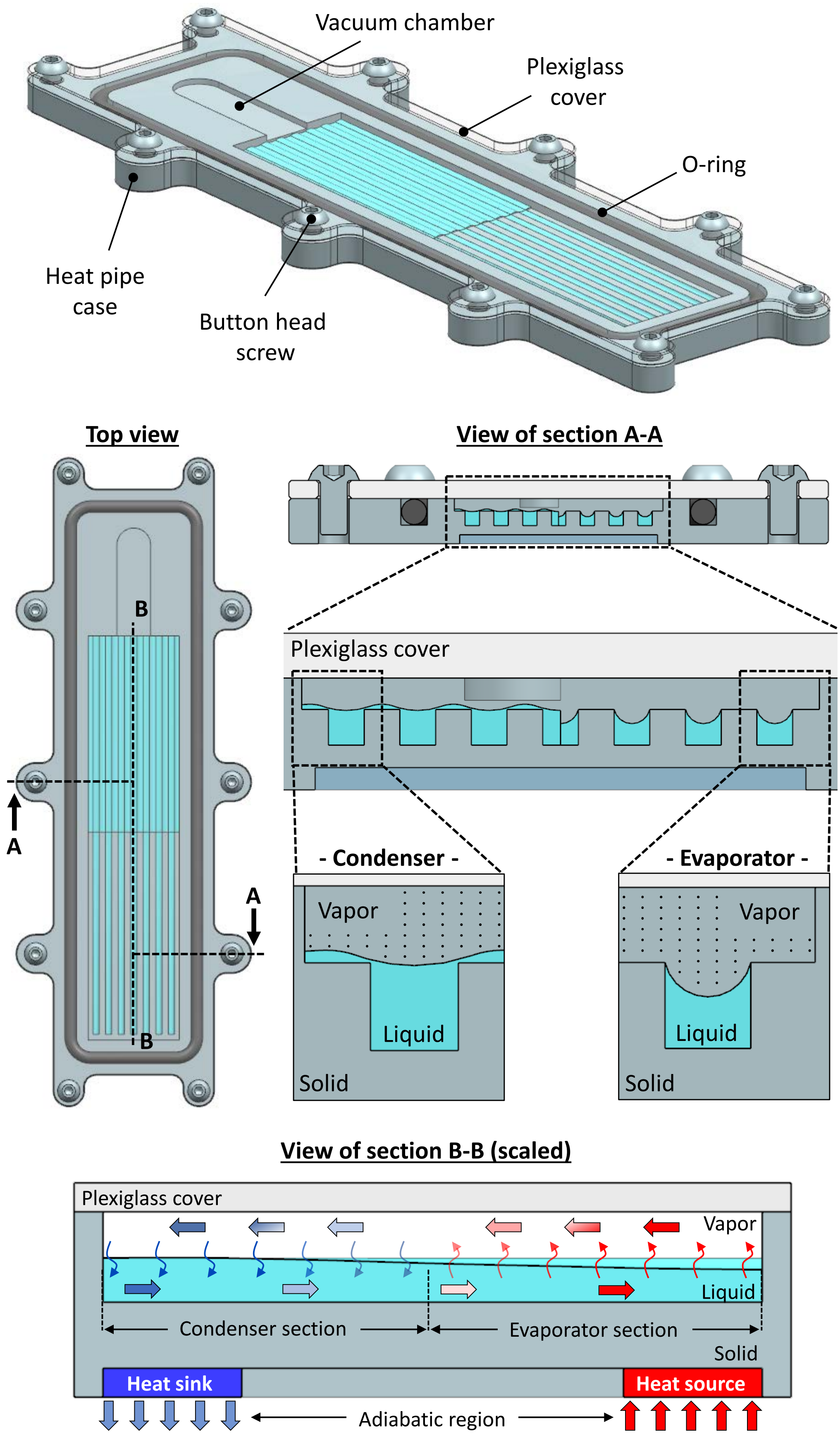


Figure 1.1: Detailed view of a flat grooved heat pipe

Capillary action can be explained as the movement of liquid within the space of channels or porous medium due to adhesion — force of attraction between the molecules of different substances — and cohesion — force of attraction between molecules of the same substance or surface tension — Capillary action occurs when the adhesion to the solid molecules is stronger than the cohesive forces between the liquid molecules.

Heat pipes can be categorized according to capillary structure used i.e. the wick. Wick is located inside the heat pipe which facilitates the flow of the condensed liquid to the evaporator side by the capillary action. Three most-common types of wick structures are the screen wicks, sintered wicks and grooved wicks (Reay et al., 2014). The selection of the wick depends on the cooling application, properties of the working fluid used and orientation of the heat pipe. Sintered wicks yield low permeability but porous structure yields large pressure drop along the pipe because low permeability increases capillary pumping effect (Peterson, 1994). Compared to other structures, porous wick provides higher effective thermal conductivity and can be used effectively against gravity (De Schampheleire et al., 2015). Screen wicks are the simplest and the most common type of the wick structure. Screen wicks yields low pressure drop along the pipe with moderate capillary action. This type of wick can be used within complicated heat pipe shapes, where sintered wicks cannot be used. Grooved wicks have good permeability while capillary pumping capability of grooved wicks is low compared with other wick structures because the size of the grooves is larger than sintered and mesh screen wicks (Faghri, A., 2014). Therefore, their low capillary pumping capability may limit the usage of grooved wicks i.e. grooved heat pipes are not preferred in adverse gravity. Moreover, manufacturing of grooves (especially those with high aspect ratio) can be difficult and generally more expensive than screen wicks (Galvan et al., 2016). Different types of wick structures are shown in Figure 1.2.

Recently, some studies in the literature divulge improvements in wick structures. New designs such as composite screens and screen-covered grooves appear in industrial use with promising performances. These solutions provide high-capillary pressure with high permeability; however, manufacturing these designs is challenging (Paiva and Mantelli, 2015; Franchi and Huang, 2008; Jiang et al., 2014; Ling et al., 2016).

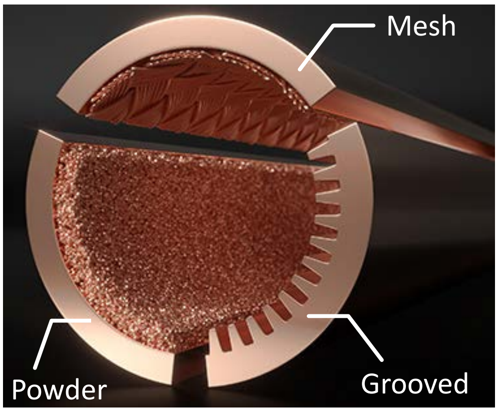


Figure 1.2: Different types of wick structures (*Cooler Master Co.* 2020)

Heat pipes that do not contain wick structures (wickless design) are also possible and available in the industry. However, they may not be suitable for some cases. Hu et al. (2016) stated that the inclination angle has a strong effect on the thermal performance of wickless heat pipes, and these types of designs yield better performance above 20° inclination angle.

Although various types of wick structures are used in industry as stated above, this thesis focuses on developing a modeling approach for the design and performance assessment of grooved wick heat pipes. Their manufacturing is cost effective and relatively easy compared to other types of wicks, moreover; mathematical modeling of other wick structures requires parameters (e.g. permeability) which cannot be analytically modeled and have a strong effect on the predicted results.

Working fluid in heat pipe plays an important role on the design and selection. Numerous working fluids are employed in the heat pipes depending on cooling application, such as water (Poston et al., 2014), methanol (Lefèvre et al., 2008), ammonia (Stephan and Busse, 1992), isopropyl alcohol (Alijani et al., 2018). Choosing the working fluid becomes one of the vital steps considering heat transfer performance. The working fluid should be selected in accordance with temperature range of the application also compatibility of the material-fluid pair. Any change in physical properties of fluid with temperature may negatively affect the performance. In studies (Lee et al., 2020; Barba et al., 2019; Zhao et al., 2019; Sun et al., 2019; Gully, 2014; He et al., 2017), heat pipes operating in cryogenic temperature range (below 100 K) are investigated. Hydrogen (Sun et al., 2019), nitrogen (Lee et al., 2020; Zhao et al., 2019), neon (Barba et al., 2019; He et al., 2017), helium (Gully, 2014) are selected as working fluids. Heat pipes are also used in high-temperature applications above 800 K (Liu et al., 2020; Meisel et al., 2015). In these high temperature applications liquid-metals are preferred as working fluid, e.g. lithium (Liu et al., 2020) and sodium (Meisel et al., 2015). Working fluid should be in the liquid state as long as the heat load is not applied on it which requires the melting temperature of the fluid should be less than the operating temperature and critical temperature should be higher than the operating temperature. Melting, boiling points at atmospheric pressure and useful temperature range values of commonly used working fluids in heat pipe applications are given in Table 1.1.

Table 1.1: Physical properties of commonly used working fluids in heat pipe applications (Reay et al., 2014)

| Fluid | Melting Point (°C) | Boiling Point at Atmospheric Pressure (°C) | Useful Range (°C) |
|---|---|---|---|
| Helium | −271 | −261 | −271 to −269 |
| Nitrogen | −210 | −196 | −203 to −160 |
| Ammonia | −78 | −33 | −60 to 100 |
| Pentane | −130 | 28 | −20 to 120 |
| Acetone | −95 | 57 | 0 to 120 |
| Methanol | −98 | 64 | 10 to 130 |
| Flutec PP2 | −50 | 76 | 10 to 160 |
| Ethanol | −112 | 78 | 0 to 130 |
| Heptane | −90 | 98 | 0 to 150 |
| Water | 0 | 100 | 30 to 200 |
| Toluene | −95 | 110 | 50 to 200 |
| Flutec PP9 | −70 | 160 | 0 to 225 |

**Table 1.1 continued**

| Fluid | Melting Point (°C) | Boiling Point at Atmospheric Pressure (°C) | Useful Range (°C) |
|---|---|---|---|
| Thermex | 12 | 257 | 150 to 350 |
| Mercury | −39 | 361 | 250 to 650 |
| Caesium | 29 | 670 | 450 to 900 |
| Potassium | 62 | 774 | 500 to 1000 |
| Sodium | 98 | 892 | 600 to 1200 |
| Lithium | 179 | 1340 | 1000 to 1800 |
| Silver | 960 | 2212 | 1800 to 2300 |

The working fluid must be compatible with the material of the wick, otherwise, corrosion may occur inside the structure or heat pipe may not perform at full capacity (i.e. dry out occurs or heat would not be transferred via phase-change). Considering the physical properties of the working fluid; latent heat and surface tension should be high unlike the fluid viscosity to transfer heat via phase-change with minimum fluid flow which yields lower pressure drop. High value of thermal conductivity would yield a more uniform temperature distribution throughout the heat pipe.

The criterion — known as Merit number — was defined to assess the impact of working fluid on heat pipe performance by Chi. Correlation of the merit number is given in Equation 1.1 (Chi, 1976)

$$Me = \frac{\rho \sigma h_{fg}}{\mu} \tag{1.1}$$

where $\rho$ is the liquid density, $\sigma$ is the liquid surface tension, $h_{fg}$ is the latent heat of evaporation, $\mu$ is the liquid dynamic viscosity. A working fluid which has a high value of merit number should be preferred to maximize the performance.

There are some limitations that restraint the operation of heat pipes such as, boiling limit, entrainment limit, sonic limit and viscous limit (Peterson, 1994; Reay et al., 2014).

Heat pipes can be manufactured by various ways owing to developments of the manufacturing techniques depending on the heat pipe material. For silicon micro grooved heat pipes machining (Peterson et al., 1993), etching (Kang et al., 2002), wafer sawing (Peterson, 1994), photo-lithography (Kang et al., 2002) processes are mainly used. On the other hand for the metallic heat pipes, electric discharge machining (EDM) (Cao et al., 1997), CNC milling (Lefèvre et al., 2008), drawing and extrusion (Moon et al., 2004), metal forming and laser-assisted wet etching (Lim et al., 2008) techniques are commonly used.

## 1.1 Literature Review

The idea of multi-phase heat transfer goes back to 1831. A.M Perkins invented a device known as Perkins tube (Reay, 1982). It is basically a sealed chamber with the working fluid inside. The liquid evaporates when heated and evaporated vapor flows to the upper part of the tube where it condenses and returns to the bottom because of gravity. Heat pipe concept was first presented in a patent file submitted by R.S Gaugler (Gaugler, 1944), working for General Motors Corporation in 1942 in which the operating principle of a 2-phase heat transfer device was explained in the document. Gaugler described the design as a capillary heat transfer device for refrigerating apparatus, not a heat pipe. In 1962, Trefethen (Bejan, 2003) studied the capillary action concept and evaporation-condensation heat transfer in scope of the research related to the space program. The idea of heat pipe came out again in a patent file introduced by T. Wyatt (Zohuri, 2020) in 1963. The author developed a self-operating, stabilization system for temperature control of an orbiting space satellite based on two-phase heat transfer and fluid flow through a wick. The definition of heat pipe was first used in a paper published by the scientists of the Los Alamos Laboratory (Grover et al., 1964). The authors designed and manufactured simple devices to transfer large amounts of heat with a small temperature difference benefiting from the phase change phenomenon. In that paper, operational principle of heat pipes was explained, simple theoretical calculations were presented. The authors stated that heat pipe could work under no-gravity environments, and the device had the potential to be utilized in space applications, however, the pipe was not tested in gravity-free conditions in the study. Several experiments were conducted in a wide temperature range in the scope of the study. Water was selected as the working fluid for the applications about the room temperatures, while sodium was adopted for high-temperature applications (~1100 K). It was aimed to transfer 30 W/cm$^2$ heat flux; however, dry-out phenomenon occurred during the operation, and the authors stated this phenomenon as a significant limitation on the performance of heat pipes. Since then, heat pipes have attracted substantial interest from scientists worldwide due to their advantages.

In 1984, correlation for the capillary limit of a heat pipe was put forward by Cotter (1984) based on the following simplifications: the maximum limit of the heat transfer capacity for a triangular grooved heat pipe was determined by solving the 1-D steady and incompressible momentum equation for both of the liquid and vapor phases by neglecting the gravitational effect. Writing energy balance locally with utilizing the mass flow rate obtained from the momentum equation and integrating along the pipe gave maximum heat transfer capacity. Author defined local axial heat transfer capacity in the energy equation and shape of liquid film which were assumed to be known *a priori.* The term can be seen as a correction factor which was used to simulate experimental data. The other assumption in this study was that velocity at the liquid-vapor interface was taken as zero which could lead to improper results.

In addition to Cotter's model, an experimental setup was built by Babin et al. (1990), and findings were compared to evaluate the validity of the numerical model. Underlying assumptions were shared except the zero-velocity assumption at the interface and neglecting the effect of gravity during the development of the mathematical model. Dry out limit and maximum heat transfer capacity were determined as a part of the study.

Another significant contribution to mathematical modeling of the heat pipes was provided by Stephan and Busse (1992). Heat transfer inside the heat pipes with open trapezoidal grooves was investigated. Until this study, many models in the literature assumed that liquid-vapor interface temperature was equal to vapor saturation temperature, or variation in the liquid-vapor interface is not considered. Schneider et al. (1976) showed that by conducting experiments, such simplifications cause an over prediction of the phase change heat transfer coefficients. To address this, the solution domain was divided into two zones as micro and macro-regions and modeled separately. For the micro-region, flow and heat transfer was considered as 1-D. The continuity, momentum, and energy equations were coupled and governing differential equation was treated as an initial value problem and solved using the Runge-Kutta method. The variation of meniscus angle and effect of disjoining pressure is taken into consideration. On the other hand, heat transfer in the macro-region was modeled as 2-D, utilizing the Finite Element Method (FEM). The authors concluded that meniscus curvature and adhesion forces have a significant impact on the temperature distribution along the groove.

Another mathematical model was built by Khrustalev and Faghri (1994a) to investigate the fluid flow and heat transfer in a heat pipe with triangular cross-section. 1-D flow models were developed for both of the liquid and vapor phases. The effect of the interfacial shear stress was not neglected in the model. Vapor flow was modeled as 1-D using the boundary layer approximations. Separate skin friction coefficient correlations for evaporator and condenser sections were adopted from the previous investigations in the literature to find the pressure variation in the vapor phase. During the calculation of the interfacial shear stress, the working fluid was assumed to be stationary because liquid velocity was small compared to the vapor velocity. The liquid flow is modeled in a similar manner. Since the Reynolds number in the grooves is less than 1, the flow was assumed to be steady and incompressible. The authors also showed that the inertia term in the momentum equation did not affect the results and could be neglected. The interface meniscus curvature variation was obtained by solving the differential form of Young-Laplace and momentum equations together, which means the effect of the meniscus angle on the phase change was considered. The energy balance was written along the groove by utilizing a liquid mass flow rate to find phase change heat transfer coefficients in the evaporator and condenser sections. Axial conduction was neglected in this study. Condensation was modeled by adopting a correlation for film thickness profile on fin top suggested by Kamotani (1976). Evaporation was modeled by following the previous approaches in literature (Stephan and Busse, 1992; Holm & Goplen 1979) based on the Clausius-Clapeyron equation. The contribution of this study was the inclusion of the effect of disjoining pressure in the mathematical model. The authors concluded that interfacial shear stress and meniscus angle had a significant impact on the maximum heat transfer capacity.

1-D steady state mathematical models for flow and heat transfer were developed to determine the maximum heat load capacity of a triangular grooved micro heat pipe by Longtin et al. (1994). Continuity, momentum and energy equations were solved together for the liquid and vapor phases, and the effect of interfacial shear stress was taken into account. Since the Reynolds number inside the groove was low, conduction and convection occurring in liquid were neglected. In this study only the evaporator and adiabatic sections were considered and included in the mathematical model due to the fact that determination of the velocity distribution in the condenser section and film thickness shape were challenging tasks. The variation of the liquid film thickness in the evaporator and adiabatic sections was taken into account during the modeling. The output of the numerical model was compared with the results obtained from experiments. Authors concluded that an approximately linear profile exists in the interfacial radius of curvature and the pressure drop in the liquid was found to be larger than that of the vapor.

Since then, various similar analytical models of heat pipes are available in literature. Zhang et al. (2009) developed a 1-D model based on thermal resistances to optimize the performance of a heat pipe with omega($\Omega$)-shaped grooves. Effect of axial conduction was neglected in this study; furthermore, radii of curvature were kept constant in evaporator and condenser regions. Modeling the change of radius of curvature could become important when the pressure drop was large through the heat pipe. The effect of axial conduction could be substantial, especially when the length of the adiabatic section was short. Do et al. (2008) also developed a 1-D mathematical model for a grooved wick heat pipe to evaluate the thermal performance characteristics. In their study, the effect of the liquid-vapor interfacial shear stress was also considered. Modified Shah method was used in the mathematical model to include the liquid-vapor interfacial shear stress. The model was validated using experimental data. Lefèvre et al. (2008) presented a more detailed model in which a 1-D flow model was coupled to a 2-D thermal model in the case of a flat grooved heat pipe and the liquid-vapor interfacial shear was neglected. The heat conduction in liquid was also neglected since the thermal conductivity of the working fluid was much lower than material of the channel. Heat transfer coefficient for evaporation region was calculated using kinetic theory and the models were validated with experiments. Odabaşi (2014) modeled a rectangular grooved heat pipe, where the flow inside the channel was 1-D and heat transfer modeled as 3-D. Energy balance was written for different regions of the heat pipe using a coordinate transformation. The effect of thermal conduction inside the liquid was accounted for in the model. Effect of various parameters like channel height, fin thickness, source heat flux, etc. was also investigated, which is important from a design point of view.

Lips and Lefèvre (2014) studied a flat micro heat pipe (FMHP) in detail by investigating the liquid and vapor phases simultaneously. The governing equations were build based on 2-D flow and 3-D thermal model assumptions; moreover, these models were coupled and solved by adopting Fourier series expressions. Similar to other studies, the temperature and pressure distributions in the heat pipe were calculated; moreover, results were supported by the conducted experiments. Authors, however considered the phase-change by equivalent thermal conductivity calculated from the kinetic theory and analytical solution was calculated by solving 3-D heat conduction equation. The flow inside the porous wick was modeled by utilizing Darcy's law,accounting for permeability. Change in the liquid-vapor interface shape was taken into account through Young-Laplace equation. The maximum heat capacity of the system was also found out as an outcome of that study.

Ternet et al. (2018) investigated the effect of the groove geometry on the performance of heat pipes both theoretically and experimentally. Rectangular, triangular and trapezoidal groove shapes were studied. Deionized water and n-pentane were used as the working fluid. Effect of the several parameters like channel height, with, length and trapezoid angle is investigated. The authors aimed to find the parameters that affect the maximum heat flux and pressure drop along the channel. Skin friction correlations were used to calculate liquid and vapor pressure drop along the heat pipe. The skin friction correlations adopted from Khrustalev, D. and Faghri, A. (1995) for rectangular grooves, Suh et al. (2001) for trapezoidal grooves and Ayyaswamy et al. (1974) for triangular grooves. The effect of interfacial shear stress between the liquid-vapor interface was not taken into account. Energy balance was written between the fluid and vapor phases to find the local heat flux which was integrated along the full length of the pipe to find the total heat transferred. At the end of the evaporator the radius of curvature was taken at its minimum value. The authors concluded that increasing channel width increased maximum heat flux up to a point and optimum values of channel width and height belonging to a particular heat pipe were found. The impact of the trapezoid angle was analyzed for various heat pipe depths. For the same trapezoid angle, increasing channel height increased the maximum heat transferred. For higher values of channel height, maximum value of heat transferred increased with trapezoid angle, however, if the channel height was reduced, maximum value of heat transferred became inversely proportional to the trapezoid angle. Rectangular, triangular and trapezoidal channels were studied to reveal the effect of channel geometry following two different approaches. First, the channel cross-sectional area was kept the same for all geometries by changing the channel height. The maximum heat was transferred with the rectangular configuration whereas the minimum value of heat was transferred with the triangular shape. The second approach was keeping the hydraulic diameters and the cross-sectional areas the same. This time the maximum heat was transferred with the trapezoidal channel, whereas minimum value of heat transfer occurred with the rectangular configuration. Heat pipe having a rectangular channel was manufactured and experiments were performed to asses the validity of the developed analytical model. De-ionized water was used as the working fluid during the experiments. Tests showed that measurements were in good agreement with analytical predictions. The drawback of this modeling methodology was that one could get a maximum heat flux value of the investigated heat pipe, not a complete result set i.e. the radius of curvature or temperature variation along the channel. Furthermore, the correlations needed to model heat and fluid flow inside the channel for new geometries like star or omega-shaped grooves. The methodology could be used as a quick comparison tool for choosing a convenient heat pipe for a specific application; however, from the design point of view, it should be beneficial to have a rigorous and detailed model.

Desai et al. (2019) built a mathematical model to determine the maximum heat carrying capacity of a trapezoidal-shaped axial grooved heat pipe. Liquid and vapor flows were modeled using the Young-Laplace equation based on the laminar flow assumption. Poiseuille number (fRe) correlation was adopted from the study performed by Schneider and Devos (1980) to obtain the skin friction coefficient which was used for calculation of the pressure drop along the grooves. Heat source and heat sink were operated uniformly and heat flux was kept constant in time. Change in the liquid cross-sectional area from the condenser to the evaporator was taken into account. The model was build based on thermal resistance analogy. The effect of micro evaporation was taken into account with the thermal resistance correlation, which was developed by Do et al. (2008). Drawback of this approach was the uncertainty of the correlation, which may not be valid for all circumstances. Further investigations were put forward by altering various parameters such as the number of grooves, groove height and groove inclination to maximize heat carrying capacity. Increasing the number of grooves and their inclination caused to decrease in overall thermal resistance, which was an indication of the maximum heat carrying capacity. Moreover, experiments were performed to find the validity of estimation. Good agreement was found between the experimental results and the estimates of the heat-carrying capacity (Only 2.5% difference was observed).

CFD methods are another numerical technique to model heat pipes. The main idea behind the computational fluid dynamics was the numerical solution of the governing differential equations such as; continuity, Navier-Stokes and energy equations. Analytical solution of the equations is possible for limited cases and basic geometries. However, in practice, it may not be possible to solve real engineering problems analytically. In these situations, numerical methods like CFD can be chosen as a powerful tool. Several approaches can be used during the numerical solutions of the heat transfer and fluid flow, such as Finite Element Modeling (FEM), Finite Volume Modeling (FVM) and Finite Difference modeling (FDM). All of these methods have their benefits and limitations. Because of that, the method should be selected in accordance with the application. Various parameters like robustness, computational cost and applicability must be taken into account.

Most commonly used CFD approach to obtain flow and temperature fields of a heat pipe is the Volume of Fluid (VoF) method. Taking advantage of its mass conserving definition (Hirt and Nichols, 1981), the technique has been used to simulate the phase-change phenomenon in heat pipes such as evaporation and condensation. VoF method was used for computing the location and shape of the free surface during each time step. In the VoF method, different phases in the solution domain are represented by volume fractions ranging between 0–1. For two-phase systems, 0 is used with the cell is fully occupied by phase-1 while 1 means that the cell is fully occupied by phase-2. By definition, the summation of volume fractions must be unity. When the volume fraction of the cell becomes different than 0 and 1, that cell is considered as an interface. One drawback of the method is the fluid properties such as density, viscosity, and thermal conductivity at each cell must be calculated according to their volume-weighted average, and the continuity, momentum, and energy equations are solved by standard solution procedures. Since the volume fraction equation is solved using a classic implicit or explicit scheme, the interface can quickly lose resolution due to numerical diffusion. Numerical diffusion may occur due to the velocity jump at the interface and may yield an inaccurate solution. Therefore, the grid resolution must be fine enough to capture the movement of the interface. This will increase the solution time.

Zainal et al. (2017) modeled a heat pipe heat exchanger (HPHE) using a commercial CFD program, AcuSolve®. There is no indication that phase change calculations were performed in the study. Only effective thermal conductivity and heat flux boundary condition is assigned to the heat exchanger to model the heat pipe. From the CFD analysis, velocity and temperature distributions were obtained and these results were used as a guide for design improvement.

Barari (2012) constructed a 2-D model for the investigation of heat transfer and fluid flow in a micro heat pipe and determine the effect of the channel aspect ratio on heat pipe performance. In the study, the heat pipe was divided into three main sections; evaporator, adiabatic and condenser sections. Constant heat flux was assigned to the evaporator, while the convective heat transfer coefficient was defined in the condenser. Effective thermal conductivity was represented in terms of the heat input and maximum temperature difference along the heat pipe (i.e. the temperature difference between condenser and evaporator sections). Continuity, momentum and energy equations were solved for the liquid-vapor mixture along the channel. Finite volume method (FVM) was adopted and the SIMPLE algorithm was selected to tackle the velocity-pressure coupling. First-order upwind scheme and unstructured triangular mesh were employed for discretization. No information provided about the variation of meniscus curvature along with the heat pipe; however, the capillary effect was taken into account with the source terms of surface tension. Heat transfer coefficients in evaporator and condenser sections were obtained from forced convection heat transfer correlations.

The CFD methods can be also employed to handle similar complicated problems including nontraditional boundary conditions or the presence of boundaries whose locations are unknown *a priori* such as phase-change governed by phenomenological laws. Moreover, optimization problems require repeating the solution more than once which is time consuming and requires intensive effort. Currently, the usage of CFD is growing due to the disadvantages of experimental studies. Because, full scale tests are expensive and require more effort compared to CFD methods. Moreover, measuring some quantities may not be easy even with sophisticated instruments.

Various studies exist the literature that consists of the nontraditional use of commercial and open-source numerical solvers. Kim et al. (2020) developed a user-friendly CFD automation tool using the open-source program OpenFOAM® to analyze internal airflow patterns and ventilation rates of naturally ventilated buildings. The study was aimed at unprofessional CFD users because CFD simulations require heavy workloads and experienced users. The automation process is developed using Visual Basic (VB) programming language. The developed code automates the pre-processing, solution, and post-processing stages of CFD simulations and to analyze the ventilation performance of naturally ventilated agricultural buildings. Geometry generation, meshing and post-processing the results are embedded into one program, which is controlled by a graphical user interface (GUI). The GUI allowed users to generate the geometry and define boundary conditions (e.g. wind speed) without opening solver or CAD program.

Feenstra et al. (2018) developed an automated solution procedure for one-way and two-way coupling of CFD fire simulations to thermo-mechanical finite element analyses. The coupled analysis consists of sub-steps, namely; fire simulation, heat transfer analysis and structural response analysis. In the two-way coupling method, mechanical effects on fire propagation were taken into account. Therefore, it was required to deliver the results of finite element analysis back to CFD analysis in an iterative manner. Since the structural parts burn and the geometry changes significantly during the sub-steps, these changes must be defined in relevant sub-models. Due to this reason, the necessity of automation has emerged. Fire Dynamics Simulator (FDS) was used for the CFD solution, and Abaqus® was chosen to handle the structural sub-model.

Zhang et al. (2017) developed an automated solution procedure for solving fluid flow, design and optimization in aerodynamics field. The study focuses on aerodynamic shape optimization (shape parameters like camber, twist and thickness of a wing) of an aircraft model to reduce drag. This will enable designer to produce lighter, fuel efficient and quieter aircraft. Since the optimization process requires performing CFD analysis repeatedly, automation of the procedure becomes crucial. The open source CFD solver and optimization package SU2 is used in calculations.

Fernengel et al. (2018) focused on simulation automation for packed bed catalytic reactors based on open-source software OpenFOAM®. In this study, it was aimed to embed multiple simulations into one program which performs pre-processing (geometry set up and mesh generation), reaction simulation and post-processing. Mesh generation and simulations were performed with OpenFOAM®. The random packing was generated with commercial software known as Blender. ParaView was used for data analysis and visualization. Software packages were integrated via scripting interfaces written in the Python environment.

Gu et al. (2017) developed an automated multidisciplinary design methodology to predict aerodynamic behavior for conventional and unconventional aircraft configurations in the earlier design stages. Since including interdisciplinary analyses into the design process is time-consuming, automation process becomes imperative. Therefore, automated CFD-based analysis developed via using scripts written in the Python environment was integrated into the process. The procedure was applied to the design of the DLR-F6 aircraft configuration. The inviscid analysis was performed with the open-source CFD solver SU2® and ANSYS Fluent® solver was used for viscous simulation. This design structure was not developed in an iterative manner. The developed program performed the necessary step for one time.

In summary, various theoretical and experimental studies have been conducted to assess the thermal performance of grooved heat pipes for numerous sections (e.g. trapezoidal, rectangular and triangular grooves). However, the available studies of flat grooved heat pipes do not pay not enough attention to the comprehensive and rigorous modeling of both fluid flow and heat transfer. Moreover, from the experimental studies it is concluded that a number of factors are effective on the performance of heat pipes: i) the choice of the micro-channel geometry ii) type and quantity of the working fluid and the material from which the grooves are manufactured. These factors have an influence on liquid and vapor flow interaction, fill ratio, contact angle and phase change rates. Experimental studies mainly provide external temperature measurements to characterize the heat pipe. Therefore, further numerical studies which are compatible with experimental data are necessary to fully understand the complex phase-change, fluid flow and heat transfer phenomena to rigorously investigate the flat plate heat pipes. From a design point of view, it is essential to obtain a detailed and parametric model to reveal and understand which affects thermal performance, in addition, a complete understanding of heat transfer performance requires a coupled model in which the continuity, momentum and energy equations are solved sequentially in an iterative manner. To obtain further insights into grooved heat pipes above mentioned model is generated in the scope of this thesis.

## 1.2 Objective of the Thesis

Heat pipes have been widely used in a wide range of applications—from thermal management of electronic components to satellites—owing to their superior ability to transfer significant amounts of heat with small temperature gradients. Diverse and complicated phenomena such as phase-change, fluid flow and heat transfer are involved during the operation of heat pipes. This makes it challenging to build a mathematical model to predict the performance of heat pipes. For this reason, modeling and design processes of the heat pipes draw substantial interest from engineers and scientists.

During the investigation of such a challenging structure, experimental studies appear to be a first choice considering the fact that the experimental approach is regarded as the most reliable technique which reflects the real-life phenomena and can be employed to reveal and understand the parameters that may affect the performance of a heat pipe. Nevertheless, full-scale tests can be expensive most of the time and require enormous efforts to build. Depending on the study, more than one prototype may be required to reveal the effect of a parameter. Generally, it would be impractical to investigate all parameters in detail. Therefore, case-specific results may be obtained because the number of controlled parameters is limited. Another difficulty encountered during the experiments is the precise measuring of some quantities may not be possible even with contemporary instruments.

As mentioned in the previous section, a number of experimental and numerical studies related to a wide range of applications of heat pipes are available in the literature. Most of the experimental studies provide only external temperature measurements to characterize the heat pipe, and the locations where the temperature data is collected are limited. From the design point of view, it is essential to understand all parameters and observe the variables not only in measured points but also for the entire system. Therefore, the necessity of a mathematical model that can be used to assess characteristics of a heat pipe emerges.

Although computing capabilities have advanced over the decades, modeling the phase-change flow and heat transfer comes with its own challenges. The numerical studies are performed with simplifications based on approximations, which may result in inaccurate predictions, such as regarding the problem as 1-D or 2-D, neglecting the effect of the liquid-vapor interface shape along the groove, assumption of fixed evaporation and condensation rate along the channel, neglecting axial conduction along the groove and utilizing approximate correlations based on free surface flow to for the skin friction coefficient to obtain pressure drop. 3-D modeling approaches are also available in the literature; however, in these studies, the coordinate transformation technique is employed, and the application of this technique is limited to simple geometries such as rectangular channels. It would be impractical to apply a coordinate transformation technique to complex groove shapes.

To realistically predict the performance of grooved heat pipes, it is necessary to include all of the mentioned effects to a developed methodology by setting up a physical-based, 3-D, comprehensive and rigorous mathematical model; however, currently there is no such comprehensive and rigorous mathematical modeling methodology reported in the literature. In this study, it is aimed to build a mathematical model that predicts flow field, heat and phase-change characteristics of a grooved heat pipe. Utilizing commercial CFD codes, complex and innovative channel geometries are suggested and investigated for performance improvement.

## 1.3 Outline of the Thesis

In this part, a summary of the content of the chapters in the thesis is stated. Beginning with the description of the working principle of heat pipes and their utilization areas, information about the main components (i.e. wick structures), working fluids and manufacturing techniques are provided in Chapter 1. Since the modeling methodology of a grooved heat pipe is studied in the scope of this thesis, literature review about the modeling approaches of grooved wick structures are predominantly provided. Moreover, non-traditional usage of the CFD codes in the wide range of application areas such as aerospace, fire dynamics and packed bed catalytic reactors is mentioned.

Modeling stages of the flow, heat and the mass transfer of a grooved heat pipe are explained step by step in Chapter 2. After the commentary on the motivations behind this study, sub components of the developed methodology (i.e. phase-change calculations, CFD modeling and solution, result evaluation) are explained in detail. First, phase change mass transfer models based on kinetic theory and Clausius-Clapeyron relation for evaporation and condensation phenomena are developed. CFD models for the determination of the flow and heat transfer characteristics are constructed. As a result, velocity, pressure and temperature variations for a rectangular channel are obtained. As these quantities do not converge their final values in one step, further calculations are performed for the interpretation of the results to sustain the iterative solution process. The findings of the converged solution are compared with the corresponding values obtained from the literature. Finally, the parametric study is employed to investigate the possible effects of the design parameters.

After obtaining a solution for the rectangular cross sectional channel, the developed methodology is used for the solution of the channels whose cross-sections are designed as simple geometries such as trapezoidal, wedge, omega etc. Shape effect on the heat pipe performance is investigated in this chapter. The advantages and disadvantages of various cross-sections are put forward. Inspiring and using these results, innovative groove cross-sections are designed to improve heat pipe performance in Chapter 3.

In Chapter 4, the implementation of the possible uses of the developed solution methodology is discussed, and as an extension, the solution procedure is used to determine flow and temperature fields of multi-channel grooved heat pipes. The results (phase change heat transfer coefficients) that are obtained from the single channel are used as a boundary conditions during the modeling of multi-channel heat pipes with different groove densities and heat loads. The results are compared with the experimental data to assess the validity of the mathematical model. Another possible extension of the solution methodology is modeling dry out phenomena, and the developed methodology is also applied to simulate the dry out characteristics of a grooved heat pipe.

Finally, conclusions and the recommendations for future work are presented in the last chapter.

# CHAPTER 2

# COMPREHENSIVE AND NOVEL APPROACH FOR THE MODELING OF GROOVED HEAT PIPES

Due to the enhancements in simulation technology, more engineering questions can be answered realistically with computers in a virtual environment. However, some problems still cannot be modeled and solved in a single step due to the non-linear and complex nature of the underlying psychics, such as problems including nontraditional boundary conditions or the presence of boundaries whose locations are unknown a priori such as phase-change governed by phenomenological laws. Detailed and sophisticated solution procedures are required to handle this kind of the problems.

This chapter focuses on an approach that is developed to simulate flow, heat and mass transfer characteristics inside the flat grooved heat pipe. Owing to the working nature of heat pipes, the effect of diverse complex phenomena should be accounted for during the development of mathematical model. Therefore, different physical sub-models such as; solution of in-groove flow; modeling evaporation and condensation to evaluate phase-change mass transfer; solution of 3-D heat transfer model emerge. The sub-models must be solved coupled and consecutively to obtain a particular solution for the grooved heat pipe. To address this, a computer code is developed in Python environment via scripts to build an automated framework that combines different physical models.

Starting with providing an information about the automated solution procedure, detailed insights about the evaporation and condensation phase-change calculations based on kinetic theory and Clausius-Clapeyron equation is provided. After that, individual flow and heat transfer models are explained in-detail.

Commercial CFD programs — Fluent® and CFX® — are employed for the solution of flow and heat transfer through the heat pipe. The output data such as vapor saturation temperature and pressure drop along the groove obtained from both software are compared and found that negligible difference exists between the results. Therefore, only Fluent® results are presented in the following chapters. The liquid-vapor interface shape, pressure, velocity and temperature variations inside the heat pipe are obtained with the developed methodology. The findings are compared with the corresponding values available in the literature. Finally, parametric studies are performed to assess the thermal performance of heat pipes with various geometric design.

## 2.1 Automation of the Modeling Approach

Although commercial CFD programs have capabilities for the solution of two-phase heat and mass transfer, some problems still cannot be comprehensively modeleded via standardized CFD tools in a single step due to the complex non-linear interaction of the physical phenomenon such as in a flat grooved heat pipe, where the problem includes nontraditional boundary conditions and the liquid-vapor interface CAD model changes with iterations during the solution.

In most of the fluid flow and heat transfer problems, CAD model of the solution domain and boundary conditions are known at the beginning and these parameters do not change with the solution. On the other hand, modeling of the grooved heat pipes is more complicated, since the geometry of the working fluid inside the channels (shape of the liquid-vapor interface), and boundary conditions at the interface are not known *a priori*. To be more specific, shape of the interface is dictated by the pressure variation along the groove. Moreover, the amount of evaporated vapor and condensed liquid are variables and their values strongly depend on the temperature distribution inside the channel and the saturation temperature of the vapor. All of these parameters are also unknown *a priori*. This situation is illustrated on the half channel in Figure 2.1. In this figure, $T_w$ is the wall temperature variation along the red line and vapor saturation temperature is denoted by $T_v$. The subscripts 1 and 2 indicate the hypothetical values of the mentioned parameters on the heat pipe.

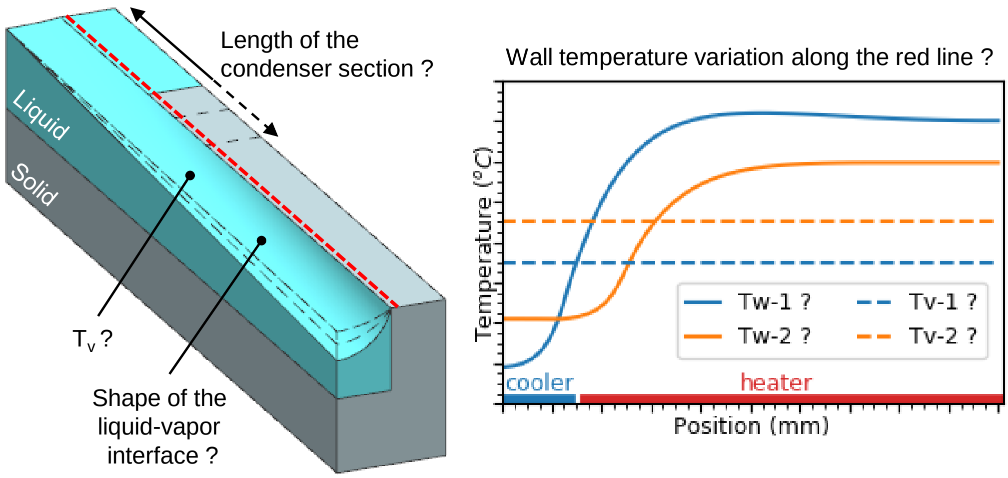


Figure 2.1: Shape of liquid-vapor interface and corresponding boundary conditions that are unknown a priori

To address such a complicated issue, the problem is divided into successive sub-steps and at each step a different physical phenomenon is addressed comprehensively. These steps can be expressed as; (i) generation of the liquid-vapor interface CAD model; (ii) modeling the mass transfer encountered with evaporation and condensation phase-change phenomena; (iii) 3-D in-groove flow modeling to predict pressure distribution and 3-D modeling of the heat transfer inside the solution domain to get wall temperature variation. These steps must be handled sequentiality and coupled to obtain a unique solution. However, these steps are dependent on each other in such a way that numerous output parameters of a particular step are used as an input in the following step. Furthermore, due to the excessive number of data to be loaded in every iteration, a manual implementation of the data set would be impractical, rendering automation of the iterative process imperative. This brings into prominence the necessity to establish an automated solution procedure.

The sub-steps consisting of the determination of the flow and temperature fields are solved with the help of the commercial CFD program, Fluent®, since the solution of the conservation equations based on phenomenological laws especially for the complex geometries would be computationally challenging.

It is aimed to embed all of the consecutive incremental steps into *one program* which will perform the iterative calculations automatically. Process involves the 3-D CAD model generation, discretization of the solution domain, determination and assignment of the materials and relevant boundary conditions to the CFD program (e.g. phase-change mass flow rates, heat transfer coefficients, saturation temperature), running the CFD code, post-processing results and evaluating results to be fed to the next iterative step and repeating the entire process until the prescribed convergence criteria are satisfied.

The main script (driver) that runs the iterative loop is written using Python® programming language. In addition, the computer code used to determine phase-change mass flow rate values and compute the liquid-vapor interface shape at each step is also developed in Python® environment. 3-D parametric heat pipe design is obtained through the use of a Computer Aided Design (CAD) tool Siemens NX 12. A parametric CAD model is crucial to handle the necessity for generation of the liquid-vapor interface for each iteration. Employed software for the automation process are depicted in Figure 2.2.

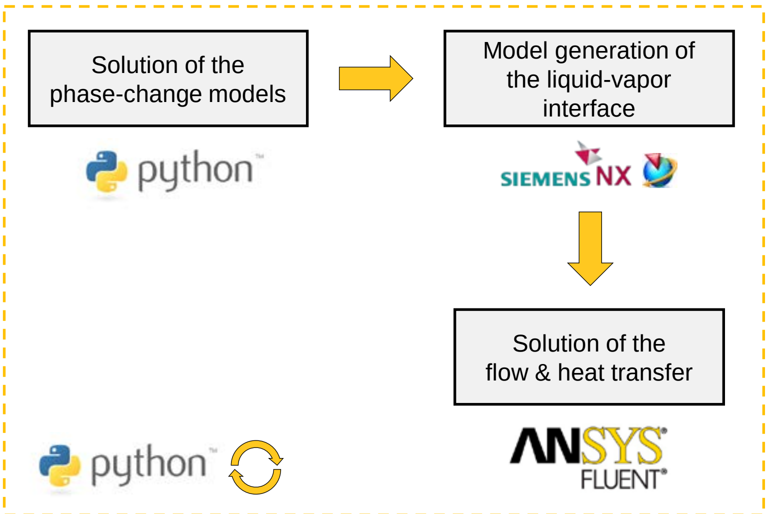


Figure 2.2: Employed software for the modeling of heat pipes

Solution procedure begins with the estimation of the initial guesses for the shape of the liquid-vapor interface, wall temperature distribution and vapor (saturation) temperature. Initial wall temperature distribution is assumed to be linear and calculated using a simple 1-D modeling of the heat pipe. The iterations are continued with the calculation of phase-change mass flow rate values for guessed models and parameters.

Applying phase-change mass flow rate values as boundary conditions, in-groove flow model is solved using the CFD program (Fluent) to predict pressure distribution along the channel. The pressure distribution obtained is used to regenerate the liquid-vapor interface along the groove by employing the Young-Laplace equation (2.1). The same procedure is continued with the new geometry and corrected mass flow rate values until the shape of the interface converges.

$$P_l - P_v = -\frac{\sigma}{R} \tag{2.1}$$

Next step is the calculation of the effective phase-change heat transfer coefficients with the procured interface geometry. Heat transfer coefficients are obtained by solving phase-change model and utilized as boundary conditions in the model which is built using Fluent® to predict the temperature distribution throughout the heat pipe. Newly calculated temperature distribution will yield improved estimates of effective phase-change heat transfer coefficients. Therefore, the iterative calculations are continued until the wall temperatures and effective phase-change heat transfer coefficients converge.

Liquid-vapor interface model and wall temperature distribution converge at a particular value of the vapor (saturation) temperature, however in this case, the global solution of the problem may not be achieved. One criterion is left to be checked which is a main balance of the working fluid at the convergence. The amount of evaporated vapor and condensed liquid should balance. To satisfy the mass balance, vapor saturation temperature is altered in an iterative manner and all of the mentioned calculations are re-performed. The secant method is employed to find new estimates of vapor temperature which is expressed in equation (2.2). During the calculations of the secant iteration process, an objective function $f(T_v)$ is defined as the ratio of evaporation and condensation mass flow rates $\left|\frac{\Sigma \dot{m}_e}{\Sigma \dot{m}_c}\right|$ which must converge to 1 at the end of the calculations. Superscripts $(i-1)$ and $(i-2)$ indicate the current and previous estimated or calculated values.

$$T_v^i = T_v^{i-1} - (f(T_v^{i-1}) - 1)\left(\frac{T_v^{i-1} - T_v^{i-2}}{f(T_v^{i-1}) - f(T_v^{i-2})}\right) \tag{2.2}$$

The solution procedure is summarized in Figure 2.3. Input parameters are depicted in red and output parameters in green.

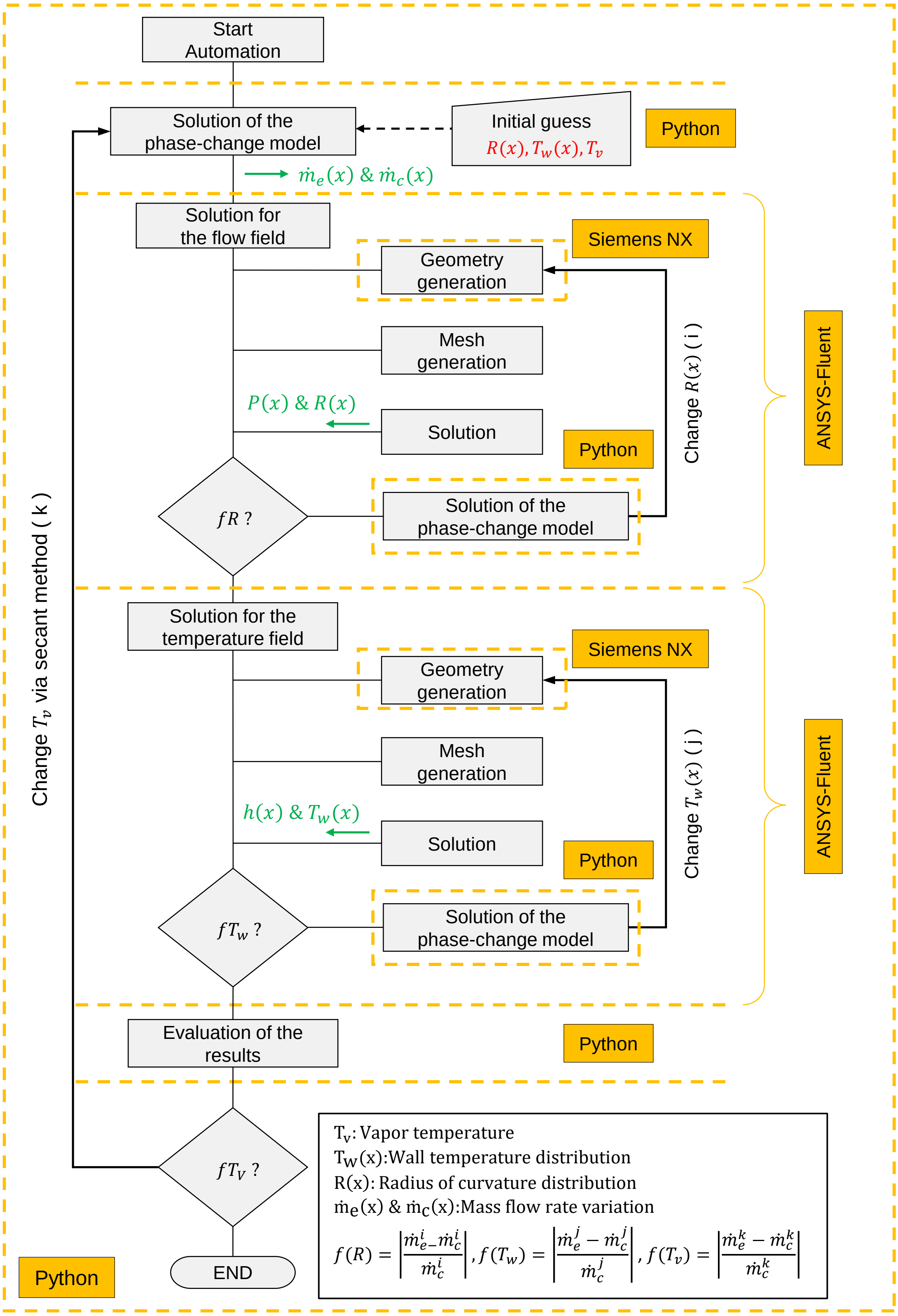


Figure 2.3: Solution procedure

1. The solution starts with the initial guesses of liquid-vapor interface shape, wall temperature distribution $T_w(z)$ and vapor saturation temperature $T_v$.

2. Phase change model is solved to obtain evaporation and condensation phase change mass flow rates along the channel with the initial guesses.

   (a) Mass flow rate distribution along the channel obtained from the step-1 is defined as a boundary condition in the flow model, which is utilized to calculate pressure distribution along the channel. Calculations can be performed with the commercial CFD programs Fluent or CFX. The process consists of the generation of liquid-vapor interface shape, discretization of the solution domain, solution of the governing equations and post-processing the results

   (b) Utilizing the calculated pressure distribution, the radius of curvature variation (new shape of the interface) along the channel is calculated with Young-Laplace equation.

3. Steps 2.a and 2.b are repeated until defined convergence criterion for the evaluation of the interface shape is satisfied. Convergence criterion $(f(R) = |\dot{m}_e^i - \dot{m}_c^i|/(\dot{m}_c^i))$ is expressed in terms of phase change mass flow rates.

4. The equivalent phase-change heat transfer coefficients along the channel are calculated to simulate phase change with using in-house code written in Python environment.

   (a) Heat transfer coefficients are defined as boundary conditions in the energy model to obtain temperature distribution throughout heat pipe. Process involves the solution of relevant governing equations and post-processing the results. Calculations can be performed with the commercial CFD programs known as Fluent or CFX.

   (b) Utilizing the calculated temperature distribution, new heat transfer coefficients (a strong function of temperature) along the channel are calculated with the in-house code written in Python environment.

5. Steps 4.a and 4.b are repeated until the convergence criterion defined for the evaluation of the wall temperatures is satisfied. Convergence criterion $(f(Tw) = |\dot{m}_e^j - \dot{m}_c^j|/(\dot{m}_c^j))$ can be expressed in terms of phase change mass flow rates.

6. Evaporated and condensed mass flow rates are checked at this step because the amount of evaporated vapor must be compensated by the condensed liquid during the heat pipe operation.

7. Steps (2-6) are repeated with the new saturation temperature ($T_v$) until the convergence criterion defined for the evaluation of the saturation temperature is satisfied. Convergence criterion $(f(Tv) = |\dot{m}_e^k - \dot{m}_c^k|/(\dot{m}_c^k))$ can be expressed in terms of phase change mass flow rates. Saturation temperature is altered via secant method during the iterations.

## 2.2 Phase Change Phenomena

Phase change occurs when a particle changes its state. The necessary condition for a phase change is sufficient amount of energy, which must either be added to or removed from a system. The energy that is released or absorbed during the phase-change of a substance is defined as the latent heat. Phase change characteristics depend on pressure and temperature as well as the physical properties of the substance such as molecular weight and accommodation coefficient. During the operation of heat pipes, phase-change occurs in two-ways, liquid to vapor (evaporation) and vapor to liquid (condensation). Phase change phenomenon plays a vital role on the overall heat transfer because most of the heat is transferred via phase-change in heat pipes. Therefore, developing realistic and physical based evaporation and condensation models is crucially important for accurate prediction of heat pipe performance. Evaporation and condensation phase-change models developed for this study are explained in the following subsections.

### 2.2.1 Evaporation Model

In the gas phase, molecules perform a random motion, colliding with each other and the walls of their container due to the kinetic energy they possess. The kinetic energy of the molecules depends only on temperature according to the kinetic theory. In the liquid phase, however, the molecules are kept in balance by inter-molecular forces, which are stronger than in gas phase. If sufficient energy is applied to the system, some molecules overcome these inter-molecular forces, separate from the liquid surface and transform into gas phase. The mentioned phenomenon is known as evaporation phase change.

The domain in which evaporation occurs is generally divided into three sub-regions according to dominance of the different physical mechanisms involved. These sub-regions are named as intrinsic meniscus region, thin film region and non-evaporating region (Potash and Wayner, 1972). A detailed view of these regions is shown in Figure 2.4.

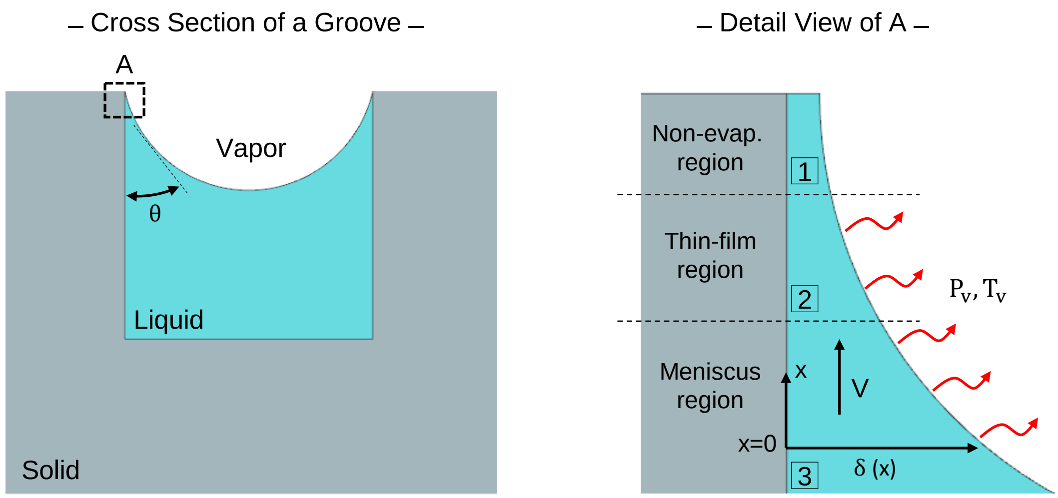


Figure 2.4: Detailed view of evaporation regions

The film thickness has its largest value in the intrinsic-meniscus region. Since the region is furthest from the wall among others, inter-molecular forces due to the presence of the wall almost have no influence and often neglected in this region. In other words, the effect of dispersion pressure is inferior and capillary forces are dominant. The shape of thin-film (liquid-vapor interface) can be found from the Young-Laplace equation with the constant meniscus curvature assumption.

The liquid flows through the thin-film region from intrinsic-meniscus region. The effect of dispersion starts to increase in this region. Therefore, both the dispersion and capillary forces are essential and must be accounted for in the mathematical model. The shape of liquid-vapor interface is influenced by the wall (dispersion effects) that make the meniscus-curvature changing. The heat flux rates are high due to the thin film thickness. Wang et al. (2007) showed that more than 50% of the total heat is transferred from this region.

In non-evaporating region, the liquid film thickness becomes relatively small. Intermolecular forces (i.e. Van der Waals forces) due to the presence of the wall become significant and dominant. Since the film thickness value in this region is order of 1 $\mu$m (Wang et al., 2007), modeling a non-evaporating region is a computationally challenging task and can be studied with the molecular dynamics simulations. In this study, Hamaker constant is employed to calculate the Van Der Waals force of interaction in terms of dispersion pressure. It is assumed neither heat nor mass transfer is occurred in the non-evaporating region.

A detailed investigation and a better understanding of the evaporation phenomenon play a vital role in mathematical modeling of heat pipes since the main heat transfer mechanism inside the heat pipes is heat transfer via phase-change. There are studies in literature in which evaporation phenomenon is investigated in detail. Stephan and Busse (1992), Schonberg et al. (1995), Ha and Peterson (1996) and Wang et al. (2007) modeled evaporation in micro-grooves and concluded that substantial amount of heat is transferred through the region around the wall where the liquid layer is small and taken into consideration for accurate prediction of the phase-change heat transfer. The heat transfer coefficient in thin-film region is affected by meniscus radius and superheat.

Inspiring from the previous models, it is aimed to develop a realistic and accurate evaporation model for the calculations of the heat pipes.

From kinetic theory evaporative mass flux can be written in terms of temperature difference and pressure jump at the interface (Equation 2.3) (Potash and

Wayner, 1972; Wayner et al., 1976)

$$\dot{m}_e'' = a\,\Delta T_{int} \,+\, b\,\Delta P_{int} \tag{2.3}$$

Equation 2.3 can be expanded as;

$$\dot{m}_e'' = a\,(T_{lv} - T_v) \,+\, b\,(P_l - P_v) \tag{2.4}$$

Coefficients a and b in Equation 2.4 is defined as;

$$a = \frac{2c}{2-c}\left(\frac{\overline{M}P_v h_{fg}}{R_u T_v T_{lv}}\right)\sqrt{\frac{\overline{M}}{2\pi R_u T_{lv}}} \tag{2.4a}$$

$$b = \frac{2c}{2-c}\left(\frac{V_l P_v}{R_u T_{lv}}\right)\sqrt{\frac{\overline{M}}{2\pi R_u T_{lv}}} \tag{2.4b}$$

Where $T_{lv}$ is temperature of the liquid-vapor interface, $T_v$ is vapor temperature, $P_l$ is liquid pressure, $P_v$ is vapor pressure, $c$ is accommodation coefficient and its value is 1 for non-polar liquids (Schonberg and Wayner Jr., 1992). $\overline{M}$ is the molar mass, $V_l$ is the molar volume of the liquid. $R_u$ is the universal gas constant. Necessary condition for evaporation to occur is that temperature of the liquid-vapor interface must be above the vapor temperature. However, saturation temperature ($T_{lv}$) in Equation 2.4 is unknown.

Energy balances at the wall and the liquid-vapor interface are written to eliminate saturation temperature ($T_{lv}$). Resulting equation can be expressed in terms of the wall temperature ($T_w$);

$$\dot{m}_e'' h_{fg} = [\,a\,(T_{lv} - T_v) \,+\, b\,(P_l - P_v)\,]\,h_{fg} = k_l\frac{(T_w - T_{lv})}{\delta} \tag{2.5}$$

If $T_{lv}$ is eliminated from the Equation 2.4 , mass flux can be rewritten as;

$$\dot{m}_e'' = \frac{a\,(T_w - T_v) \,+\, b\,(P_l - P_v)}{1 + a\,\delta\,h_{fg}/k_l} \tag{2.6}$$

According to augmented Young-Laplace equation (Wayner et al., 1976), vapor pressure is balanced by liquid ($P_l$), capillary ($P_c$) and disjoining ($P_d$) pressures.

$$P_v = P_l + P_c + P_d \tag{2.7}$$

Young-Laplace equation can be used to define capillary pressure $P_c$;

$$P_c = \sigma\left(\frac{1}{R_1} + \frac{1}{R_2}\right) \tag{2.8}$$

$R_1$ and $R_2$ are the two principal radius of curvatures which are orthogonal to each other and $\sigma$ is surface tension of the liquid. The radius of curvature along the groove is much larger as compared with the radius of curvature of other axis therefore, Equation 2.8 reduces to;

$$P_c = \frac{\sigma}{R} \tag{2.9}$$

If the curvature $(1/R)$ is defined in terms of the film thickness $\delta$, Equation 2.9 becomes;

$$P_c = \frac{\sigma\delta_{xx}}{(1+\delta_x^2)^{3/2}} \tag{2.10}$$

For a non-polar liquid, the disjoining pressure $(P_d)$ can be expressed as (Derjaguin and Zorin, 1992);

$$P_d = \frac{A_d}{\delta^3} \tag{2.11}$$

During the phase change, not a significant change is expected in vapor pressure $(P_v)$. Therefore, its value can be assumed as constant. Capillary and disjoining pressures are substituted in augmented Young-Laplace equation (Equation 2.7) and the resulting equation is differentiated with respect to film length (x);

$$\frac{dP_l}{dx} = \frac{3A_d\delta_x}{\delta^4} - \frac{\sigma\delta_{xxx}}{(1+\delta_x^2)^{3/2}} + \frac{3\sigma\delta_x\delta_{xx}^2}{(1+\delta_x^2)^{5/2}} \tag{2.12}$$

Considering the facts that Reynolds number is low due to the liquid velocity inside the channel and the channels have a large aspect ratio, lubrication theory is employed to model the fluid flow inside the evaporation region. 1-D, fully developed, incompressible, laminar flow characteristics are assumed. continuity equation and momentum equation in x-direction are written to obtain the liquid pressure gradient with the following boundary conditions;

$$\frac{\partial V_x}{\partial x} + \frac{\partial V_y}{\partial y} = 0 \tag{2.13}$$

$$\frac{\partial V_x}{\partial t} + V_x\frac{\partial V_x}{\partial x} + V_y\frac{\partial V_x}{\partial y} + V_z\frac{\partial V_x}{\partial z} = -\frac{1}{\rho}\frac{\partial P}{\partial x} + \nu\left(\frac{\partial^2 V_x}{\partial x^2} + \frac{\partial^2 V_x}{\partial y^2} + \frac{\partial^2 V_x}{\partial z^2}\right) + g \tag{2.14}$$

No slip boundary condition at the wall;

$$y = 0; \quad V_x = 0 \tag{2.14a}$$

No shear boundary condition at the liquid-vapor interface;

$$y = \delta; \quad \frac{dV_x}{dy} = 0 \tag{2.14b}$$

After the simplifications and solution of continuity and x-momentum equations (Equation 2.13 & Equation 2.14), evaporation mass flux is written in terms of liquid pressure gradient;

$$\dot{m}_e'' = \frac{d}{dx}\left[-\frac{\delta^3}{3\upsilon}\left(\frac{dP_l}{dx} + \rho g\right)\right] \tag{2.15}$$

where $\rho$ is the density and $\upsilon$ is kinematic viscosity of the liquid.

Equation 2.15 can be rewritten as;

$$\frac{d}{dx}\left(\frac{dP_l}{dx}\right) = -\frac{3\upsilon\dot{m}_e''}{\delta^3} - \frac{3\delta_x}{\delta}\left(\frac{dP_l}{dx} + \rho g\right) \tag{2.16}$$

Equation 2.6 , Equation 2.12 & Equation 2.15 are combined in such a way that the combined equations would give the evaporation mass flux;

$$\frac{d}{dx}\left[-\frac{\delta^3}{3\upsilon}\left(\frac{3A_d\delta_x}{\delta^4} - \frac{\sigma\delta_{xxx}}{[1+\delta_x^2]^{3/2}} + \frac{3\sigma\delta_x\delta_{xx}^2}{[1+\delta_x^2]^{5/2}} + \rho g\right)\right] = \frac{a\,(T_w - T_v) + b\,(P_l - P_v)}{1 + a\,\delta\,h_{fg}/k_l} \tag{2.17}$$

Starting from the intrinsic-meniscus region, the $4^{th}$ order differential equation is solved numerically to find mass flux along the liquid film until the point $x^*$ where non-evaporating region starts. The boundary conditions of the differential equation is;

$$x = 0 \;\rightarrow\; \delta = \delta_0 \tag{2.17a}$$

$$x = 0 \;\rightarrow\; P_l - P_v = -\frac{\sigma}{R} \tag{2.17b}$$

$$x = 0 \;\rightarrow\; \frac{\partial \delta}{\partial x} = -\tan(\theta) \tag{2.17c}$$

$$x = x^* \;\rightarrow\; \dot{m}_e'' = 0 \tag{2.17d}$$

Since the solution starts from the intrinsic-meniscus region where intermolecular forces due to the presence of the wall almost no influence on the film thickness, initial film thickness value $\delta_0$ in Equation 2.17a can be obtained with the assumption of capillary pressure is $10^5$ times greater than the disjoining pressure.

$\theta$ in Equation 2.17c is the meniscus angle and can be defined as the angle between the liquid-vapor interface and the wall. As the evaporation rate increases this angle tends to approach its limiting value known as contact angle.

There are various methods that can be followed for the solution of $4^{th}$ order differential equations like Equation 2.17. Forward Euler, backward Euler and Crank-Nicolson methods are some of the examples of the most commonly used methods.

Forward Euler method is an explicit method. The unknown value at step $(n+1)$ is evaluated explicitly with the known quantities such as function value and its derivative at the step $n$. The method is less complicated and requires fewer calculations as compared with implicit methods; therefore, it is easier to implement as compared with the implicit methods. On the other hand, numerical stability may become an issue depending on the chosen step size and convergence may not be satisfied for all cases.

Backward Euler is an implicit method. In order to find the unknown value at step $(n+1)$, the function derivative must be calculated at step $(n+1)$ implicitly. Since the derivative at step $(n+1)$ is not known *a priori*, a suitable root-finding technique must be employed, which makes the backward Euler method more time consuming and computationally intensive as compared with the explicit methods.

Formulation of Crank-Nicolson method is given in Equation 2.18. From the equation it can be seen that Crank-Nicolson method is the average of forward Euler and backward Euler methods.

$$\zeta_{n+1} = \frac{1}{2}\left[\zeta_n + h\, f(\zeta_n, x_n)\right] + \frac{1}{2}\left[\zeta_n + h\, f(\zeta_{n+1}, x_{n+1})\right] \tag{2.18}$$

During the calculations of the current study, convergence was not achieved for distinct contact angles, even with the decreased step sizes if explicit methods (e.g. Runge-Kutta & Forward Euler) are employed. To handle this issue and ensure the numerical stability, more comprehensive but numerically intense Crank-Nicolson method with adaptive step size is utilized to solve the Equation 2.17

Stephan and Busse (1992)'s study is used to assess the validity of the developed methodology. Film thickness and local heat flux variations in the micro-region are compared with the corresponding results of Stephan and Busse (1992), Odabaşi (2014), Akkuş and Dursunkaya (2016). Ammonia is selected as working fluid and heat pipe is made from aluminium. Physical properties of the working fluid are provided in Table 2.1

Film thickness variation and local heat flux distribution in micro-region belong to current study and Stephan and Busse (1992), Odabaşi (2014), Akkuş and Dursunkaya (2016) are shown in Figure 2.5 and Figure 2.6 respectively. Stephan and Busse (1992) starts the solution from non-evaporating region whereas in other studies the solution is started from the somewhere in the intrinsic-meniscus region (where the capillary effect is much more dominant than dispersion of the wall).

Explicit Runge-Kutta and forward Euler methods are utilized for the solution of the $4^{th}$ order differential equation in Stephan and Busse (1992), Odabaşi (2014)

Table 2.1: Physical properties of working fluid used in validation of evaporation model

| **Property** | **Symbol** | **Value** |
|---|---|---|
| Wall temperature [K] | $T_w$ | 301.31 |
| Vapor temperature [K] | $T_v$ | 300 |
| Vapor pressure [Pa] | $P_v$ | $1.06 \times 10^5$ |
| Surface tension [N/m] | $\sigma$ | 0.02 |
| Liquid density [kg/m$^3$] | $\rho$ | 600 |
| Latent heat of evaporation [J/kg] | $h_{fg}$ | $1.18 \times 10^{-6}$ |
| Liquid thermal conductivity [W/m . K] | $k_l$ | 0.48 |
| Dynamic viscosity of liquid [Pa . s] | $\mu$ | $1.3 \times 10^{-4}$ |
| Molar mass of liquid [kg/mol] | $\overline{M}$ | $17.3 \times 10^{-3}$ |
| Molar volume of liquid [m$^3$/mol] | $V_l$ | $28.8 \times 10^{-6}$ |
| Accomodation coefficient [-] | $c$ | 1 |
| Dispersion constant [J] | $A_d$ | $2 \times 10^{-21}$ |
| Intrinsic meniscus radius [m] | $R$ | $909 \times 10^{-6}$ |

whereas, Akkuş and Dursunkaya (2016) and the current study employ implicit Crank-Nicolson method.

From the Figure 2.5, it can be observed that film thickness values nearly coincide in all studies; however, a slight difference exists between heat flux variations in Figure 2.6. This difference causes amount of total heat transferred from the micro-region deviates within 7% between the studies. The deviation may be attributed to the followed modeling approaches.

Comparisons showed that findings are in close-agreement with the corresponding results, and modeling methodology can be utilized for calculation of evaporation mass flux and phase-change heat transfer coefficient values as a part of the automated solution methodology mentioned in the previous section.

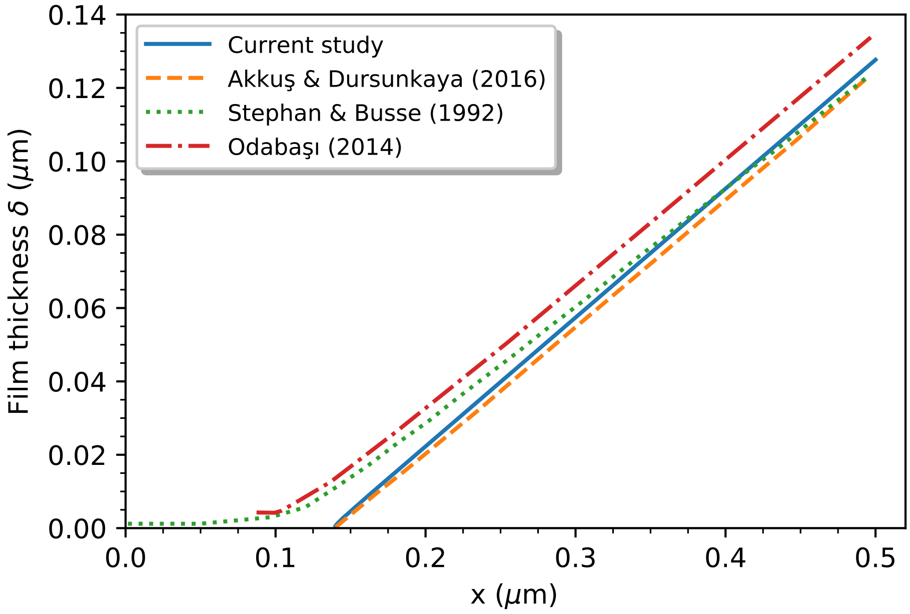


Figure 2.5: Comparison of film thickness variations in micro-region

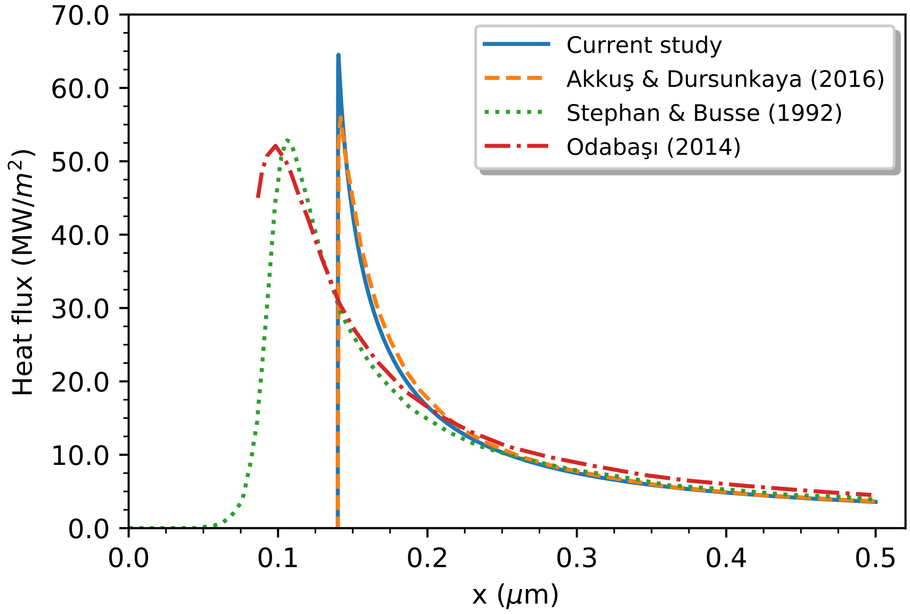


Figure 2.6: Comparison of heat flux variations in micro-region

### 2.2.2 Condensation Model

Contrary to evaporation, condensation is a process when vapor becomes liquid. Condensation mainly occurs on the fin top in grooved heat pipes where the wall temperature value decreases below the vapor saturation temperature. Modeling condensation plays a vital role during modeling of heat pipes. At the condenser section of the heat pipes, fluid attaches and forms a thin film on the fin top. The film thickness variation on the fin top is not known *a priori* and obtaining the film thickness variation can be a challenging process. There are various approaches to find film thickness variation during the condensation in the literature. Jiao et al. (2005) kept film thickness constant along the fin top. Kamotani (1976) assumed a $4^{th}$ order profile for the film thickness. Zhang and Faghri (2001) obtained film thickness with the Volume of Fluid (VOF) method. Lefèvre et al. (2008) developed an hydrodynamic model to predict the film thickness. Authors divided the fin top into several sections and wrote the mass, momentum and energy balance equations each of those sections.

Kamotani (1976) modeled condensation inside the axially rectangular grooved heat pipe to find the steady state thermal behavior under laminar and incompressible flow assumptions. Author divided the fin into 2 regions as flat and round corner regions. $4^{th}$ order profile for the film thickness variation in the flat region is assumed. It was concluded that shape of the fin top and radius of curvature effects the condensation rate. Author computed the overall heat transfer coefficient and observed that the results are aligned with the experimental data.

Zhang and Faghri (2001) studied condensation in a grooved channel with a different approach called Volume of Fluid (VOF) method. Continuity, momentum, energy and VOF equations for liquid and vapor phases and additional source terms of each equation to model phase change are written. From the results, it was concluded that condensation mainly occurs on the fin top due to very thin-film thickness compared to large thickness value in the meniscus region. Authors compared their study with the other approaches in literature (Khrustalev and Faghri, 1994b) and found out that convection effects can be neglected during the determination of film thickness on the fin top.

Lefèvre et al. (2008) modeled flat plate heat pipe with rectangular channels. Authors used nodal thermal model based on resistances. The heat pipe was divided into many sections and calculated wall temperature distribution and radius of curvature variation. In part of that study condensation model was generated. Authors emphasized that heat transfer because of condensation took place on fin top as compared with the grooves due to the fact that thermal resistance of the liquid is higher than the thermal resistance of the fins. Authors also developed a hydrodynamic model to find the liquid film thickness variation on the fin top. In the model, a steady state flow and one dimensional velocity and liquid film thickness along the fin top were assumed. The condensation inside the grooves was neglected in their study. Due to the large vapor volume, the shear stress at the liquid-vapor interface was neglected to obtain pressure distribution on the fin top as well.

In the scope of current study, it is aimed to develop a simple but realistic condensation model to predict characteristics of grooved heat pipe. Since Kamotani (1976) results are aligned with the experimental data, $4^{th}$ order film thickness profile assumption is adopted to predict total condensation mass flux on the fin top. Illustration of the condensation phenomenon in a flat grooved heat pipe is depicted in Figure 2.7

$4^{th}$ order profile for the film thickness variation of liquid profile on the fin top is given with the following formula;

$$\delta = c_0 + c_1(x-w) + c_2(x-w)^2 + c_3(x-w)^3 + c_4(x-w)^4 \tag{2.19}$$

The boundary conditions for the condensation on fin top is;

$$x = 0 \Rightarrow \delta'(x) = 0 \tag{2.19a}$$

$$x = w \Rightarrow \delta'(x) = -\tan(\pi/2 - \theta) \tag{2.19b}$$

$$x = w \Rightarrow \delta''(x) = 0 \tag{2.19c}$$

$$x = 0 \Rightarrow \delta'''(x) = 0 \tag{2.19d}$$

Using boundary conditions (2.19a-2.19d), coefficients in the equation 2.19 can

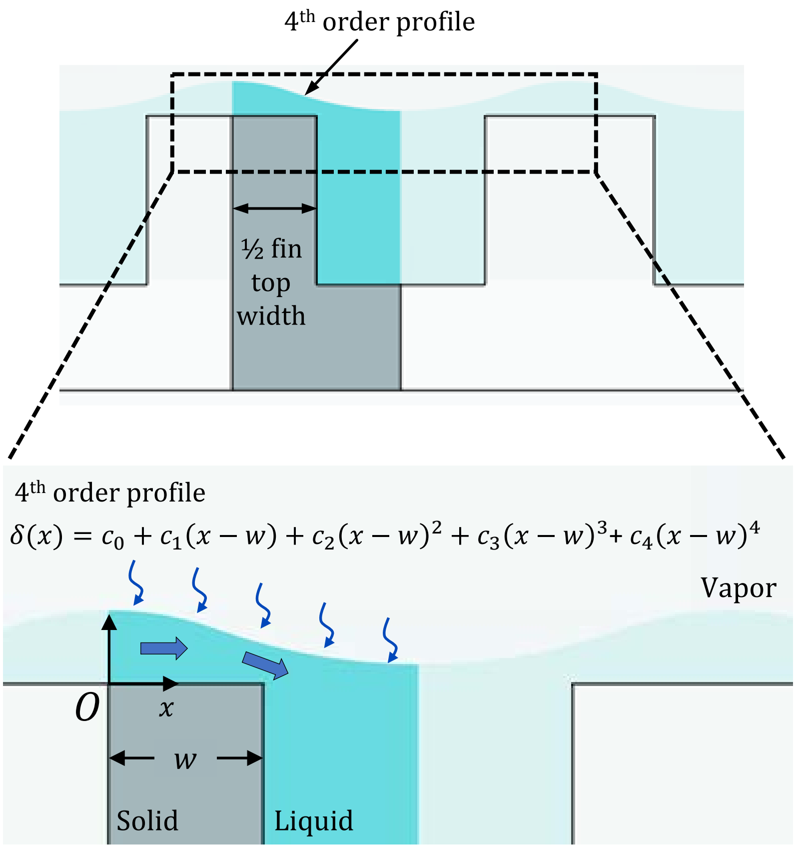


Figure 2.7: Illustration of the condensation phenomenon

be calculated as;

$$c_1 = -\tan(\pi/2 - \theta) \tag{2.19e}$$

$$c_2 = 0 \tag{2.19f}$$

$$c_3 = -c_1/2w^2 \tag{2.19g}$$

$$c_4 = -c_1/8w^3 \tag{2.19h}$$

Similar to evaporation, condensation is modeled with the kinetic theory. Since the liquid is too thick to influence from the wall, disjoining effect is neglected. Vapor pressure is balanced with liquid and capillary pressures. Due to kinetic theory Equation 2.17 can be simplified as;

$$\frac{d}{dx}\left[-\frac{\delta^3}{3\upsilon}\left(-\frac{\sigma\delta_x}{(1+\delta_x^2)^{3/2}} + \frac{3\sigma\delta_x\delta_{xx}^2}{(1+\delta_x^2)^{5/2}}\right)\right] = \frac{a\,(T_w - T_v)\, +\, b\,(P_l - P_v)}{1 + a\,\delta\, h_{fg}/k_l} \tag{2.20}$$

Equation 2.20 is integrated along the fin top (from 0 to $w$) after film thickness and its derivatives are substituted into left side of equation. Resulting integral can be solved numerically using the secant method with 2 initial estimates of film thickness at the edge of the fin top, $c_0$, values.

2 different cases in the literature are selected to validate the developed condensation model. As a part of the validation, film thickness and local heat flux variations on the fin top are plotted. Physical properties of working fluids and dimensions of the channel used in validation cases are given in Table 2.2.

Table 2.2: Physical properties of working fluid used in validation studies of condensation model

| **Property** | **Symbol** | **Value (Case-1)** | **Value (Case-2)** |
|---|---|---|---|
| Wall temperature [K] | $T_w$ | 363 | 340.5; 342.9 |
| Vapor temperature [K] | $T_v$ | 373 | 343.15 |
| Vapor pressure [Pa] | $P_v$ | $1.033 \times 10^5$ | $1.31 \times 10^5$ |
| Surface tension [N/m] | $\sigma$ | 0.0589 | 0.0185 |
| Liquid density [kg/m$^3$] | $\rho$ | 1000 | 792 |
| Latent heat of evaporation [J/kg] | $h_{fg}$ | $2.3 \times 10^6$ | $1.085 \times 10^6$ |
| Liquid thermal cond. [W/m . K] | $k_l$ | 0.6 | 0.2 |
| Dynamic viscosity of liquid [Pa . s] | $\mu$ | $2.79 \times 10^{-4}$ | $3.14 \times 10^{-4}$ |
| Molar mass of liquid [kg/mol] | $m$ | $18 \times 10^{-3}$ | $32 \times 10^{-3}$ |
| Molar volume of liquid [m$^3$/mol] | $V_l$ | $18 \times 10^{-6}$ | $42 \times 10^{-6}$ |
| Accomodation coefficient [-] | $c$ | 1 | 0.139 |
| $\frac{1}{2}$ fin top width [$\mu$m] | $w$ | 20 | 200 |
| Meniscus angle [deg] | $\theta$ | 84; 88 | 77.1; 80.2 |

Water is selected as working fluid for the validation case-1. Effect of the meniscus curvature is investigated for 10 K superheat. Liquid film thickness variation and local heat flux distribution obtained from the developed condensation model are compared with the corresponding values of (Zhang and Faghri, 2001) in Figure 2.8.

From the Figure 2.8, it is observed that the film thickness value is maximum in the middle of the fin top and reaches its minimum value at the edge of the fin top. Thinner film thickness yields more local heat flux, which means local heat flux value is proportional to film thickness and reaches its maximum value at the edge of the fin top. Comparing the results obtained from the 2 different meniscus angles, it can be concluded that film thickness value increases with the meniscus angle; on the other hand, the local heat flux value (accordingly condensation rate) shows a decreasing trend with the same parameter.

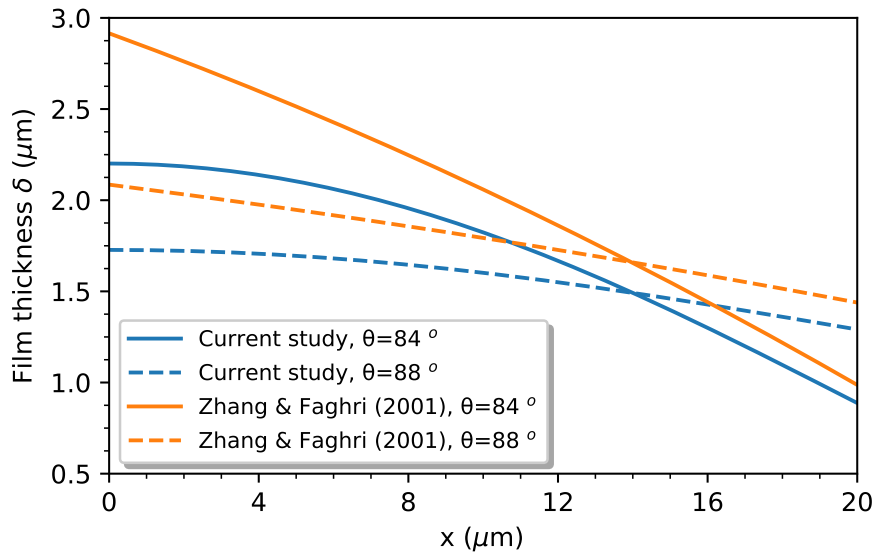


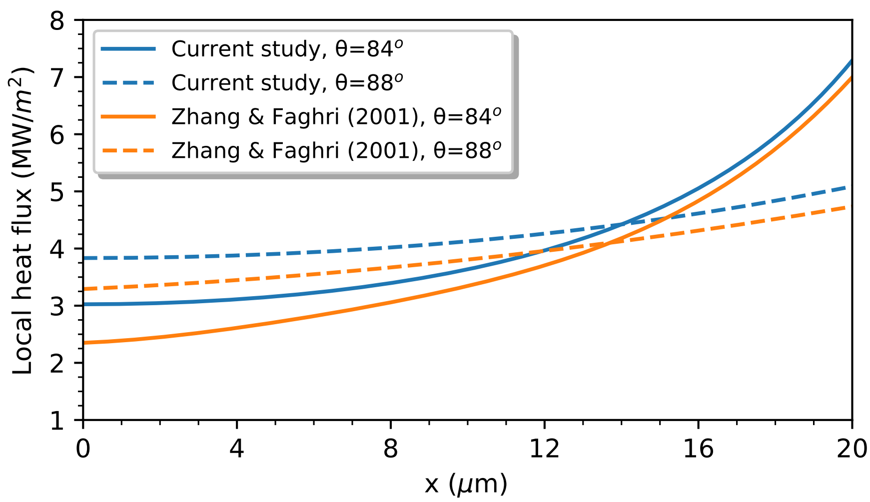


Figure 2.8: Liquid film thickness variation and local heat flux distribution for validation case-1

Methanol is selected as working fluid for the validation case-2. In this study, liquid film variations for different positions inside the condenser section of a grooved heat pipe are plotted. Film thickness variations obtained from the developed condensation model and Lefèvre et al. (2008) at 2 different positions are compared in Figure 2.9. z/L=0 indicates the end of the channel (evaporator side) and z/L=1 indicates beginning of the condenser section.

Investigating the Figure 2.9, it is observed that the film thickness variation along the fin top shows similar trend with the results of validation case-1. From the middle of the fin top to the edge, the film thickness value decreases.

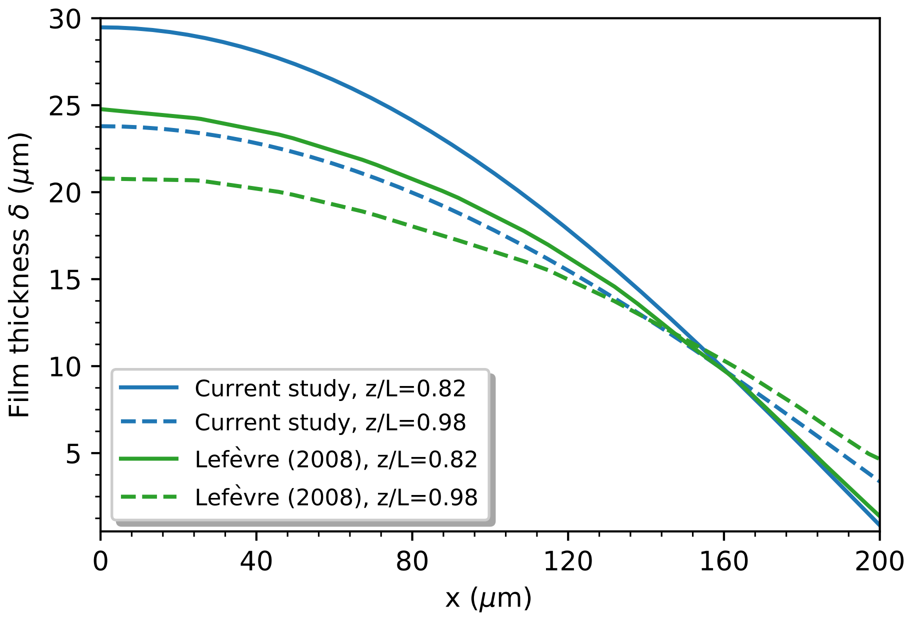


Figure 2.9: Liquid film thickness variations for the current study and validation case-2 for the different axial positions

Comparisons showed that results are in good agreement with other approaches. Therefore, developed model can be used to predict the heat transfer characteristics of grooved heat pipes.

## 2.3 1-D Modeling of Grooved Heat Pipes

In this section, simplified 1-D model of a grooved heat pipe are constructed and the predictions of the temperature variations are put forward to assess the validity of the 1-D model.

Energy balance at an arbitrary cross-section of a heat pipe can be represented by the concept of thermal resistances. Since evaporation and condensation are phenomena that affect the heat transfer differently, their representations should be handled separately. Hence, the heat pipe is divided into two sections as the evaporator and condenser. Models of the thermal resistances for evaporator and condenser are shown in Figure 2.10

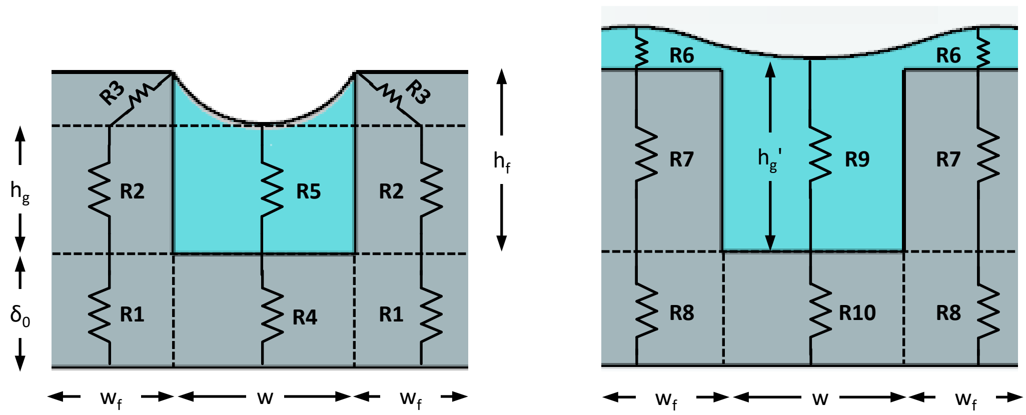


Figure 2.10: Thermal resistance circuits evaporator (left) and condenser (right) sections

The difference in evaporation and condensation models arises from the micro evaporation and fin top condensation. Micro evaporation is represented by the resistance R3, and fin top condensation is represented by the resistance R6. Since the 1-D model does not take into account axial conduction, the adiabatic section is not modeled.

Thermal resistances in Figure 2.10 can be expressed in the following equations;

$$R_1 = \frac{\delta_0}{k_s W_f L_e}, \qquad R_2 = \frac{h_g}{k_s W_f L_e}, \qquad R_3 = \frac{1}{\alpha_{film}(h_f - h_g) L_e} \tag{2.21a}$$

$$R_4 = \frac{\delta_0}{k_s W L_e}, \qquad R_5 = \frac{h_g}{k_l W L_e}, \qquad R_6 = \frac{\delta_{film}}{k_l W_f L_c} \tag{2.21b}$$

$$R_7 = \frac{h_f}{k_s W_f L_c}, \qquad R_8 = \frac{\delta_0}{k_s W_f L_c}, \qquad R_9 = \frac{h'_g}{k_l W L_c} \tag{2.21c}$$

$$R_{10} = \frac{\delta_0}{k_s W L_c} \tag{2.21d}$$

where, $k_s$ is thermal conductivity of the solid, $k_l$ the thermal conductivity of the liquid, $\delta_{film}$ is the mean condensate liquid film thickness at the fin top, $L_e$ and $L_c$ are the lengths of condenser and evaporator sections and $\alpha_{film}$ is the evaporating thin-film heat transfer coefficient and expressed in a correlation given in Zhang et al. (2009) as,

$$\alpha_{film} = \frac{k_l}{0.185 W_f} \tag{2.22}$$

Total resistance at the evaporator is,

$$R_e = \frac{1}{N}\left[\frac{(R_1 + R_2 + R_3)(R_4 + R_5)}{R_1 + R_2 + R_3 + 2(R_4 + R_5)}\right] \tag{2.23}$$

where N is the total number of grooves.

Total resistance at the condenser is,

$$R_c = \frac{1}{N}\left[\frac{(R_6 + R_7 + R_8)(R_9 + R_{10})}{R_6 + R_7 + R_8 + 2(R_9 + R_{10})}\right] \tag{2.24}$$

and the resistance due to vapor flow is given as,

$$R_v = \frac{T_v(P_{v,e} - P_{v,c})}{\rho_v h_{fg} Q_{in}} \tag{2.25}$$

where, $T_v$ is the saturation temperature, $P_{v,e}$ and $P_{v,c}$ are vapor pressures at the evaporator and condenser section, $\rho_v$ is the density of the vapor, $h_{fg}$ is the latent heat of the working fluid and $Q_{in}$ is the heat transferred to the heat pipe. In (Lefèvre et al., 2008), it is shown experimentally that when the phase change occurs interfacial stress at the liquid-vapor interface can be neglected when the volume of the vapor is large. Therefore, vapor resistance is neglected in this study.

The total thermal resistance, $R_{tot}$ is,

$$R_{tot} = R_e + R_c \tag{2.26}$$

The temperature difference between the two ends of the heat pipe can be found through,

$$\Delta T = Q_{in} R_{tot} \tag{2.27}$$

The resistance R3, which is used to model micro evaporation, is expressed in the 1-D model over the length of $(h_f - h_g)$ in (Zhang et al., 2009). However, micro condensation occurs in a small region around the vicinity of the wall (~10 µm), and this region is simulated in the 3-D model developed in the current study. Considering this fact, and accounting for the difference between the corresponding heat transfer areas of Zhang et al. (2009) and the current 3-D model, the constant equal to 0.185 is recalculated to be in the range of 0.020 – 0.025, and the thin-film heat transfer coefficient, $\alpha_{film}$, becomes approximately,

$$\frac{k_l}{0.025 W_f} < \alpha_{film} < \frac{k_l}{0.02 W_f} \tag{2.28}$$

It should be noted that 1-D model does not take into account either axial conduction or the meniscus curvature variation (free surface flow) along the channel. Therefore, a 3-D model including the fluid domain is necessary to predict the temperature variation on the heat pipe.

## 2.4 Development of Physical Based CFD Models

In this section, two important steps of the automated solution algorithm expressed in Section 2.1 are explained in detail; predicting the in-groove flow field and calculation of temperature distribution for the entire heat pipe. Computational Fluid Dynamics (CFD) methodology is employed for determination of the flow field and heat transfer phenomena.

The main idea behind the computational fluid dynamics (CFD) is to produce quantitative predictions of fluid flow, heat and mass transfer phenomena. Differential equations of phenomenological laws such as; continuity, Navier-Stokes and energy equations are discretized over the solution domain after that resulting set of algebraic equations are solved numerically using various algorithms.

CFD procedure consists of three fundamental stages; pre-processing; in which the geometry of the solution domain is generated and divided into small segments known as mesh. Boundary conditions and materials are also assigned in this stage. Solution; the step in which the proper numerical technique is selected to solve conservation equations in accordance with the physics behind the phenomena. Post processing; the results such as vectors, contours, streamlines etc. are provided.

CFD solution stages are applied to one channel of a flat grooved heat pipe. The study (Lefèvre et al., 2008) which is selected for the validation of developed automated solution methodology. The details are provided in the following subsections.

### 2.4.1 Geometry Generation and Physical Properties of Materials

First stage of the CFD solution procedure is preparing a Computer Aided Design (CAD) model for the domain of interest. Schematic view of a rectangular grooved heat pipe selected for the validation study and its main dimensions are demonstrated in Figure 2.11. Since the channels are symmetric and equally distributed along the lateral direction in periodic manner, only half of one channel is modeled and investigated. Building a parametric CAD model is crucial and beneficial to handle the necessity for generation of the liquid-vapor interface shape for each iteration also for the assessment of distinct geometric effects such as channel length, height and width. Preparing a parametric CAD model allows researchers to alter their geometry and explore the different alternatives in a systematic way. Parameterization can be made very effectively by defining dimensions that govern the model and creating relations (constraints) through geometric features. When the dimension or geometric feature is changed, the new model is automatically regenerated. The most challenging issue of parametric modeling is maintaining consistency of the CAD model. Sketch relations and constraints must be properly defined because missing or wrong definitions may yield a physically invalid model. Therefore, 3-D parametric CAD models of flat grooved heat pipes are generated in Siemens NX 12.

The channel is divided into several sections in longitudinal direction to define relevant boundary conditions which are varying with space i.e. phase change mass flow rates and heat transfer coefficients. At each section, meniscus curvature radius values are parameterised and their initial estimates are assigned. Then, liquid-vapor interface is split near the vicinity of the wall to generate micro-region where some of the boundary conditions are defined. Bottom face of the model is also divided into sections to define heat source and heat sink.

Solid and liquid bodies are grouped to obtain shared topology which is required for conformal mesh where the different bodies meet. Shared topology is important to ensure the mesh quality at the intersection of different bodies. Parametric model is sent to ANSYS-Workbench environment directly from the CAD program for discretization of the solution domain.

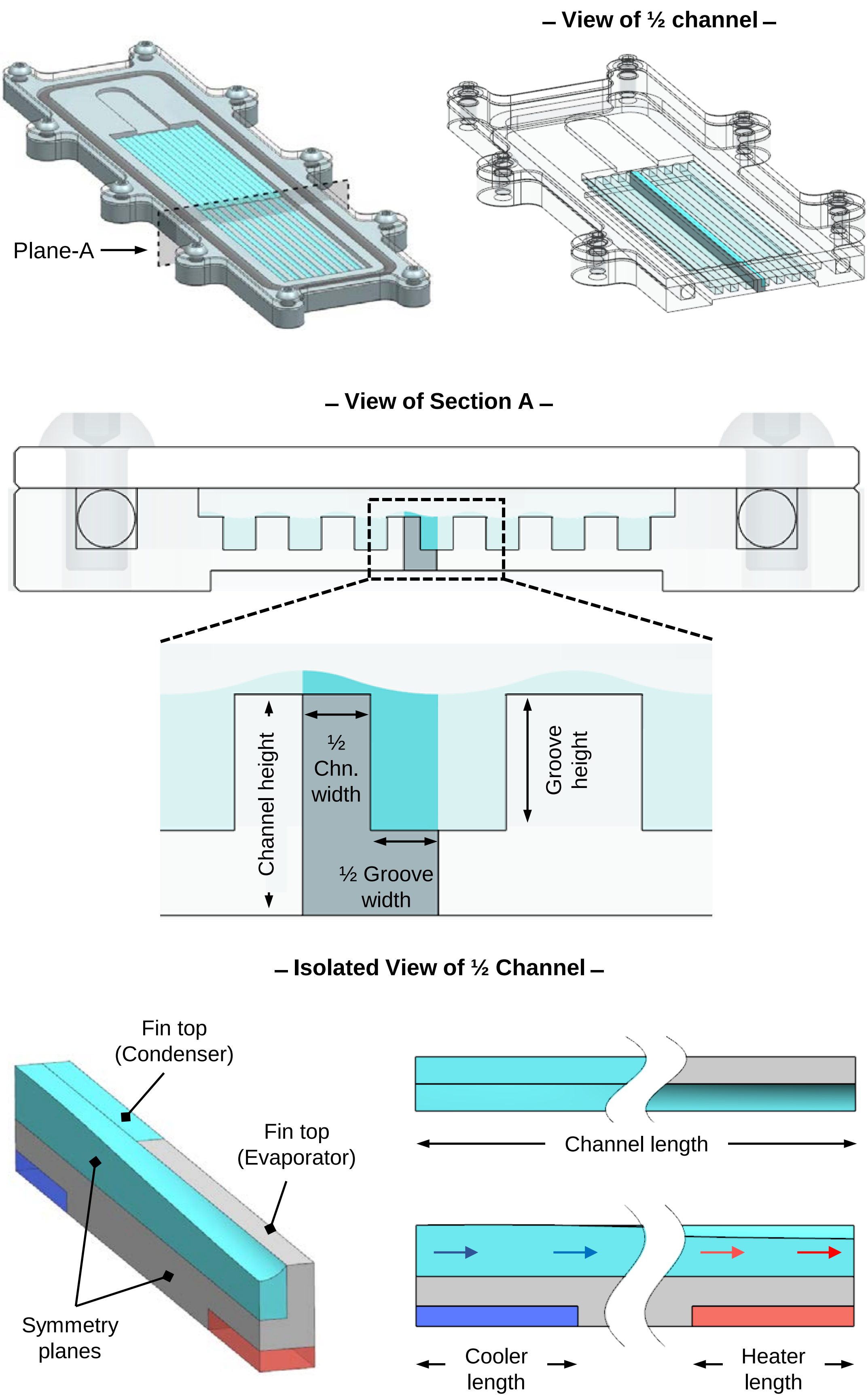


Figure 2.11: Heat pipe and its dimensions

CAD generation is implemented to the mathematical model via a Python script. Utilizing the script, heat pipe model is generated from a Graphical User Interface (GUI) without opening the CAD program in foreground (it is run in batch mode). Following this methodology, substantial amount of solution time is saved.

Next step in the CFD procedure is the material assignment. Generic material model is created in Fluent environment and material properties such as density, viscosity, thermal conductivity of the working fluid are defined parametrically and controlled via Python script. In (Lefèvre et al., 2008) the channel is made from copper, and methanol is selected as working fluid. Main dimensions of the model, operating conditions, physical properties of the working fluid and channel material are provided in Table 2.3.

Table 2.3: Main dimensions of the groove geometry, operating conditions, physical properties of the working fluid and channel material

| **Property** | **Symbol** | **Value** |
|---|---|---|
| Height of the channel [mm] | $H_c$ | 0.38 |
| Height of the pipe [mm] | $H_p$ | 2.38 |
| Length of the pipe [mm] | $L_p$ | 230 |
| 1/2 Groove width [mm] | $w_g$ | 0.2 |
| 1/2 Pipe width [mm] | $w_c$ | 0.4 |
| Length of the cooler [mm] | $L_c$ | 30 |
| Length of the heater [mm] | $L_h$ | 190 |
| Thermal conductivity of solid [W/m . K] | $k_s$ | 400 |
| Heat load (flux) [W/m$^2$] | $q$ | 5000 |
| Sink heat transfer coeff. [W/m$^2$ . K] | $h_{amb}$ | 2100 |
| Sink temperature [°C] | $T_{amb}$ | 51 |
| Dynamic viscosity of liquid [Pa . s] | $\mu$ | 0.00013 |
| Thermal conductivity of liquid [W/m . K] | $k_l$ | 0.2 |
| Surface tension [N/m] | $\sigma$ | 0.01846 |
| Molar mass of liquid [kg/mol] | $m$ | 0.0173 |
| Molar volume of liquid [m$^3$/mol] | $V_l$ | $2.88 \times 10^{-5}$ |
| Accomodation coefficient [-] | $c$ | 0.139 |

**Table 2.3 continued from previous page**

| Property | Symbol | Value |
|---|---|---|
| Dispersion constant [-] | $A_d$ | $2 \times 10^{-21}$ |
| Vapor pressure [Pa] | $P_v$ | 106000 |
| Latent heat of evaporation [J/kg] | $h_{fg}$ | 1085000 |

### 2.4.2 Discretization of the Solution Domain (Mesh Generation)

Discretization of the solution domain is another important stage of the CFD solution. In this stage, solution domain is divided into small regions called control volumes or cells. The conservation equations based on phenomenological laws are solved in these control volumes.

There are vital issues must be taken into consideration while generating mesh for the solution domain. Mesh quality has a strong effect on the accuracy of the simulation. If bad elements exist in the solution domain, simulation may diverge due to these low quality elements. Meshing method should be properly selected in accordance with the application moreover, number of elements must be sufficient enough to capture the gradients (i.e. velocity, pressure and temperature). Furthermore, in the regions where large gradients (i.e. pressure, velocity or temperature), separation, vortex or flow reversal occur, extra care should be taken and the grid should be refined locally especially around these areas.

Design of the groove model (constant cross-section along the longitudinal direction and high aspect ratio) provides a flow-aligned geometry. Fluid flow due to capillary action is almost unidirectional inside the groove which makes the model convenient to employ the sweep mesh method. For this reason, sweep mesh algorithm is preferred and the solution domain is filled with hexahedral elements. Solution domain is divided into three regions (2 solid regions + 1 fluid region) to improve element quality and reduce the number of elements. Shared topology is set in all domains to achieve a conformal mesh between adjacent bodies that coincide.

If the selected mesh size is sufficient and mesh distribution is suitable enough for the investigated model, results would not change even if number of elements is increased. The results which is obtained by using that sufficient mesh size is called the mesh independent solution.

Starting from coarser grid size, several analysis are performed by refining element size and taking mesh metrics (i.e. orthogonal quality and aspect ratio) into consideration to achieve a mesh-independent solution. It was mentioned in the previous section that two distinct CFD models are built in scope of the automated solution procedure; First model is prepared to model in-groove flow and with another model temperature distribution over the entire domain can be predicted. Approximately 712.000 elements, 780.000 nodes exist in the first model whereas the second model consist of a larger number of elements (approximately 1.380.000 elements, 1.500.000 nodes).

Analyses performed with different number of elements to obtain a mesh-independent solution is depicted in Figure 2.12. Pressure drop along the groove and vapor saturation temperature values are selected to control mesh-independence. Mesh settings employed for the number of elements which are shown inside the dashed rectangle can be utilized to assess the validity of the developed solution methodology and further parametric analyses.

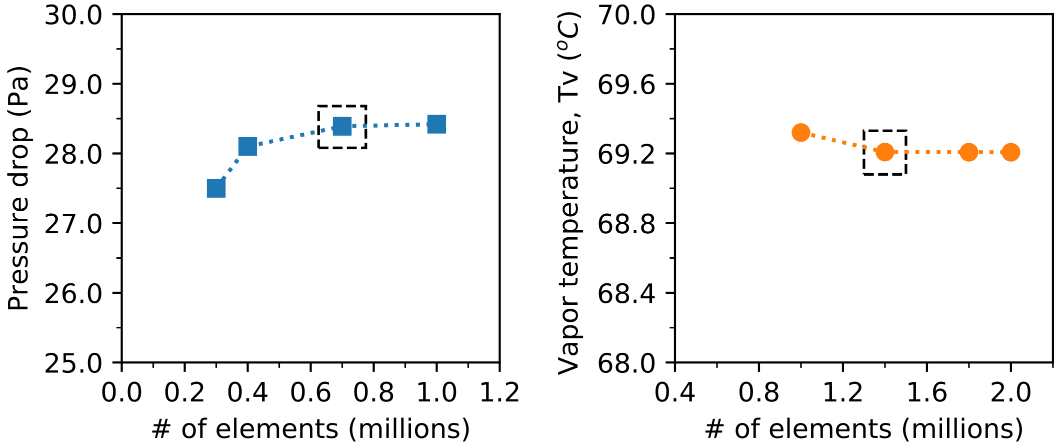


Figure 2.12: Various case studies to find optimum mesh

Obtained optimum grids for the validation case is shown in Figure 2.13. Grid structures belong to heat transfer and flow models are depicted in left and right of the figure respectively. In the second model, mesh is refined along the vicinity of the wall due to occurrence of high gradients and grid size getting coarser near the symmetry plane.

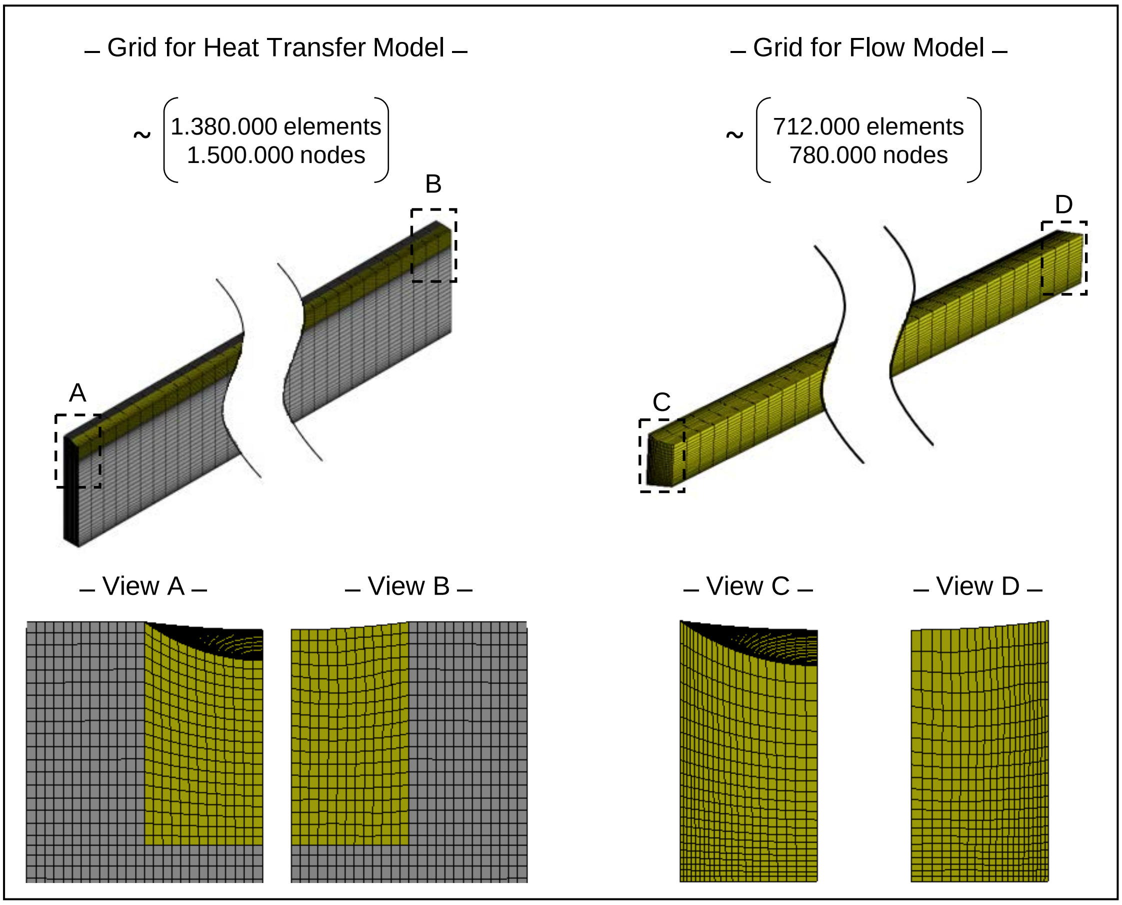


Figure 2.13: Optimum mesh for the validation case

### 2.4.3 Boundary Conditions and Solution Scheme

After the mesh generation, relevant boundary conditions can be assigned to the prepared CFD models. Determination of the boundary conditions is one of the challenging parts of CFD solution procedure. Boundary conditions must be selected in accordance with physical phenomena because improper assignments may not reflect the real situation and may yield inaccurate results.

It was mentioned in the previous section that in-scope of the automated solution procedure, two distinct CFD models were prepared to reveal in-groove flow and heat transfer characteristics. CFD models are built based on the same geometry but subjected to different boundary conditions.

To accurately predict the flow and heat transfer characteristics of a grooved heat pipe, one channel is divided into several sections (100 for validation case) along the longitudinal direction to include varying effect of the phase-change phenomenon. Evaporation and condensation mass flow rate values and the phase-change heat transfer rates are not constant. Because mentioned parameters are strong functions of both temperature and interface shape.

The boundary conditions employed for the flow and heat transfer models are written in red and blue respectively in Figure 2.15. Focusing on the flow model; small region (has a thickness 10-20 $\mu$m in lateral direction) around the vicinity of the wall is created on the fluid-vapor interface to define phase-change mass flow into or out of the system. Zero shear stress (free slip condition) is assumed on the interface since Rullière et al. (2007) indicated that interfacial shear stress has a negligible effect on the results. Since the model is symetric to the $y-z$ plane, symmetry boundary condition is assigned to surfaces that lies in the $y-z$ plane. Micro evaporation and condensation mass flow rates are considered in accordance with the calculation method expressed in section 2.2. On the other hand, to take into account phase-change from the macro region, amount of heat is transferred obtained from the macro-region is utilized. Heat transfer from the macro region can be expressed as;

$$\dot{q}_{macro} = \dot{m}_{macro} \times h_{fg} \tag{2.29}$$

Total mass transfer through the phase-change can be calculated as;

$$\dot{m}_{total} = \dot{m}_{micro} + \dot{m}_{macro} \tag{2.30}$$

At the interface and symmetry plane, the normal component of velocity and shear stress are set to zero.

$$\overrightarrow{V} \cdot \overrightarrow{N} = 0 \quad \& \quad \tau_{ij} = 0 \tag{2.31}$$

Variable phase-change mass flow rates can be defined along the groove with 2.32. If condensation occurs ($T_w < T_v$), liquid is supplied to the system unlike the case of evaporation.

$$\dot{m}(z) = \dot{m}_{total}(z) \quad \text{at} \quad 0 < z < L; \quad x_{micro} < x < 0; \quad y_{micro} < y < H_c \tag{2.32}$$

It was mentioned in section 2.1 that until the convergence the global mass balance (difference between evaporated and condensed amounts) may not be satisfied. It means that in interval steps mass conservation inside the groove are not satisfied. CFD model would not converge in this circumstance. Moreover, for the solution of CFD at least one pressure boundary condition must be applied to the system along with the mass flow rate boundary condition. To address this issue pressure boundary condition is applied to the first segment of the interface ($z = 0$). With this definition excess or insufficient amount of fluid would be compensated by the CFD solution at each iteration.

In the heat transfer model, solid domain is also included to the solution. Similar to the flow model, heat transfer via phase-change occurred in the micro-region is considered in accordance with the calculation method expressed in section 2.2. The phase-change heat transfer is added to the CFD model with convection boundary condition ($h_{pc}$) which is assigned to the fin top (for the condenser part of the groove, because liquid film resides on the fin top) or the micro-region on the liquid-vapor interface (for the evaporator part, no fluid on the fin top therefore fin top is assumed to be adiabatic)

$$\begin{aligned} q_{pc}(z) = h_{pc}(z)\,[T_v - Tw(z)] \quad \text{at} \quad 0 < z < L\,; & \qquad\qquad\qquad (2.33) \\ T_w(z) < T_v \quad \rightarrow \quad x_{micro} < x < 0\,; \qquad y_{micro} < y < H_c & \\ T_w(z) > T_v \quad \rightarrow \quad 0 < x < w_{fintop}\,; \qquad y_{micro} < y < H_c & \end{aligned}$$

Vapor temperature is assumed to be a constant during the phase-change. Therefore, constant temperature boundary condition is assigned to the liquid-vapor interface.

$$T = T_v \quad \text{at liquid-vapor interface} \tag{2.34}$$

Heat source and heat sink is simulated via constant heat flux and convective heat transfer coefficient respectively.

$$\begin{aligned} q &= q_{heater}\,; \quad \text{at} \quad L_{heater} < z < L_{groove} \\ q_{sink} &= h_{env}(T - T_{env})\,; \quad \text{at} \quad 0 < z < L_{sink} \end{aligned} \tag{2.35}$$

In validation study, thermal load is given as 5000 W/m$^2$. It is assumed that heat is transferred from the heat sink to the environment with the rate of 2100 W/m$^2$.K and ambient temperature is kept at 324.2 K. All of the other surfaces which are not mentioned are assumed as adiabatic.

The continuity, momentum and energy equations are solved in the Fluent. The conservative form of the mentioned equations are written for the Cartesian coordinate system;

The continuity equation;

$$\frac{\partial \rho}{\partial t} + \nabla \cdot (\rho \overrightarrow{V}) = S_m \tag{2.36}$$

Momentum equation;

$$\frac{\partial}{\partial t}(\rho \overrightarrow{V}) + \nabla \cdot (\rho \overrightarrow{V} \overrightarrow{V}) = -\nabla P + \nabla \cdot (\overline{\overline{\tau}}) + \overrightarrow{F} \tag{2.37}$$

$\overrightarrow{F}$ represents the external body forces and $\overline{\overline{\tau}}$, is the stress tensor. It can be expressed as;

$$\overline{\overline{\tau}} = \mu \left[ \left( \nabla \overrightarrow{V} + \nabla \overrightarrow{V}^T \right) - \frac{2}{3} \nabla \cdot \overrightarrow{V} I \right] \tag{2.38}$$

Energy equation;

$$\frac{\partial}{\partial t} (\rho E) + \nabla \cdot \left[ \overrightarrow{V} (\rho E + P) \right] = \nabla \cdot \left[ k_{eff} \nabla T - \sum_j h_j \overrightarrow{J}_j + \left( \overline{\overline{\tau}}_{eff} \cdot \overrightarrow{V} \right) \right] + S_h \tag{2.39}$$

Where $\overrightarrow{J}_j$ is the diffusion flux of species $j$ and $k_{eff} = k + k_t$ is the effective thermal conductivity depend on turbulent thermal conductivity $k_t$.

During the operation of the heat pipes, relatively low liquid velocities are encountered in the grooves which makes the flow incompressible and laminar. Various solver preferences are available in Fluent to treat velocity-pressure coupling namely, SIMPLE, SIMPLEC, PISO and Coupled algorithms. First three algorithms are also known as segregated solution algorithms in which momentum and continuity equations are solved separately. If the coupled solution algorithm is employed, the continuity and momentum equations are solved in a fully coupled way. A single matrix equation is generated in which the dependent variable is a solution vector that combines the $x$, $y$, $z$ velocities and pressures. Coupled algorithm improves the rate of convergence and robustness. In Fluent theory guide (ANSYS, 2019), it is stated that results are independent from the utilized solution algorithm. Algorithm only effects the solution time and robustness.

Although analyses can be run faster with segregated solution methods, divergence is observed with the SIMPLE algorithm during the solution of in-groove flow model. To address this, pressure-based coupled solution algorithm is utilized to treat velocity-pressure coupling. Furthermore, $2^{nd}$ order upwind differencing scheme is adopted for the discretization of the convective term of momentum and energy equations.

It took approximately 8 hours to get a converged solution. Generally minimum 5 iterations are required for the convergence of the in-groove flow model to obtain the shape of the liquid-vapor interface (iteration i in Figure 2.3). More number of iterations (minimum 7) are required to get a converged wall temperatures(iteration j in Figure 2.3). To satisfy global mass balance, mentioned incremental steps are repeated for at least 5 times (iteration k in Figure 2.3). In total, at least 60 iterations are performed for the simulation of only one groove. The convergence behavior of the validation case is provided in Figure 2.14. Vapor saturation temperature and $f(Tv)$ which is employed for the indication of the global mass balance is checked. From the plots, it is concluded that secant method works perfectly for the solution methodology developed.

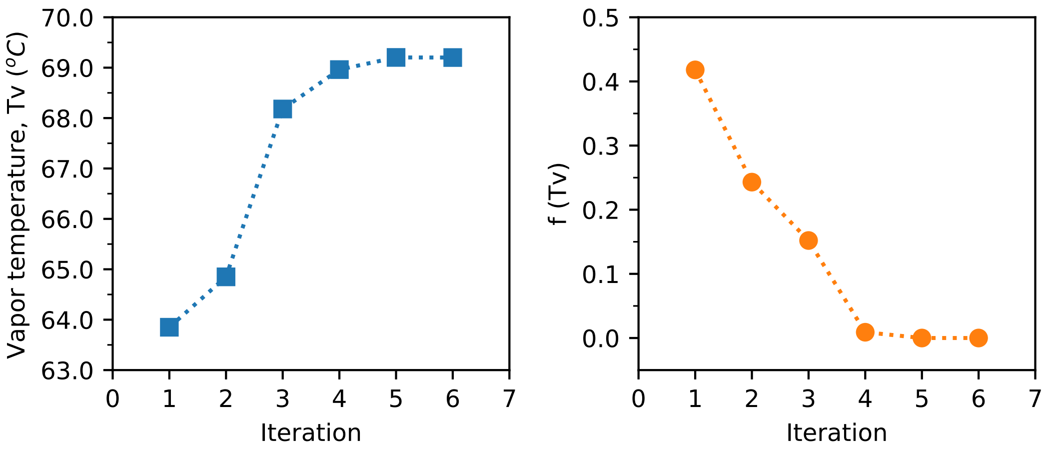


Figure 2.14: Convergence behavior of the validation case

The specifications of the utilized computer for analyses are provided in Table 2.4.

Table 2.4: Specifications of the computer used for the analyses

| Computer specifications | |
|---|---|
| CPU | Intel® Xeon® CPU E5-2620-v3 2.4 GHz |
| Memory | G8X33AV 64GB DDR4-2133MHz (4x16GB) |
| GPU | NVIDIA® Quadro® M4000 8GB 256Bit |

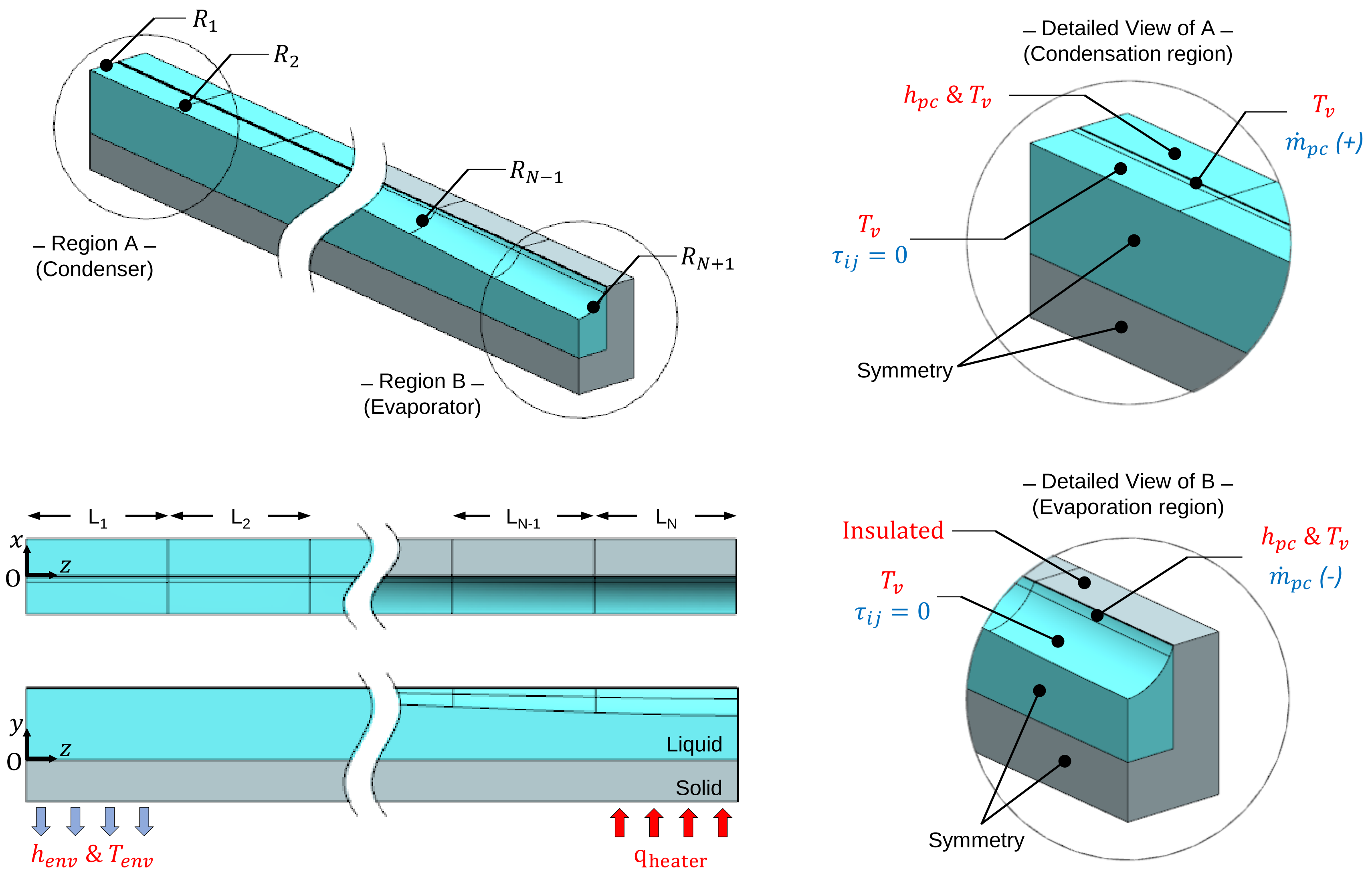


Figure 2.15: Boundary conditions

## 2.5 Results of the Validation Study

After solving sets of the incremental steps, the simulations have converged within defined convergence criteria. Data such as pressure variation, velocity profile inside the groove and temperature distribution is extracted and evaluated to gain insights to the heat transfer and fluid flow in a grooved heat pipe.

The shape of the liquid-vapor interface is usually obtained in 5–7 iterations. Employing the Young-Laplace equation (Equation 2.9) the interface shape is determined from the pressure variation along the groove. Pressure distribution of the converged solution is depicted in Figure 2.16.

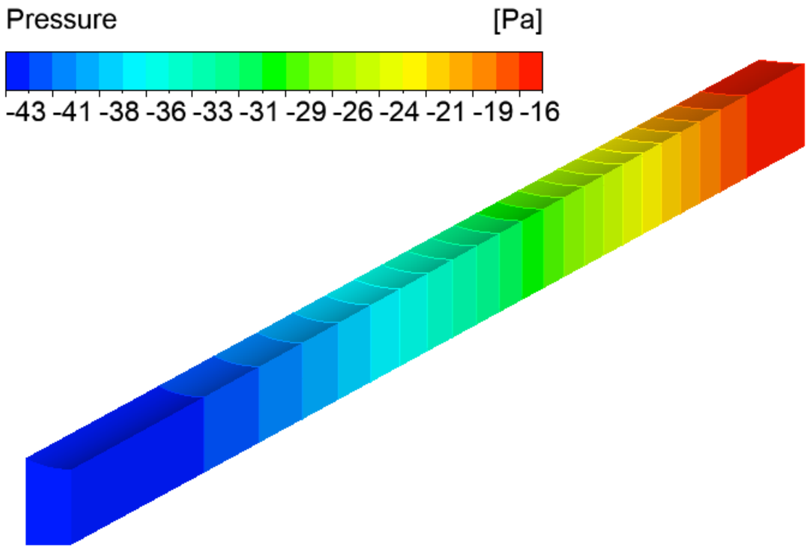


Figure 2.16: Pressure distribution along the channel

Due to the operating principle of heat pipes, starting from the condenser section of the groove, the amount of fluid inside the channel gradually increases because of the condensed liquid until the beginning of the evaporation section, where the value of wall temperature exceeds the vapor saturation temperature. After that point, evaporation occurs inside the rest of the liquid domain, and the liquid concentration inside the channel starts to decrease. This phenomenon can be observed from Figure 2.17 and Figure 2.18 in which the velocity variation along the groove is provided. From the figures it is observed that velocity is not uniform within the cross-section of the groove. Near the symmetry plane and liquid vapor-interface velocity magnitude reaches its maximum value.

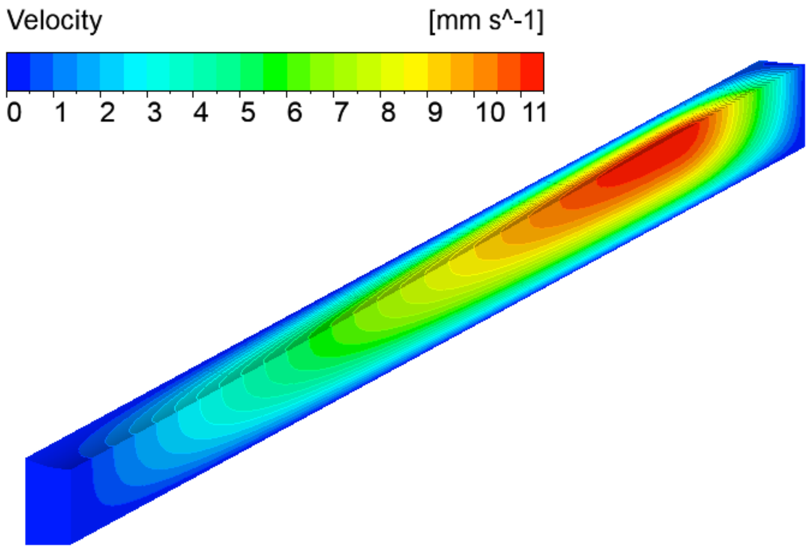


Figure 2.17: Velocity distribution along the channel

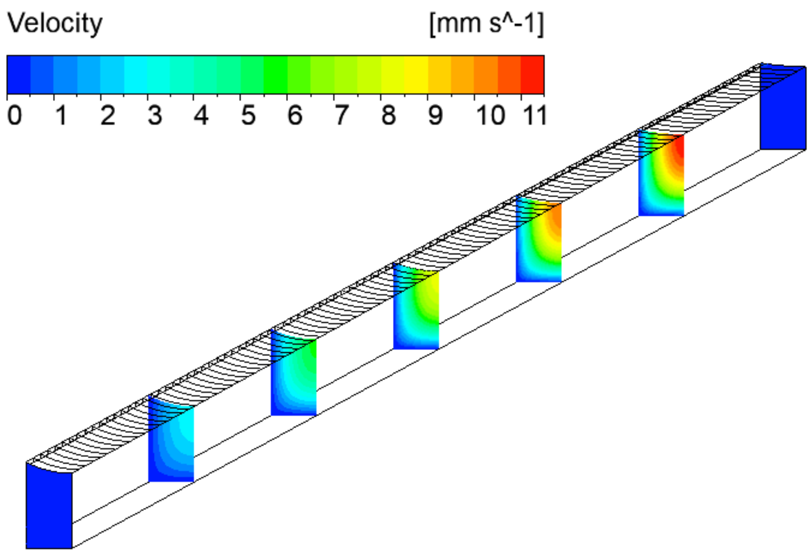


Figure 2.18: Velocity distribution at different sections along the channel

The situation mentioned in the previous paragraph can be observed more clearly if the mass flow rate variation along the groove is investigated. Rate of mass transferred due to the phase-change and instant total mass flow rate at each cross-section along the groove is plotted in Figure 2.19. From this figure it is seen that at the beginning of the condenser section, the mass flow rate inside the channel is zero as the phase-change occurs mass flow rate inside the channel increases until the evaporation region. Then decreases to zero again at the other end of the channel.

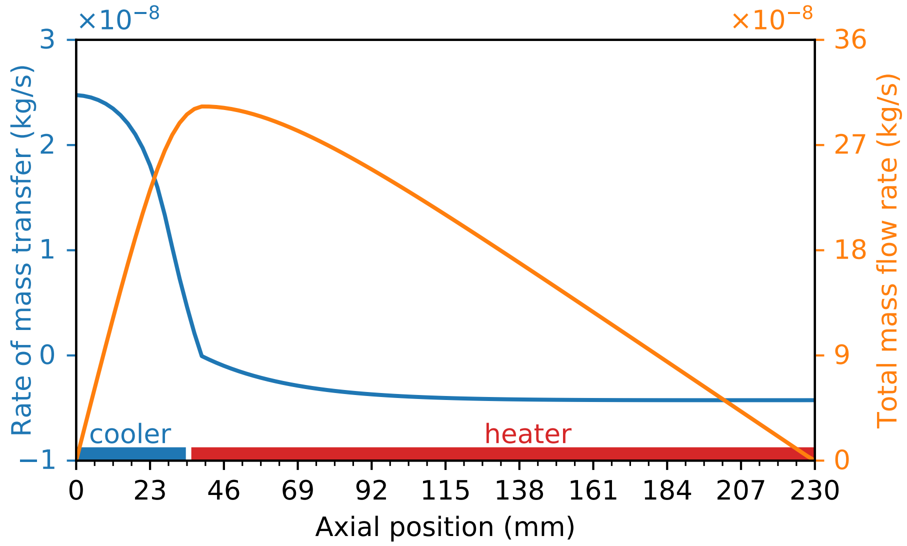


Figure 2.19: Mass flow rate contribution and total mass flow rate along the groove

Another parameter that can be useful during the investigation of the flow field is the streamlines. A streamline is a path traced out by a massless particle as it moves with the flow in steady-state conditions. Streamlines inside the flow field are plotted in Figure 2.20. Dead-zones are spotted at the bottom of the groove. Some of the streamlines can be seen as an indication of geometry revision. Dead-zones must be taken into consideration due to its negative effect on the flow field and heat transfer. Lessening the mixing has an undesirable influence on the uniformity of temperature distribution. Circular bottom shape of the groove may help to improve dead-zones and alteration of the geometry may influence the pressure drop along the groove positively. Mentioned improvements alone can provide an extra heat carrying capacity.

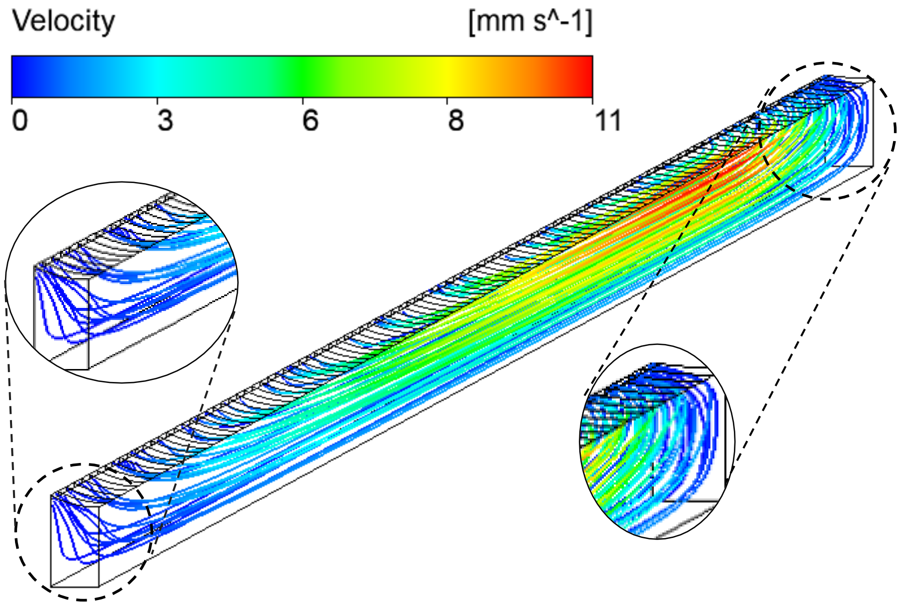


Figure 2.20: Streamlines and dead-zones along the channel

Radius of curvature variation along the groove which is an indication of the fluid-vapor interface shape is compared with the corresponding values of (Lefèvre et al., 2008 and Odabaşi, 2014). Meniscus curvature variations are plotted on the same graph in Figure 2.21.

There is no considerable difference observed between the results even when different methodologies are followed in the solution of flow field. Meniscus curvature variations are almost identical. In all studies the interfacial shear stress is not taken into account due to large volume of vapor. However, Lefèvre et al. (2008) and Odabaşi (2014) modeled the in-groove flow as 1-D and employed skin friction coefficients to calculate pressure drop along the groove. Odabaşi (2014) adopted Schneider and De Vos correlation (Schneider and Devos, 1980) whereas, Lefèvre et al. (2008) utilized Shah and London law (Faghri, 1995) to obtain the same parameter. On the other hand, the solution domain was treated as 3-D and pressure drop along the groove was calculated directly from the CFD software in the current study.

Obtaining similar results does not mean the 1-D solution of the flow field based on the skin-friction correlations would be adequate for all circumstances. 3-D modeling of the flow field may be useful for more complex geometries when no skin-friction correlation is available to calculate pressure drop or in the cases when 3-D effects are more important and become dominant such as groove models with low aspect ratio.

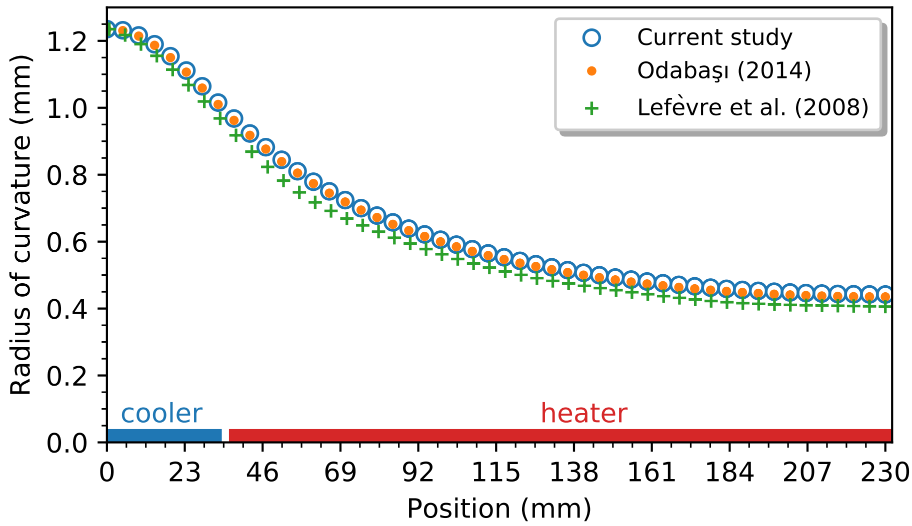


Figure 2.21: Meniscus curvature variation along the groove

After modeling the flow field, another part of the automated solution procedure is solving the heat transfer model to find temperature distribution of the heat pipe. Temperature field of the converged solution is depicted in Figure 2.22.

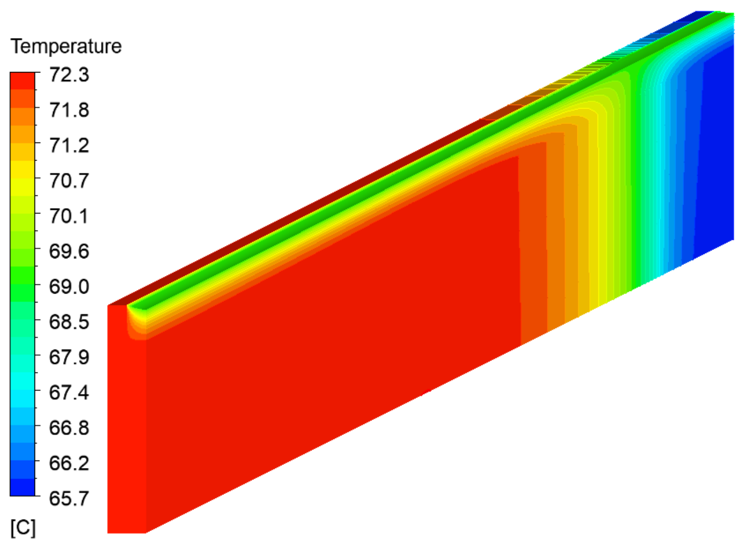


Figure 2.22: Temperature distribution along the channel

From Figure 2.22, it is seen that minimum and maximum temperature values on the channel is calculated as 65.7$^o$C and 72.3$^o$C with 69.2$^o$C saturation temperature. Results show that 87% of input heat is transferred via phase-change in this case. It was stated in the introduction section that heat pipes can transfer high amount of heat with small temperature gradients. To demonstrate this fact the same geometry is modeled with a copper block and the same amount of heat load is applied to the heat pipe. This time the heat is transferred only via conduction. Maximum temperature difference throughout the model is approximately 120$^o$C whereas corresponding value is approximately 7$^o$C when the heat pipe is operated.

Obtained temperature distribution is compared with the corresponding findings of Lefèvre et al. (2008) and Odabaşi (2014). The temperature variation along the small region at the vicinity of the liquid-solid interface is plotted for all studies in Figure 2.23.

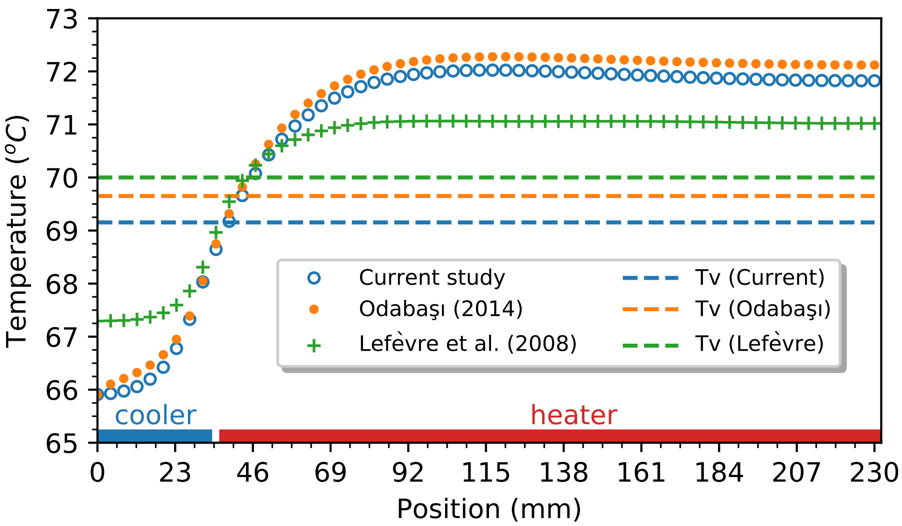


Figure 2.23: Comparison of the temperature distributions along the groove edge

The wall temperature deviations from the saturation temperatures for each study are also plotted in Figure 2.24.

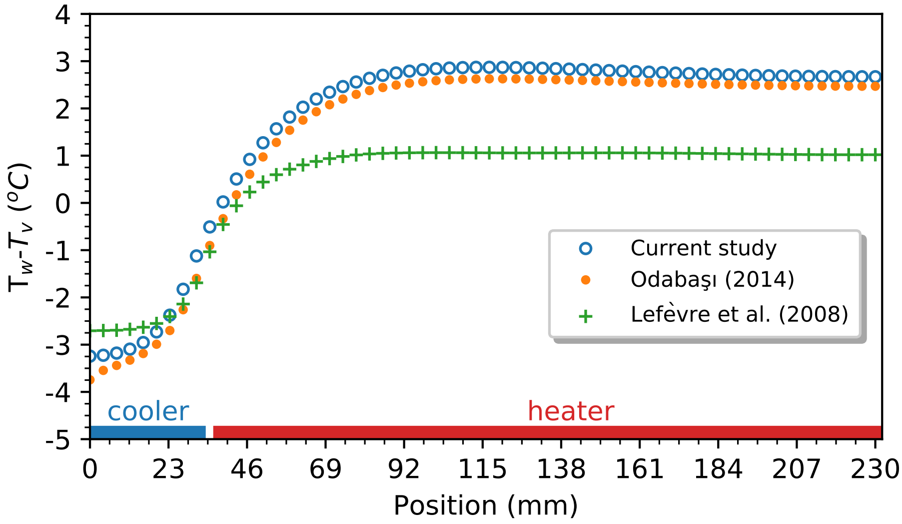


Figure 2.24: Wall temperature deviation from the saturation temperature

From figures Figure 2.23 and Figure 2.24 , it is observed that wall temperature variation trends are very close for the current study and Odabaşi (2014). However, Lefèvre et al. (2008) achieved a more uniform temperature distribution along the heat pipe. Maximum temperature difference is approximately 4.5$^o$C in Lefèvre et al. (2008), 7$^o$C in current study and also in Odabaşi (2014). Moreover, a small difference is observed between the vapor saturation temperatures of all studies.

The difference may be attributed to the phase-change models and different modeling methodologies. Odabaşi (2014) considered the problem as 3-D utilizing the coordinate transformation technique, and the phase-change from the micro region was taken into account based on kinetic theory. However, there is 7% difference noticed on micro-region evaporation heat transfer values (section 2.2.1) between the current study and Odabaşi (2014). Lefèvre et al. (2008) modeled the heat transfer as 2-D based on the thermal resistance analogy. Since the thermal conductivity of the liquid is smaller than that of the channel material, axial conduction in liquid is neglected in the 2-D model. Lefèvre et al. (2008) referenced kinetic theory to model phase change heat transfer however, micro region was not modeled in scope of the study. Phase-change was modeled with the heat transfer coefficient which was assigned to the entire liquid-vapor interface. However, in Odabaşi (2014) and the current study, heat transfer from the micro-region is modeled with the heat transfer coefficient boundary condition which is assigned to the micro-region.

Finally, 3-D temperature fields on the heat pipe between the current study and Odabaşi (2014) are depicted in Figure 2.25 . From the figure it is seen that temperature distributions are qualitatively in close agreement with each other.

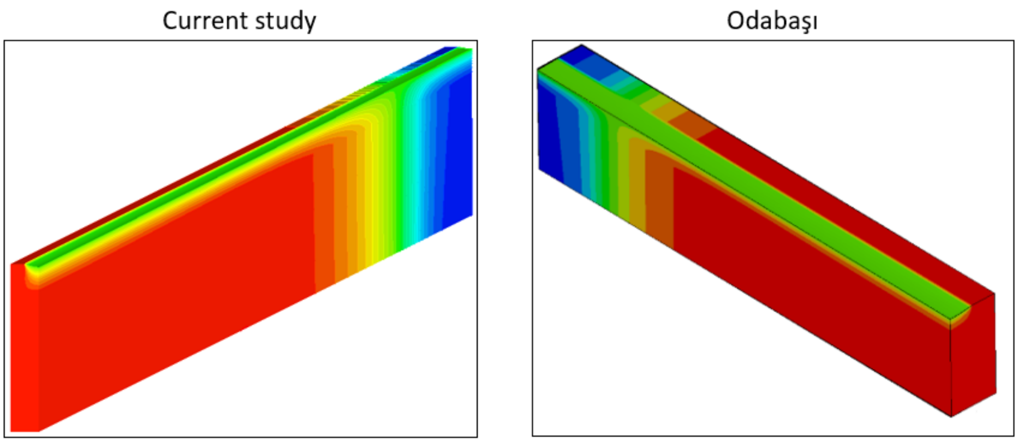


Figure 2.25: Comparison of the 3-D temperature fields

Since the findings of the current study are in close agreement with the results of other studies, the developed automated solution methodology can be used to predict flow and heat transfer characteristics of grooved heat pipes.

## 2.6 Investigating the Effect of Design and Operating Parameters

Since the modeling methodology is validated, the effect of various parameters can be investigated using the developed approach. Various cases whose details are explained in following subsections are prepared and analyses are carried out to reveal the effect of the investigated parameters. Effect of the groove height, groove width, filling ratio and length of the adiabatic section are investigated.

### 2.6.1 Effect of the Groove Height

Analyses are conducted for three distinct values of groove height to determine the effect of the groove height on heat pipe performance. The geometric parameters and operating conditions are kept the same with the validation study except for groove height. The groove height value in the validation study was 380 µm. In addition to that the channels with 760 µm and 1520 µm height values are investigated.

Meniscus curvature variation for all cases are plotted in upper left of the Figure 2.26. From the figure it is concluded that increasing the height value causes a decrease in the pressure drop along the channel due to the decrease in the liquid velocity inside the groove. Because the cross-sectional area of the liquid increases.

Wall temperature variations along the micro-region are plotted in upper right of the Figure 2.26. From Figure 2.26, it can be concluded that increasing groove height yields less uniform temperature distribution. There is no considerable difference observed between the vapor saturation temperature values (69.2$^o$C for all cases).

Mass flow rate variations along the groove are plotted in lower left of the Figure 2.26. Only 2% difference is observed in phase change mass flow rate values because the mentioned parameters are not a strong function of the channel height. Similarly, amount of heat transferred via phase-change is found almost to be identical for all cases because lower values of meniscus angle obtained with smaller groove which increases the rate of evaporation. The phase change heat transfer is compensated with lower temperature difference variation along the channel which decreases the rate of evaporation. When groove height value is 0.38 mm, approximately 87% of heat is transferred via phase change whereas the corresponding value becomes 89% when the height value is quadrupled (h=1.52 mm).

Finally, it is also concluded that the heat load capacity of the channel can be increased with selecting larger grooves but at the expense of elevated temperatures along the channel.

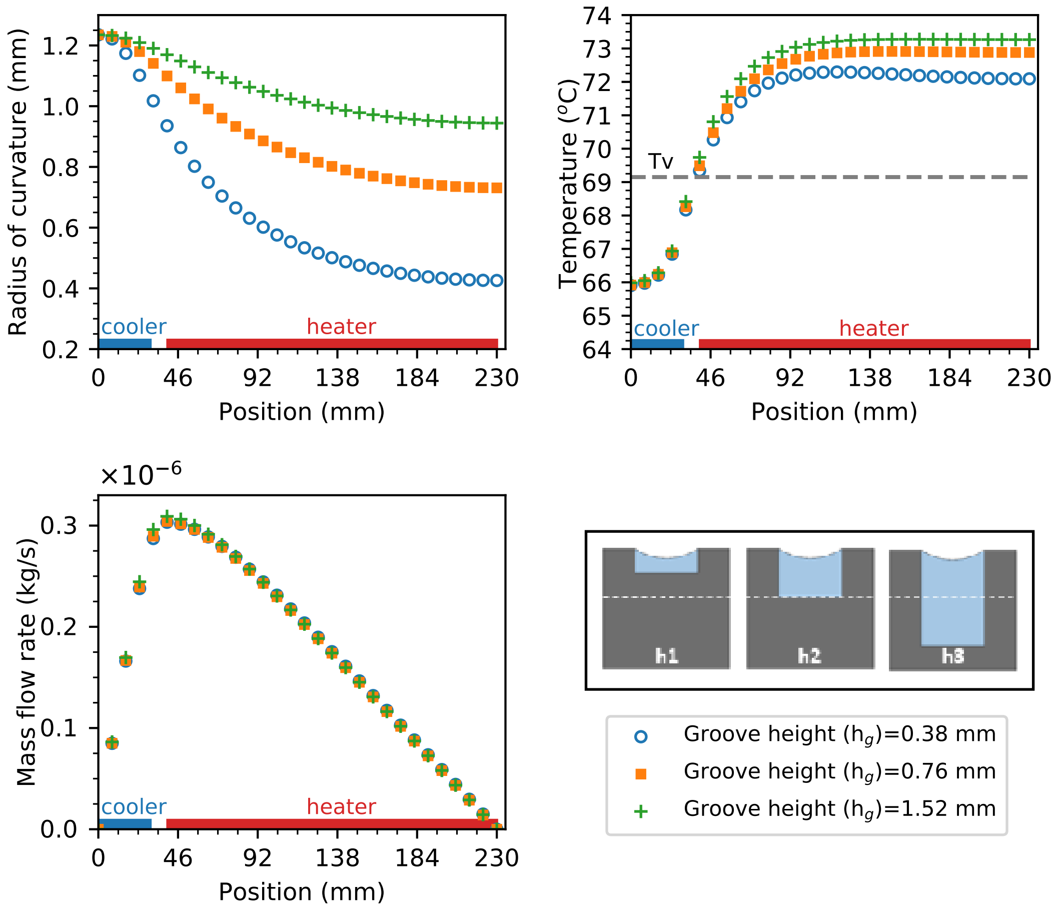


Figure 2.26: Effect of groove height on various parameters

### 2.6.2 Effect of the Groove Width

Analyses are conducted for three distinct values of groove width to determine the effect of the groove width on heat pipe performance. The geometric parameters and operating conditions are kept the same as the validation study except for the width of the grooves. The groove width value in validation study is 200 µm. In addition to that, grooves with 150 µm and 300 µm width values are investigated.

Meniscus curvature variation for all cases are plotted in upper left of the Figure 2.27. From the figure it is concluded that increasing the groove width value yields higher liquid cross-sectional area which reduces the pressure drop along the channel due to the decrease in the liquid velocity inside the groove.

Wall temperature variations along the micro-region are plotted in upper right of the Figure 2.27. From the figure, it can be concluded that increasing groove width yields less uniform temperature distribution. The vapor saturation temperature values range in $1^{o}$C interval.

Mass flow rate variations along the groove are plotted in lower left of the Figure 2.27. No difference is observed in phase change mass flow rate values because the mentioned parameters are not a strong function of the groove width. Similarly, amount of heat transferred via phase-change is found to be almost identical for all cases (approximately 87% of heat is transferred via phase change).

From Figure 2.27, it is also concluded that the heat load capacity of the channel can be increased by selecting larger grooves but at the expense of elevated temperatures along the channel.

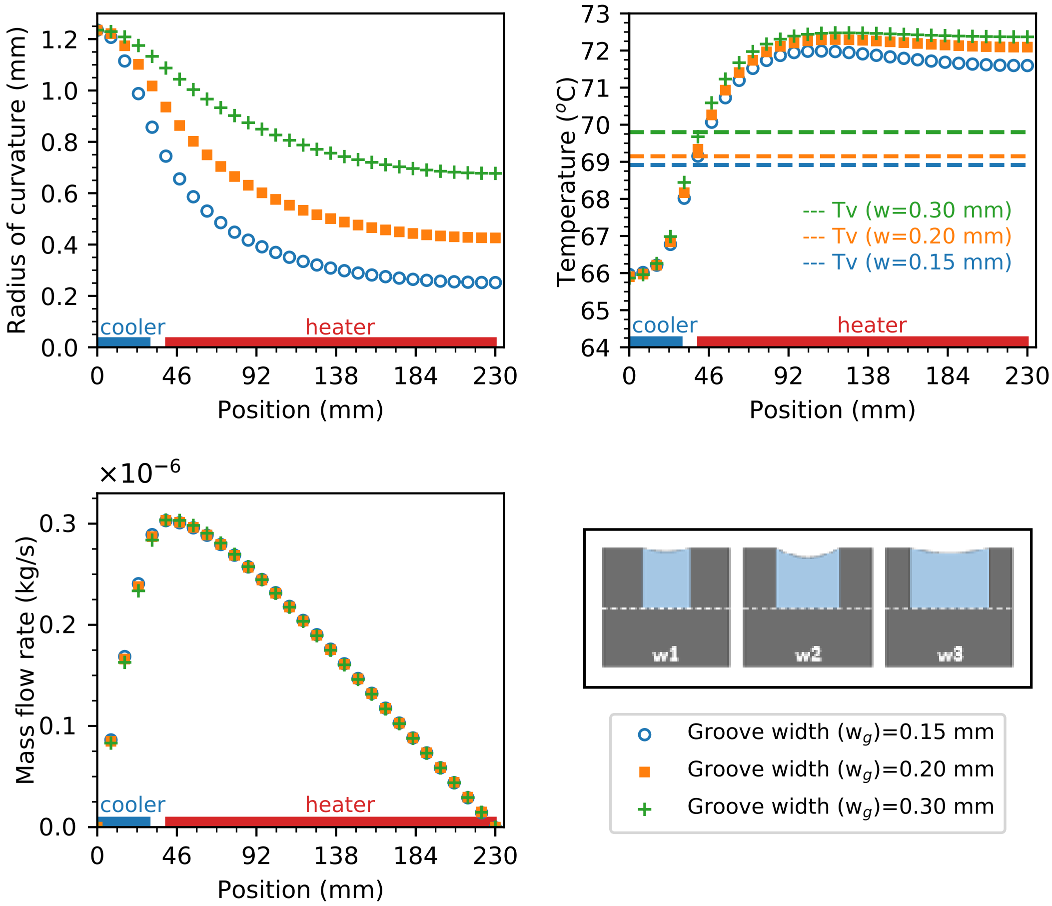


Figure 2.27: Effect of groove width on various parameters

### 2.6.3 Effect of the Filling Ratio

Analyses are conducted for six distinct values of filling ratio to determine the effect of the fill ratio on heat pipe performance. The geometric parameters and operating conditions are kept the same as the validation study except for the amount of the fluid that fill the grooves. Filling ratio can be defined as the ratio between the volume of the liquid in the groove and total groove volume. It is controlled with meniscus curvature value at the beginning of the condenser section (shape of fluid inside the grooves).

The meniscus curvature radius value at the beginning of the condenser section in validation study is 1.24 mm. In addition to that 1 mm, 1.5 mm, 10 mm, 20 mm and 25 mm initial meniscus curvature values are investigated.

Meniscus radius and temperature variations for all cases are plotted in Figure 2.28. From the figure it is concluded that increasing the filling ratio has a positive effect on the amount of heat transferred via phase-change up to a certain limit (in this case until 10 mm meniscus curvature value). Further raise in the value has a negative impact on the mentioned parameter.

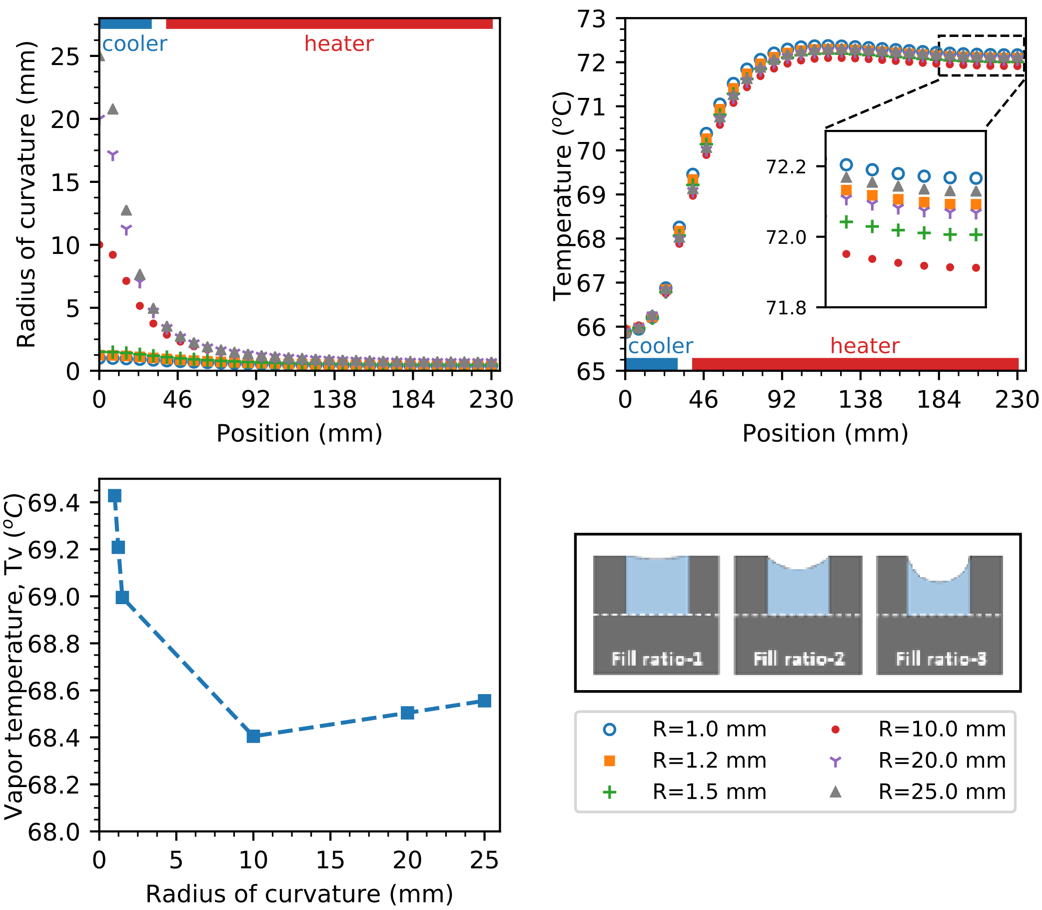


Figure 2.28: Effect of filling ratio on various parameters

Since the amount of heat transferred via phase-change has its maximum value for 10 mm initial meniscus radius, more uniform temperature variation along the channel is observed for that value as expected.

Vapor saturation temperature values lies between 1$^o$C interval and has its minimum value for 10 mm meniscus radius value.

### 2.6.4 Effect of the Adiabatic Length

Analyses are conducted for five distinct values of adiabatic section length to determine the effect of adiabatic length on heat pipe performance. The geometric parameters and operating conditions are kept the same with the validation study except for the lengths of heat source, heat sink and adiabatic sections. During the analysis adiabatic section length is changed (total length remains the same) while lengths of the heater and cooler sections are kept equal. 0 mm, 57.5 mm, 115 mm, 172.5 mm and 207 mm adiabatic length values are investigated. Bottom view of the channel and lengths of the heat source, heat sink and adiabatic sections are provided in Figure 2.29 and Table 2.5 respectively.

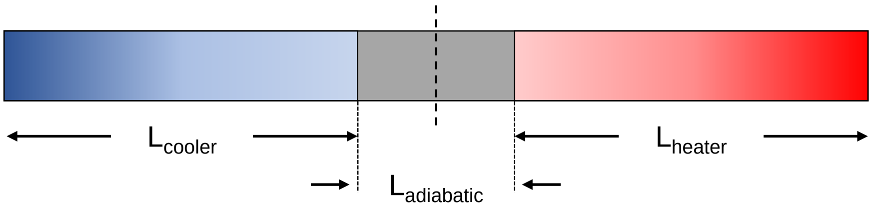


Figure 2.29: Bottom view of the channel

Table 2.5: Geometric properties of the channel to reveal adiabatic length effect

| **Case number** | $L_{cooler}$ **[mm]** | $L_{adiabatic}$ **[mm]** | $L_{heater}$ **[mm]** |
|---|---|---|---|
| Case-1 | 11.5 | 207 | 11.5 |
| Case-2 | 28.75 | 172.5 | 28.75 |
| Case-3 | 57.5 | 115 | 57.5 |
| Case-4 | 86.25 | 57.5 | 86.25 |
| Case-5 | 115 | 0 | 115 |

The radius of curvature, temperature and channel mass flow rate variations are plotted in Figure 2.30. There is no considerable difference noticed between the saturation temperatures. Its value is approximately equal to 53.8$^o$C for all configurations. From the results, it can be stated that increasing the adiabatic length yields a lower pressure drop along the groove since less amount of heat input is applied to the system. Moreover, decreasing the length of the adiabatic section has a negative influence on the uniformity of temperature distribution along the channel due to decrease in the amount of heat transfer via phase-change. 99% of heat is transferred via phase-change in case-1 while the corresponding value in case-5 is only 82%. Amounts of heat transfer via phase-change for all alternatives are provided in Figure 2.31.

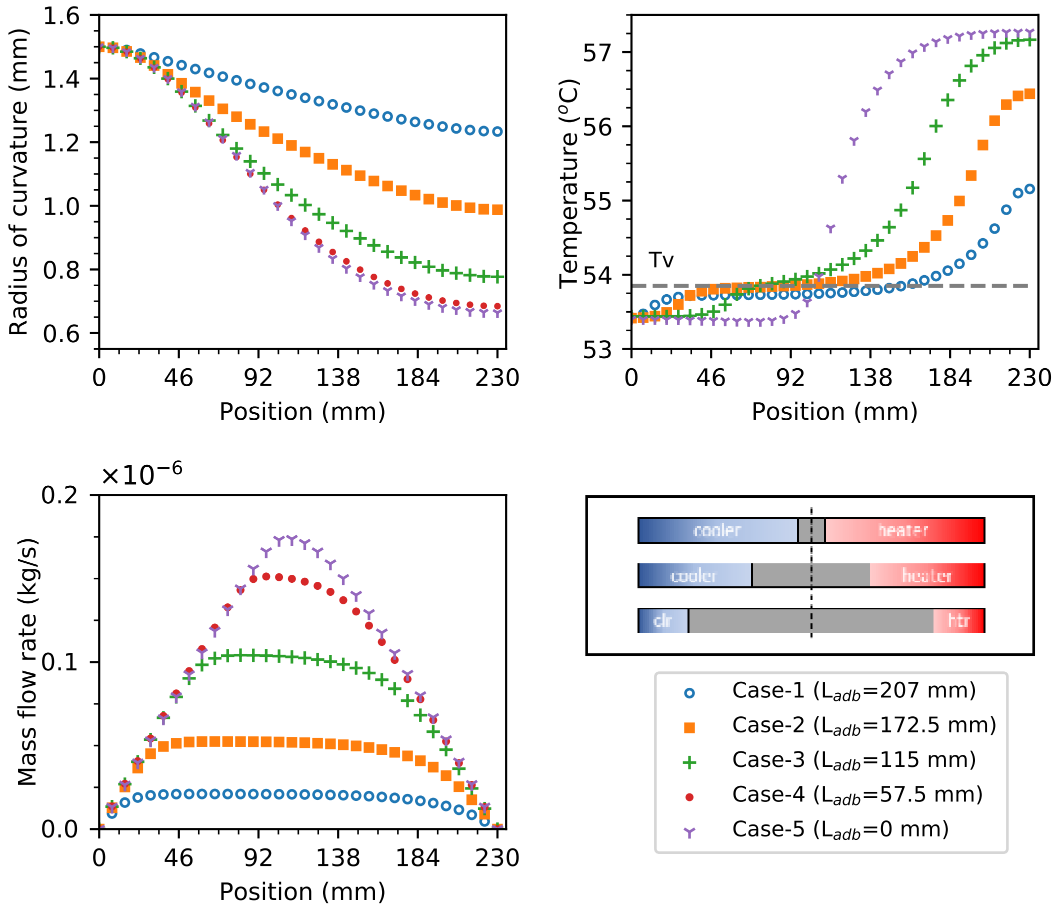


Figure 2.30: Effect of adiabatic length on various parameters

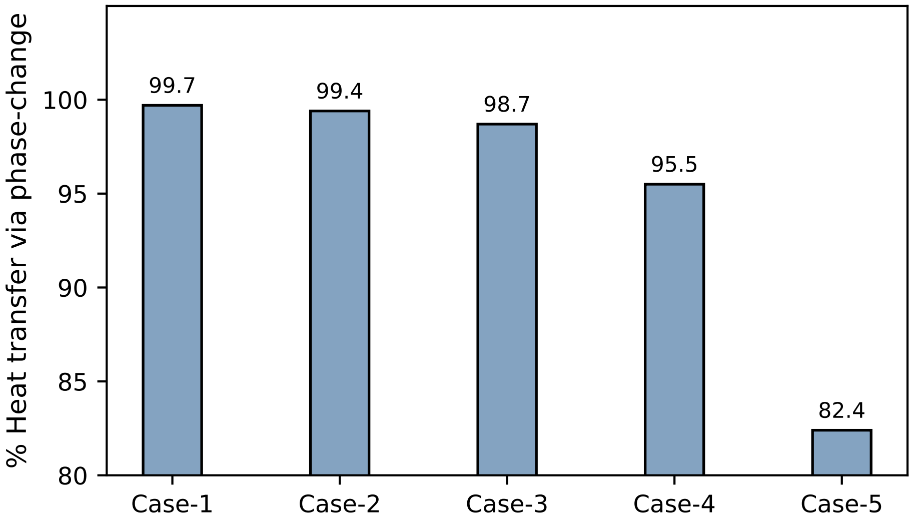


Figure 2.31: Effect of adiabatic length on phase-change heat transfer

# CHAPTER 3

# MODELING OF HEAT PIPES WITH INNOVATIVE CHANNEL GEOMETRIES FOR PERFORMANCE IMPROVEMENT

Having validated the developed methodology for the rectangular groove cross-section, the approach can now be applied to the various groove shapes. Several analyses are carried out for the performance assessment of the proposed models. It was mentioned in the introduction part of the study that there is no comprehensive and rigorous 3-D modeling methodology developed to investigate flow and heat transfer characteristics of complex groove geometries such as $\Omega$-shaped and circular cross sections. Benefiting from computational fluid dynamics (CFD), the developed automated solution methodology will be used to reveal the performance characteristics of distinct groove geometries. Trapezoidal, reverse trapezoidal, wedge, omega ($\Omega$), circular and chamfered shapes are investigated in the scope of this study.

Two different strategies are followed to enable a comparison between different geometries. First, fin top width and liquid cross-sectional area are kept constant by changing groove height. Second, channel height and liquid cross-sectional area are kept constant by changing the width of the fin top. These modeling approaches are depicted in Figure 3.1. On the left side of the figure, groove width is kept the same for all alternatives whereas, on the right side, height of the groove is kept constant. After the solution, findings are reviewed and groove shape effect on the heat pipe performance is discussed in detail.

In the final part of this section, innovative groove shapes are introduced. Shape of the groove cross-section is altered along the groove while its cross-sectional area is kept constant. e.g. condenser part is modeled as a trapezoidal whereas the evaporator part is modeled as a reverse trapezoidal. There is no such a model - which has a variable cross-section along the groove - has been presented in the literature. With this unique design, advantages of the distinct shapes are utilized for performance improvement of the flat grooved heat pipes.

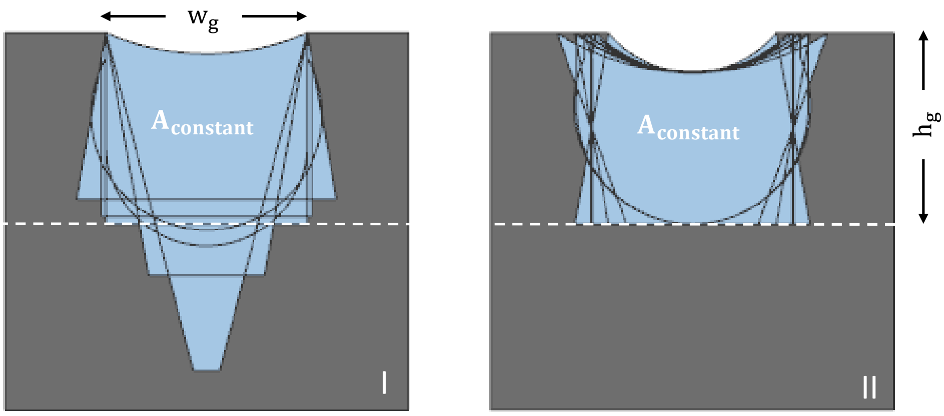


Figure 3.1: Modeling approaches to investigate groove shape effect

## 3.1 Modeling Approach #1 (Constant Fin Top Width)

The first methodology introduced for investigating the effect of different cross-sections is maintaining the same fin top width and liquid cross-sectional area while changing the groove height. Parametric sketch relations and dimensions are imposed on various geometries which are illustrated in Figure 3.2. To better understand the differences between them, all of the groove geometries are drawn with the same scale.

*Wetted perimeter* (P), which is the total length of the groove surface which is in contact with liquid. It is a useful parameter for the comparison of different groove geometries. In the current case, the longest wetted perimeter is obtained with the wedge model while the omega channel geometry satisfies the shortest wetted perimeter. Wetted perimeter values for different groove geometries are normalized with respect to the rectangular channel and shown in the in Figure 3.2.

Efficiency can also be a useful indication of heat pipe performance. It is another parameter used to describe physical phenomenon and comparison. Although efficiency can be defined in various forms, in the presented study it is defined as the ratio between the amount of heat transferred via phase-change and amount of heat input to the system. Along with the efficiency, other quantities like maximum temperature and pressure difference inside the channel are investigated. Mentioned quantities are shown all together in Figure 3.6.

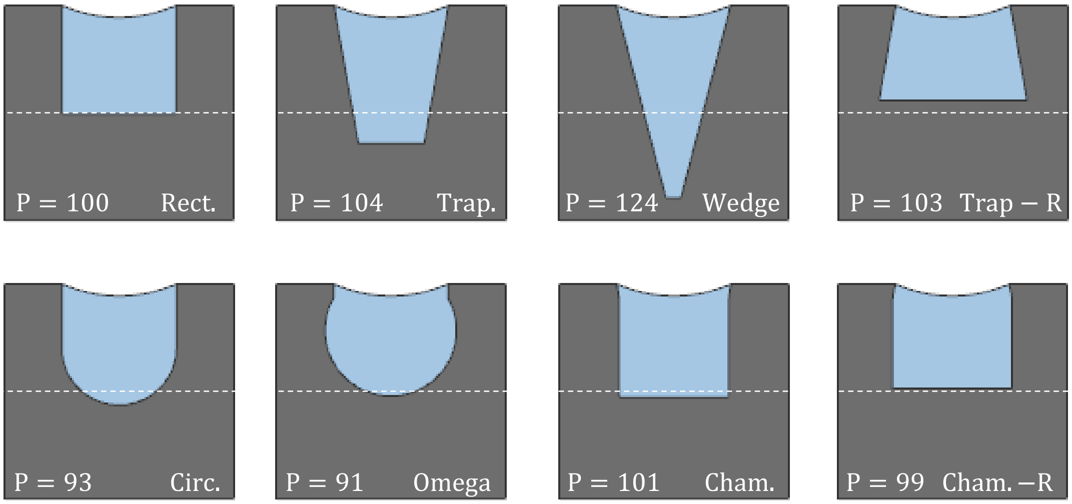


Figure 3.2: Normalized perimeters of various cross-sectional geometries with identical fin top width and cross-sectional area

The developed analysis methodology (explained in previous chapters) is employed for all of the stated models in Figure 3.2. Physical properties and boundary conditions are selected in accordance with the validation case except the cross-section of the grooves and filling ratio. Higher filling ratio is selected in this case because dry-out phenomenon has occurred in some models (i.e. trapezoidal and wedge grooves) with the filling ratio which is used in validation case.

After the achieved convergence, velocity distributions along the groove, 3-D temperature fields, meniscus curvature, wall temperature and liquid mass flow rate variations for the mentioned models are depicted in Figure 3.3, Figure 3.4, Figure 3.5 respectively.

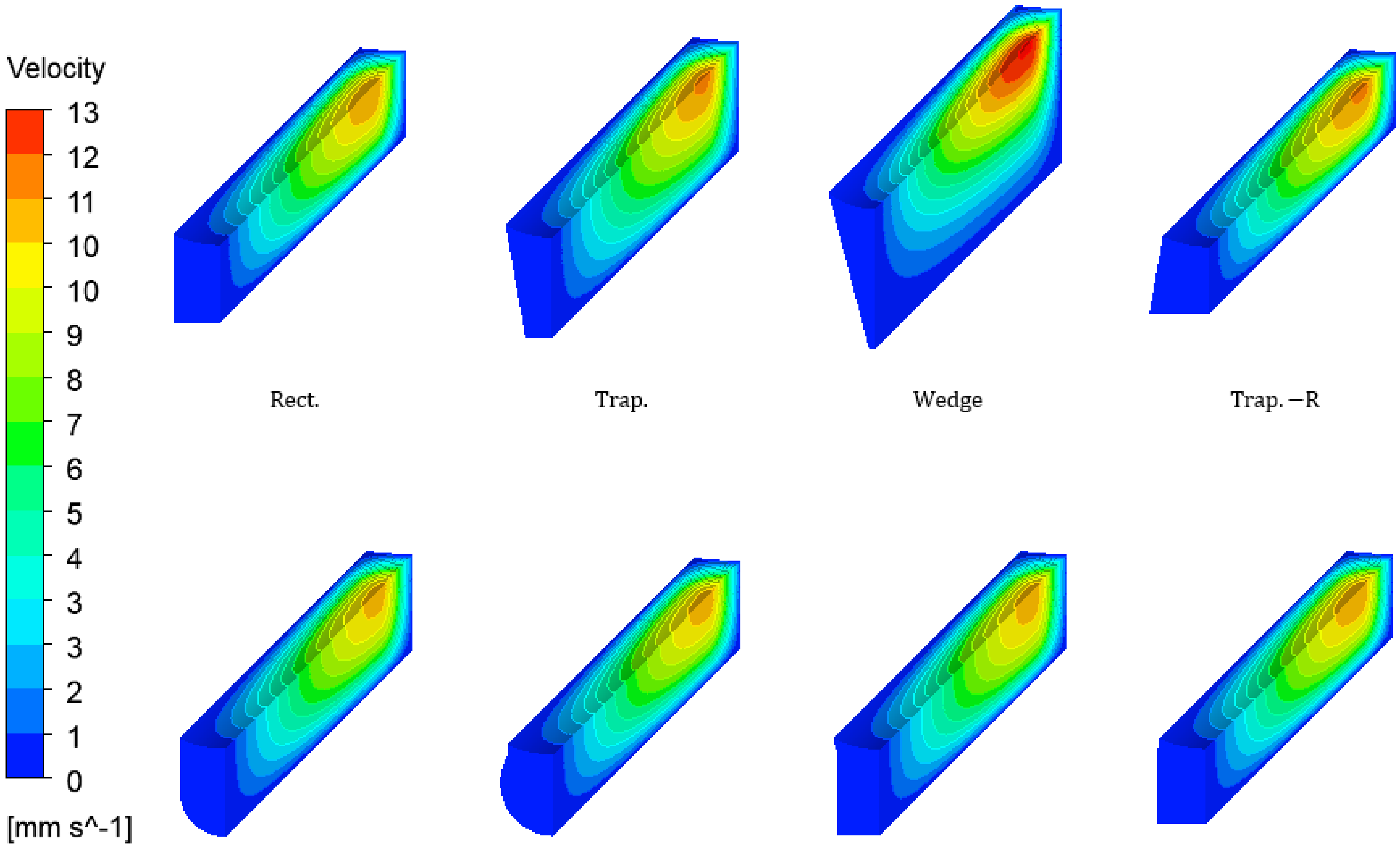


Figure 3.3: 3-D velocity fields of studied groove geometries

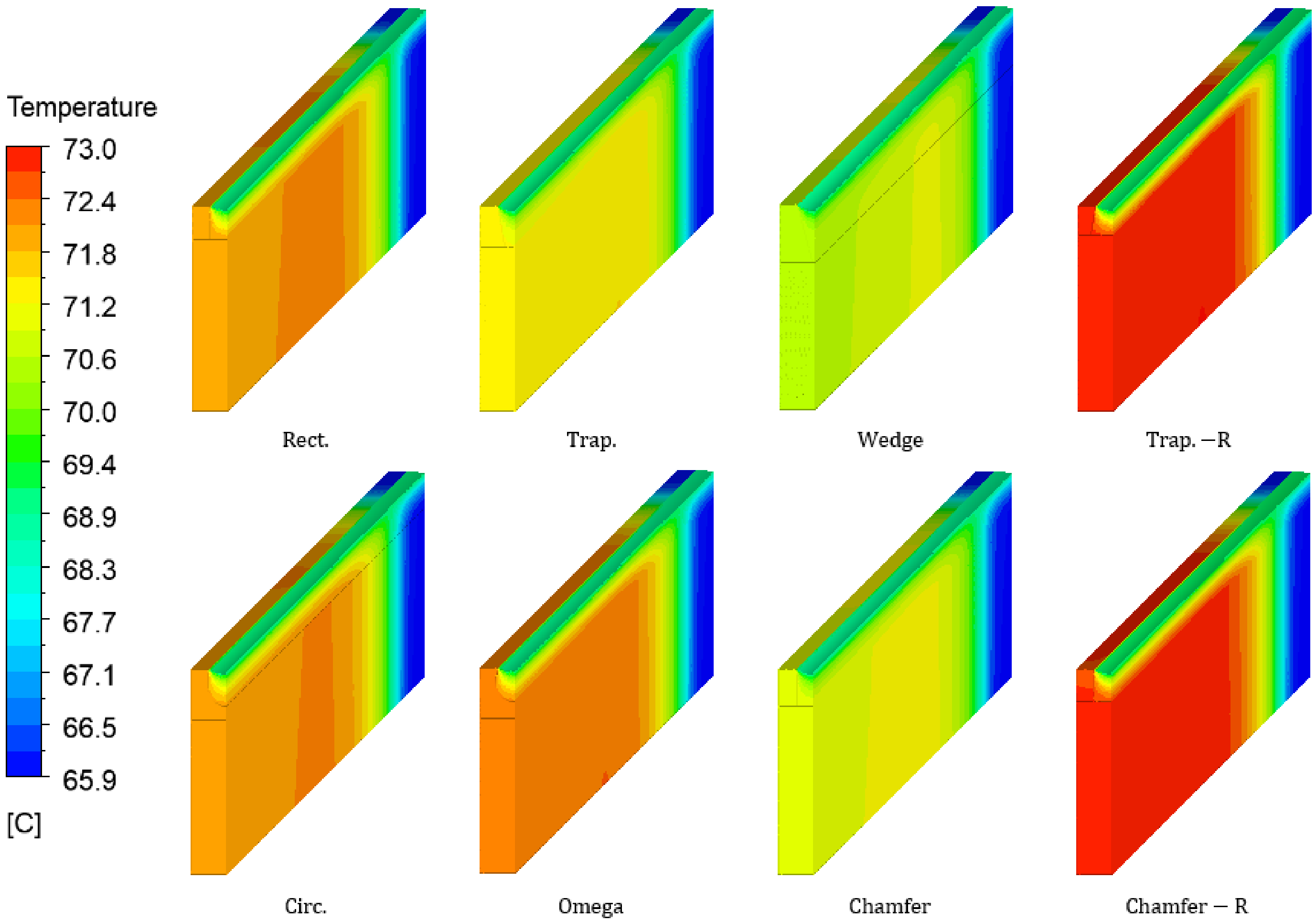


Figure 3.4: 3-D temperature fields of studied groove geometries

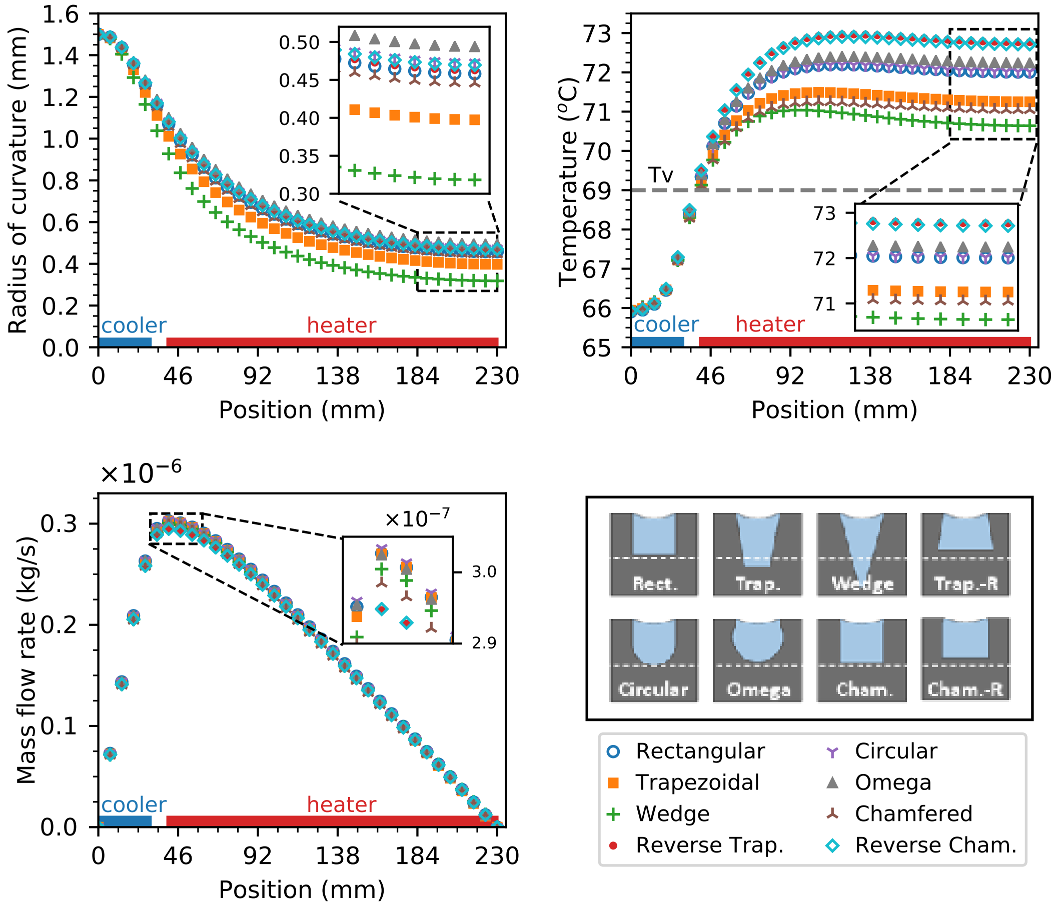


Figure 3.5: Effect of various parameters on the studied geometries

From Figure 3.3 and Figure 3.5 it can be deduced that pressure drop along the groove has its highest value for the wedge shape. The reason behind this can be attributed to a shear-induced pressure drop. The wedge geometry yields the longest wetted perimeter which increases the shear-induced pressure drop along the channel. Due to the same reason (contrary to wedge geometry), Ω-shape channel design gives the smallest pressure drop along the channel. Approximately 55% difference exists between the pressure drop values of the two shapes.

Focusing on Figure 3.4, Figure 3.5 and Figure 3.6, it is observed that all models yield approximately the same saturation temperature ($T_v$ app. 69$^o$C ). With the wedge configuration, a more uniform temperature distribution along the channel is obtained. Approximately, the same amount of heat is transferred via

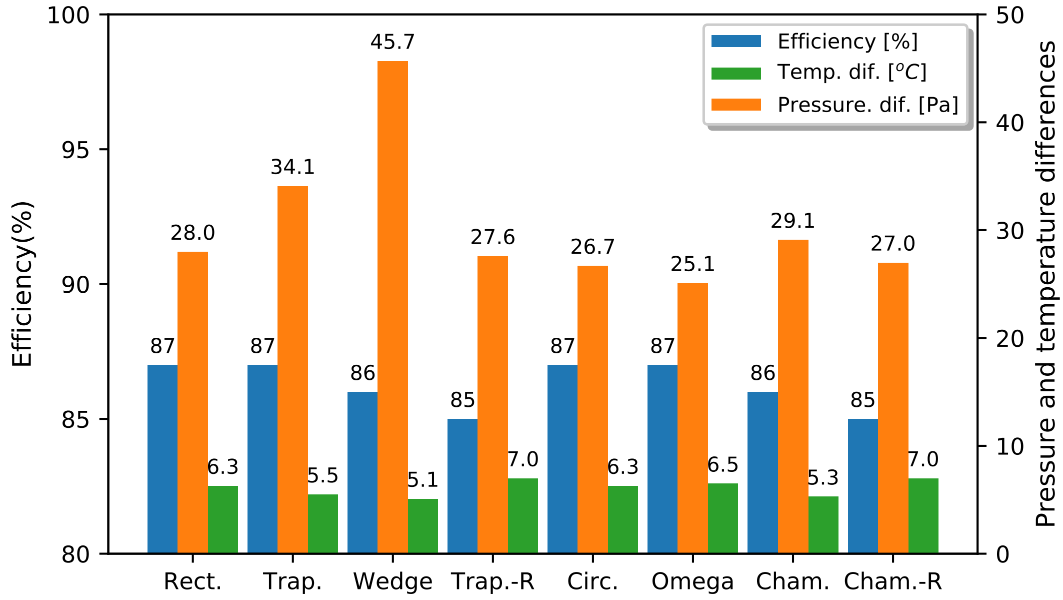


Figure 3.6: Efficiency, pressure and temperature differences for studied shapes

phase-change with a smaller temperature difference compared to other geometries. This can be attributed to the evaporation phenomenon. It was stated in the evaporation model that mass flux rate increases with decreasing meniscus angle — the angle which liquid-vapor interface makes with the wall — due to existence of a longer layer of thin film. The wedge cross-section has the smallest end angle along the evaporator region, moreover, the same model satisfies the longest wetted perimeter among others. Due to these reasons, shear induced pressure drop along the channel is found to be the highest in this shape which means that the minimum thermal load can be carried with wedge model without dry out phenomenon. However, temperature difference along the channel determines the minimum in the case of no-dry out inside the pipe.

With chamfered geometry, approximately 20% improvement on the temperature difference inside the channel as compared with rectangular groove is achieved. Improvement arises from the combination of end angle effect and the decrease in wetted perimeter. Moreover, approximately 3% decrease is obtained in pressure drop along the channel.

## 3.2 Modeling Approach #2 (Constant Groove Height)

The second methodology introduced for investigating the effect of different cross-sections is maintaining the same groove height and liquid cross-sectional area while changing the fin top width. Parametric sketch relations and dimensions are imposed on various geometries given in Figure 3.7. To better understand the differences between the shapes, all groove geometries are drawn on the same scale. In the current case, the longest wetted perimeter obtained with the trap-R geometry while the circular channel shape satisfies the shortest wetted perimeter. Wetted perimeter values for different groove geometries are normalized with respect to rectangular cross-section and shown in the same figure.

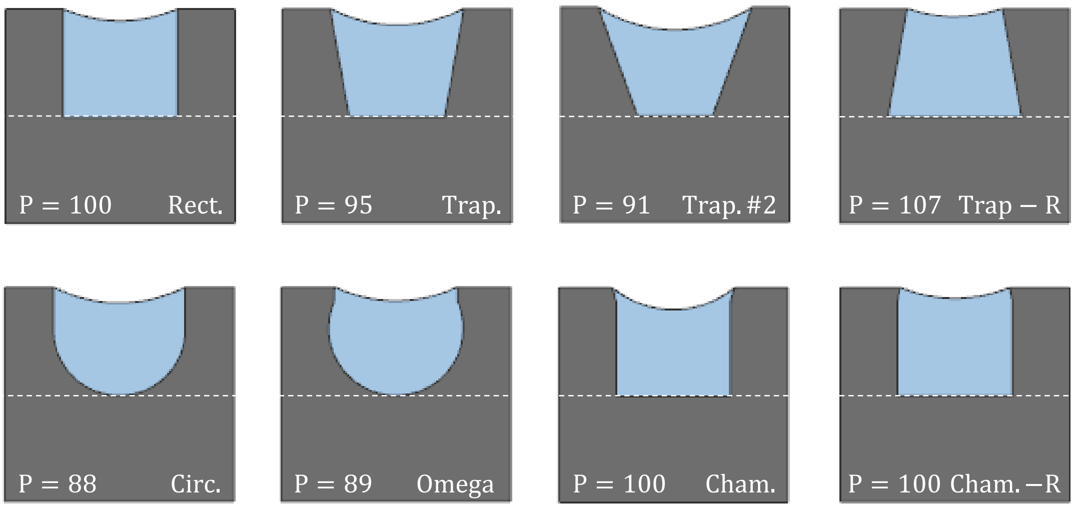


Figure 3.7: Normalized perimeters of various cross-sectional geometries with identical channel height and cross-sectional area

Developed analysis methodology (explained in previous chapters) is carried out for all of the stated models in Figure 3.7. Physical properties and boundary conditions are selected in accordance with the modeling methodology #1 explained in Section 3.1.

After numerical convergence, velocity distributions along the groove, 3-D temperature fields, meniscus curvature, wall temperature and liquid mass flow rate variations for the mentioned models are depicted in Figure 3.8, Figure 3.9, Figure 3.10 and Figure 3.11 respectively.

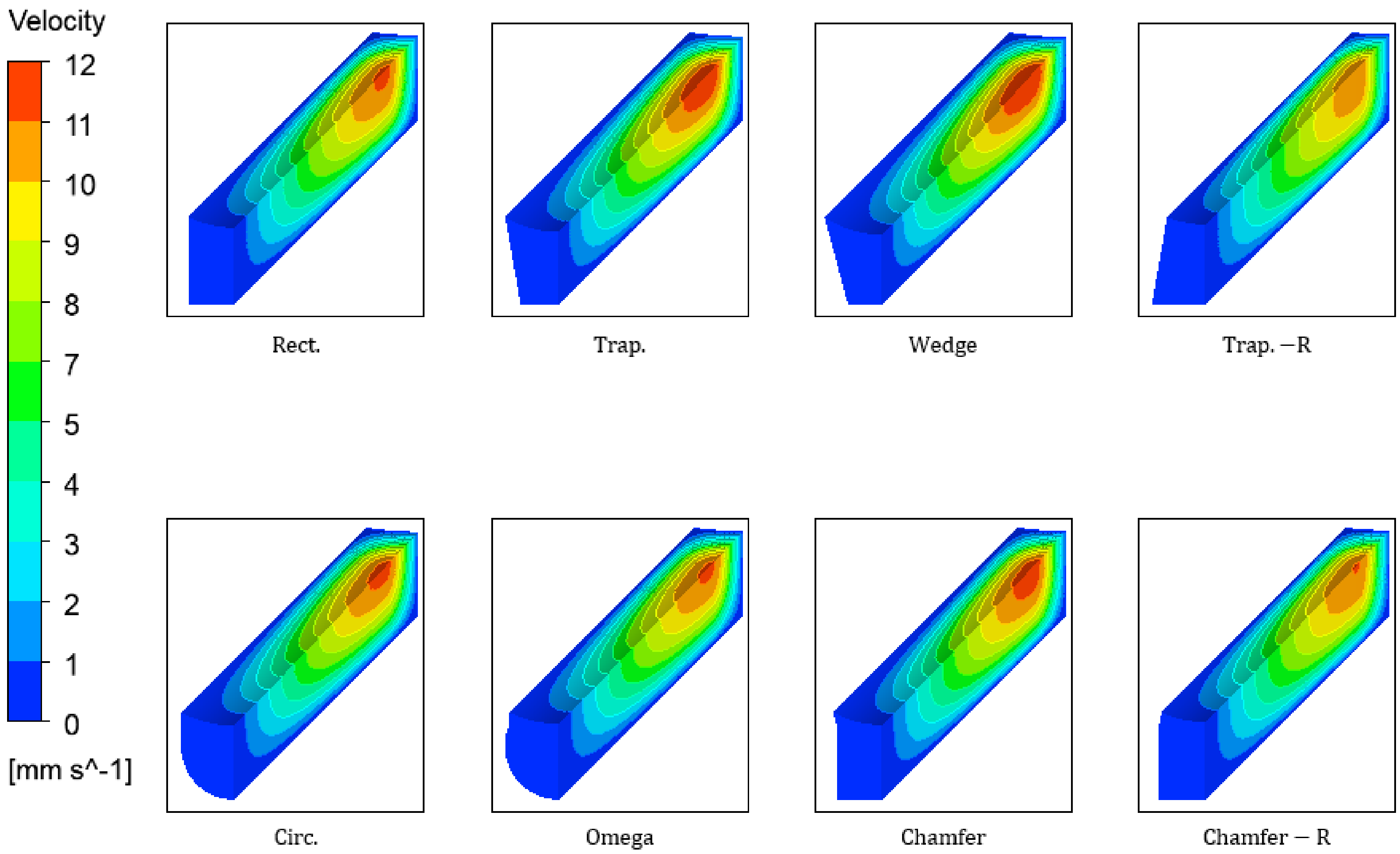


Figure 3.8: 3-D velocity fields for different groove geometries

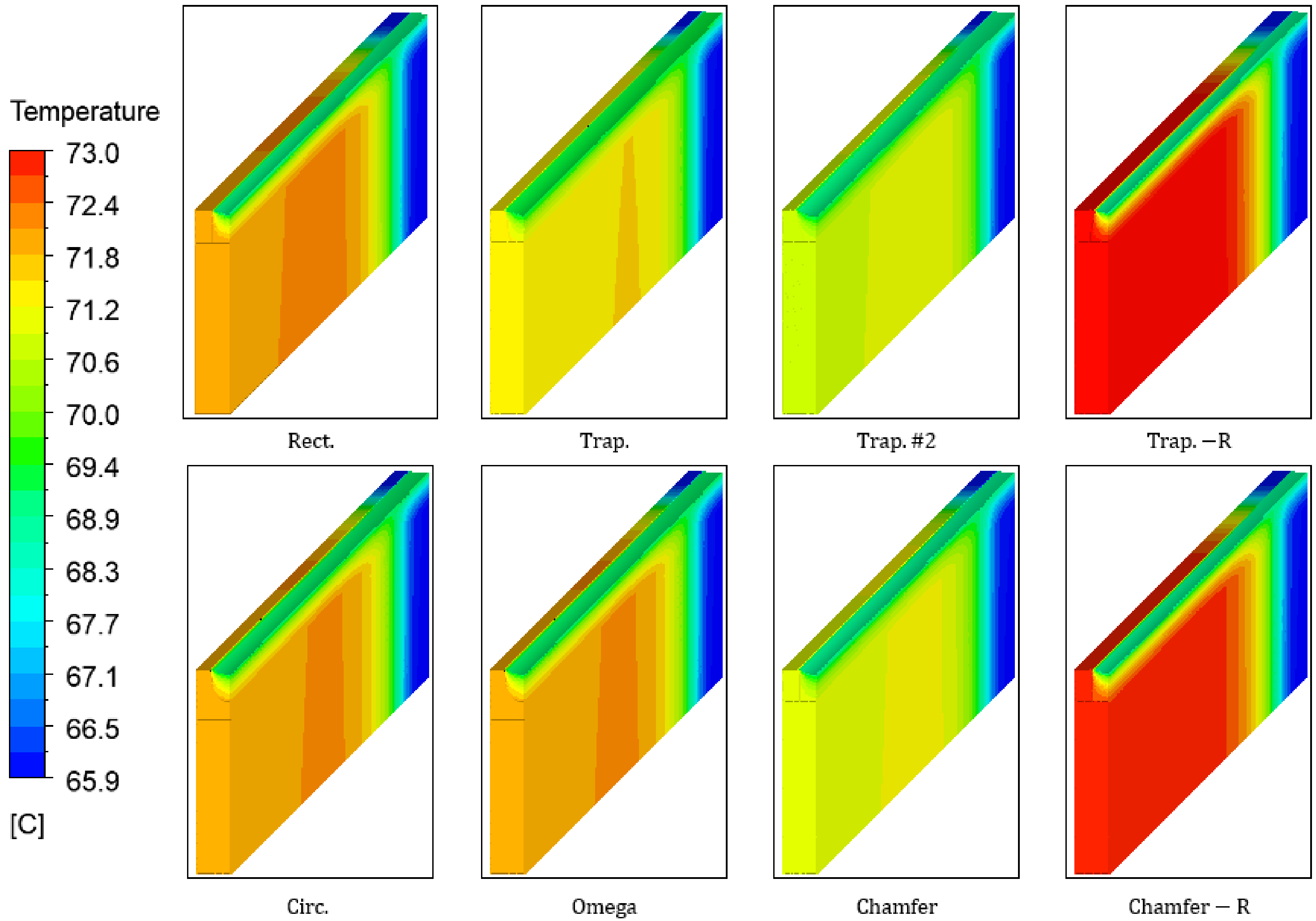


Figure 3.9: 3-D temperature fields for different groove geometries

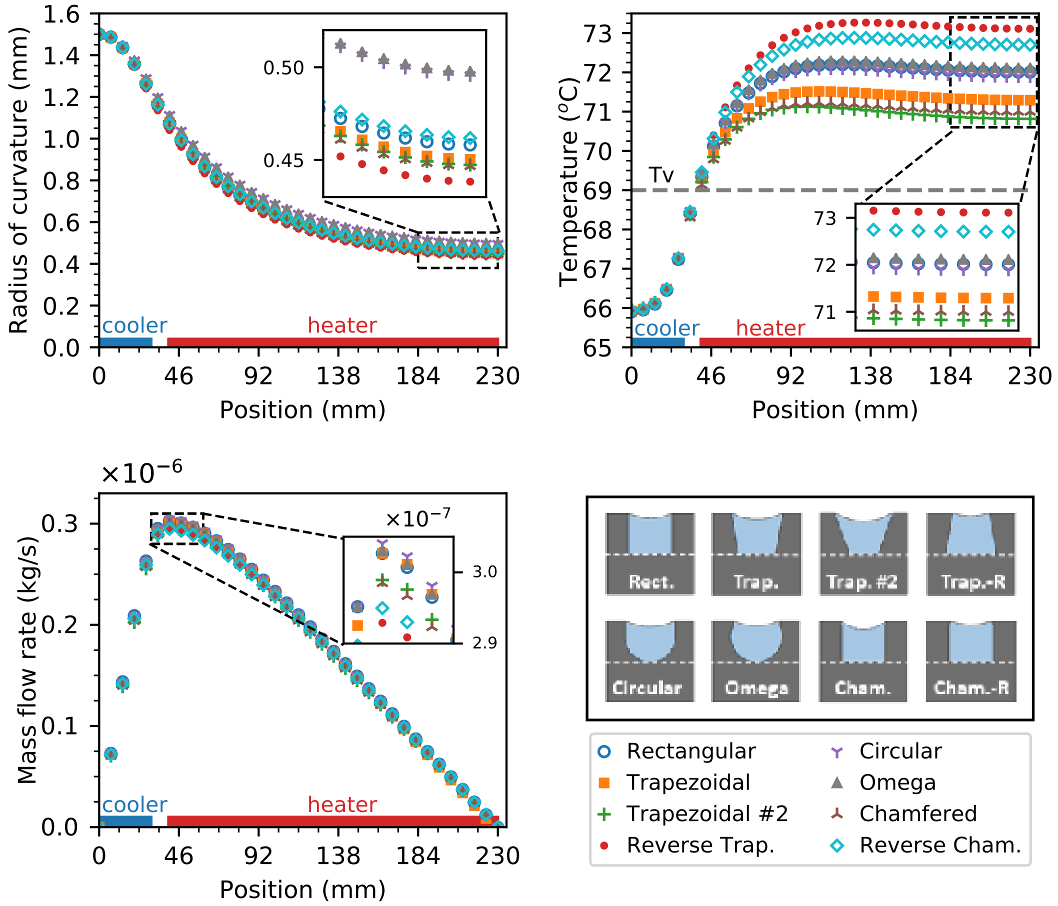


Figure 3.10: Meniscus curvature variation for different geometries

From Figure 3.8 and Figure 3.10 it can be seen that pressure drop along the groove has its highest value in trap-R model. A possible reason behind can be explained with a shear-induced pressure drop. The trap-R model yields the longest wetted perimeter which increases the shear-induced pressure drop along the channel. Due to the same reason (opposite to wedge model), circular-shape geometry gives the least pressure drop along the channel. Approximately 20% difference calculated between the pressure drop values of the two models.

Focusing on the figures Figure 3.9, Figure 3.10 and Figure 3.11, it is observed that all models yield approximately the same saturation temperature ($T_v$ app. $69^o$C ). With trap#2 configuration, more uniform temperature distribution along the channel is obtained. Approximately the same amount of heat is transferred via phase-change with less temperature difference as compared with other geometries. This can be attributed to the evaporation phenomenon. It was stated in the evaporation model (which is explained in detail in section 2.2.1) that mass flux rate increases with decreasing meniscus angle — the angle which liquid-vapor interface makes with the wall —

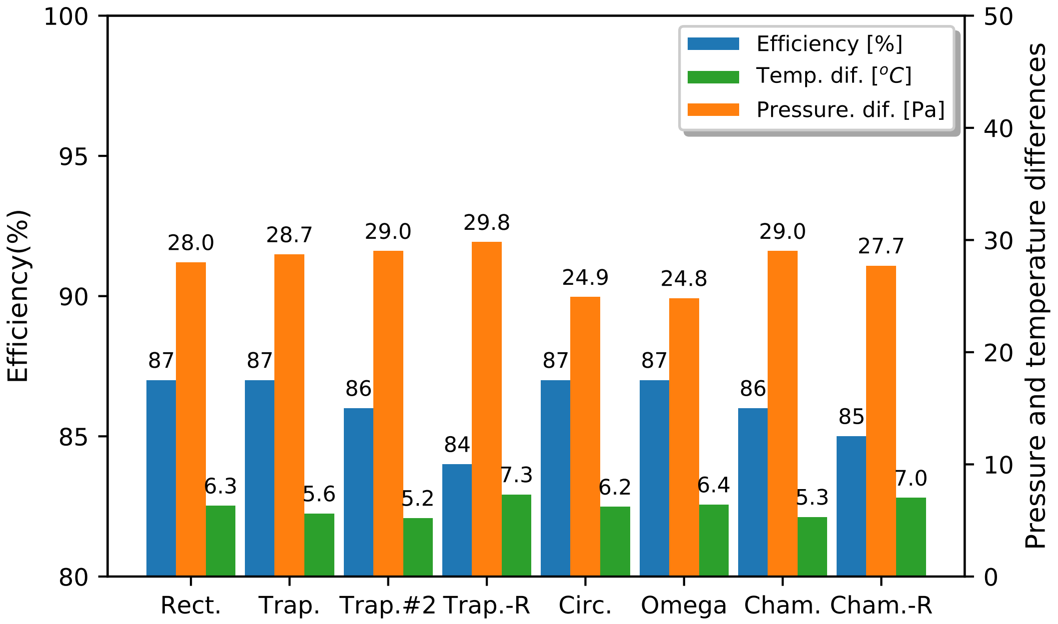


Figure 3.11: Efficiency, pressure and temperature differences for studied groove geometries

## 3.3 Novel Groove Geometries for Performance Improvement

The most common groove shapes utilized in industrial designs were put forward with using comprehensive analysis methodology in the previous section. Groove shape effect on heat load capacity (pressure drop along the channel) and maximum temperature difference inside the channel is determined. In this section, novel groove geometries are proposed for improved performance based on previous findings.

Trapezoidal cross-section helps to improve evaporation rate because the amount of evaporated vapor is negatively influenced by meniscus angle. Reverse-trapezoidal arrangement increases potential of heat load capacity. This type of design allows to start with larger meniscus angle on the condenser side. However, evaporator side would be negatively effected from this revision (trap-R cross section) owing to smaller meniscus angle which causes evaporation rate to decrease. Moreover, shear induced pressure drop increases with this configuration, because of the longer perimeter obtained as compared to the rectangular groove geometry.

Advantages of the two distinct groove geometries are combined and a new shape is proposed. In this new novel geometry, shape of the groove cross-section is altered along the channel while its cross-sectional area is kept constant. Cross-section of the channel is a reverse trapezoidal in the condenser whereas it is a trapezoidal in the evaporator. Having this arrangement, it is aimed to transfer more amount of heat with a less temperature difference.

The alternatives are not limited to trapezoidal groove geometries. Other configurations in various groove shapes can be defined in which the the groove cross-section is altered along the groove (e.g. omega shaped and chamfered grooves). It is also possible to alter the groove cross-section or fin top width along the channel to optimize the heat load capacity and temperature distribution. However, in the current study, only chamfered and trapezoidal groove shapes are investigated and their results are presented. In Figure 3.12 some innovative groove arrangements are depicted (Sections A and B are interchangeable).

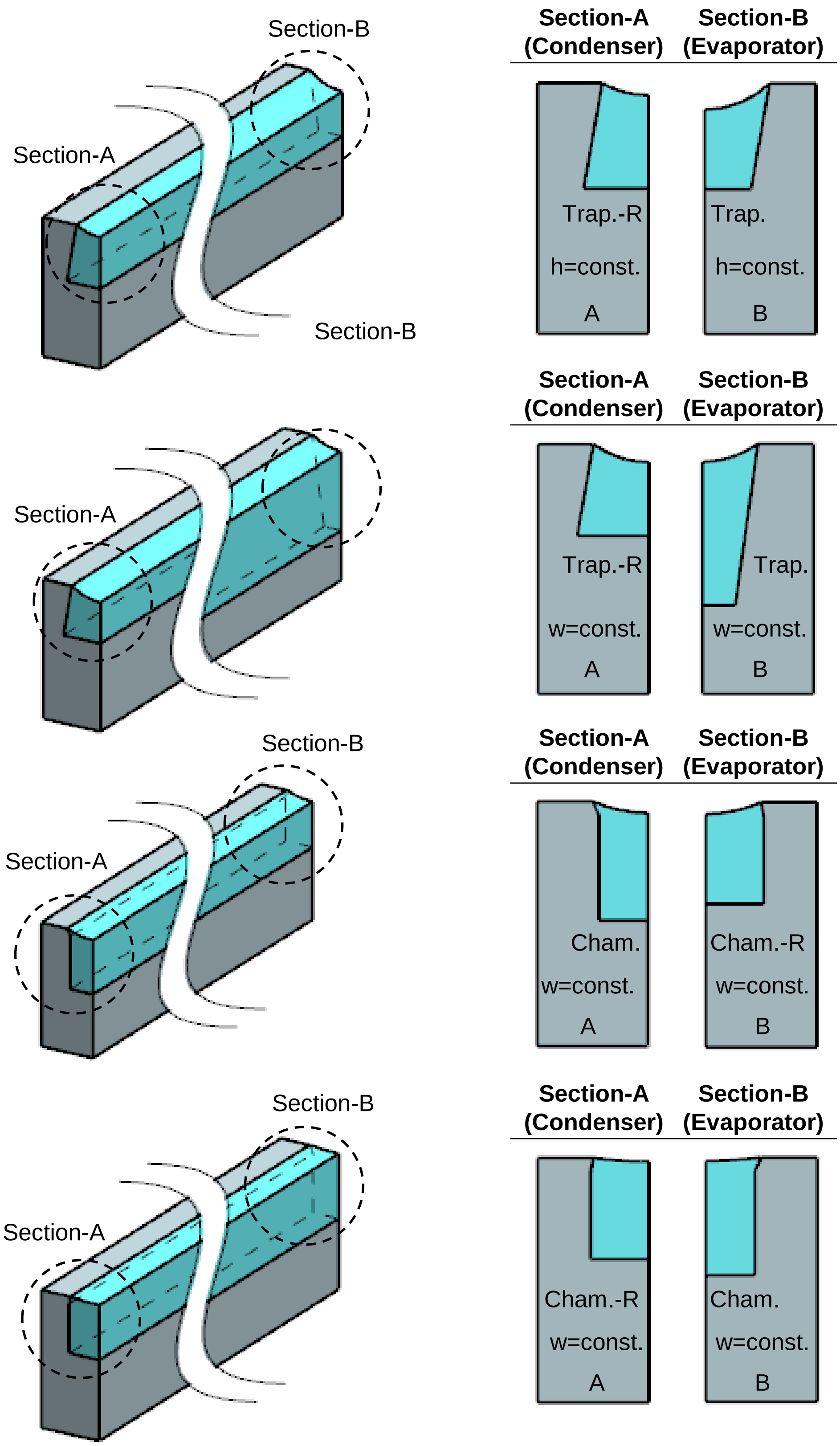


Figure 3.12: Examples of innovative groove geometries

2 distinct novel groove shapes are designed and their performance characteristics are investigated by following the developed solution methodology. For the first model, liquid cross-sectional area is kept constant along the groove at every cross-section while the condenser section is designed as reverse trapezoid and the evaporator section is designed as a trapezoid. Geometric details are provided in Table 3.1. Physical properties and boundary conditions are selected in accordance with the validation case except the cross-sections of the grooves and the filling ratio.

Table 3.1: Studied groove geometries

| Model number | Geometry of Section A/B | Length of Section-A [mm] | Length of Section-B [mm] |
|---|---|---|---|
| 1 | Trap-R/Trap | 43.7 | 186.3 |
| 2 | Chamfer-R/Chamfer | 43.7 | 186.3 |

After the convergence of the saturation temperature is achieved, 3-D temperature field, wall temperature plots and meniscus curvature variation along the groove for the geometry-1 is shown in Figure 3.13.

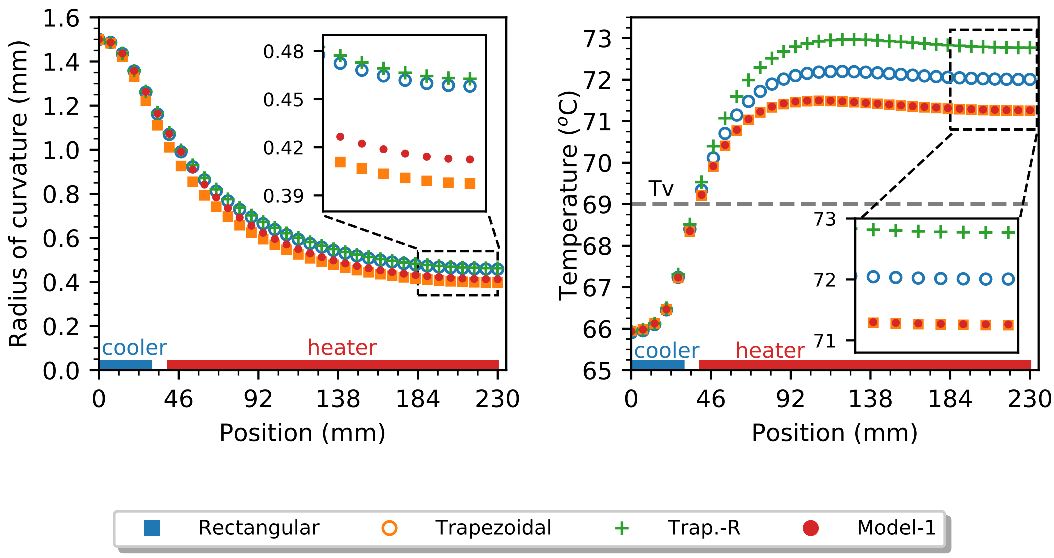


Figure 3.13: Meniscus curvatures and wall temperatures comparison for different geometries

To reveal the effect of the novel design, results of rectangular, trapezoidal and reverse trapezoidal groove shapes are provided on the same plot. From Figure 3.13, it can be seen that the novel groove design (model-1) yields approximately 10% lower pressure drop compared to trapezoidal groove.

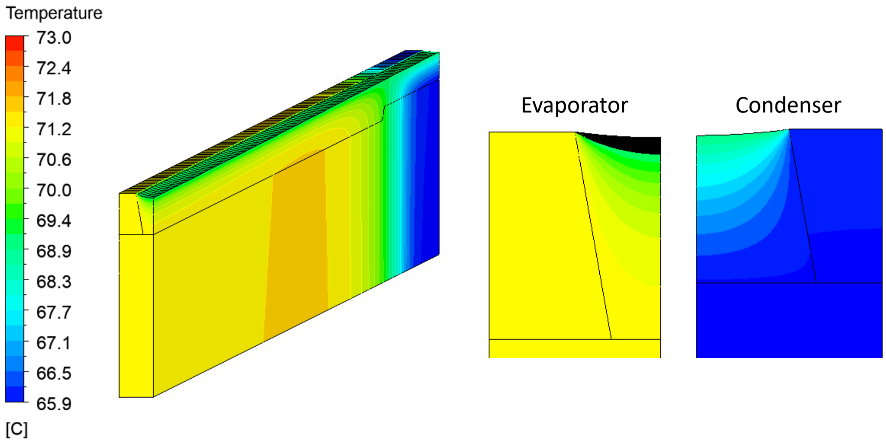


Figure 3.14: Temperature variation in model-1

If we focus on Figure 3.13 it can be seen that there is no significant difference between wall temperature distributions of the novel groove design and trapezoidal groove. Therefore it can be concluded that the novel design which has a variable cross section will provide more heat transfer capacity with approximately the same temperature difference.

The second geometry is designed very similar to the first model. But this time, chamfered groove cross-section geometry is adopted instead of a trapezoidal shape. Liquid cross-sectional area is kept constant along the groove at every cross-section while the condenser section is designed with a reverse chamfer and evaporator section is designed with a straight chamfer. Physical properties and boundary conditions are selected in accordance with the validation case except the cross-sections of the grooves and the fill ratio.

From Figure 3.15, it can be seen that the chamfered novel groove design (model-2) yields approximately 5% lower pressure drop compared to fixed chamfered groove.

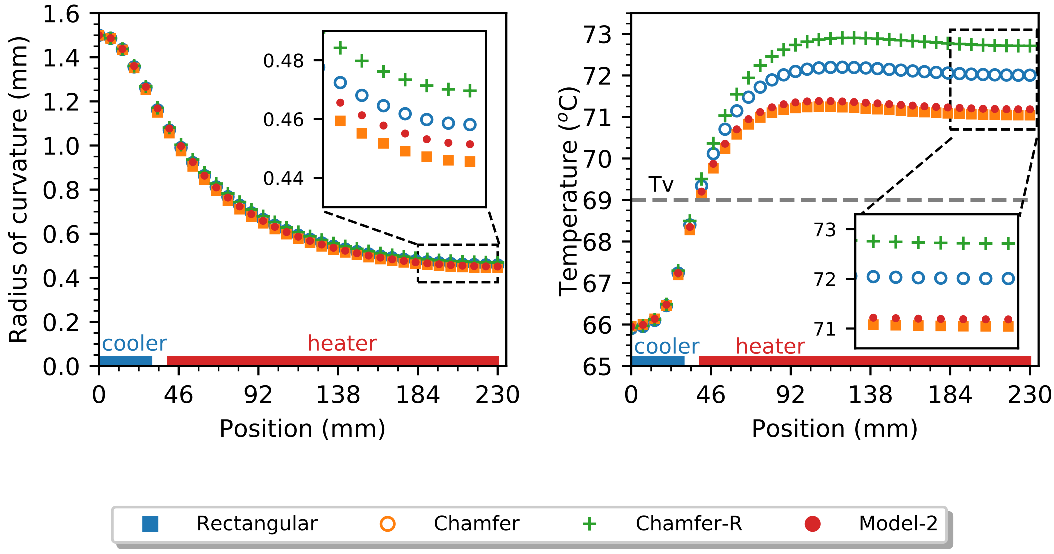


Figure 3.15: Meniscus curvatures and wall temperatures comparison for different geometries

From the same figure, it can be concluded that no significant difference exists between wall temperature distributions of the novel groove and chamfered designs. Therefore, it can be concluded that the chamfered channel which has variable cross section will provide more heat transfer capacity with the same temperature difference.

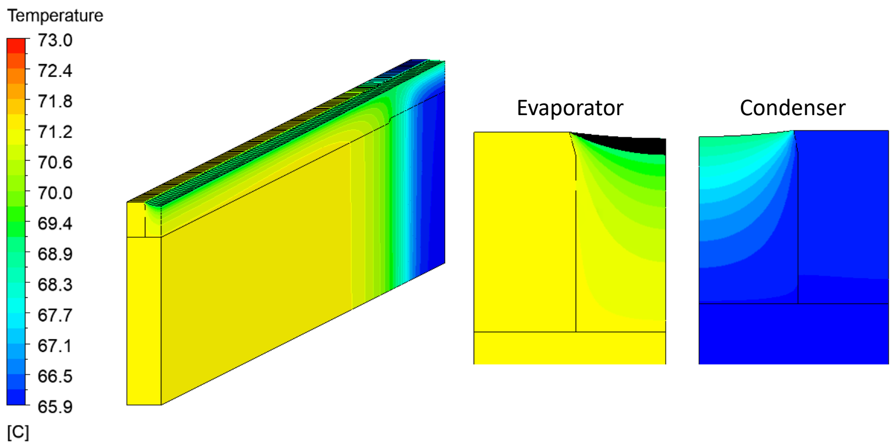


Figure 3.16: Temperature variation in model-2

# CHAPTER 4

# EXTENSION OF THE STUDY TO MULTICHANNEL HEAT PIPES AND PREDICTION OF DRY OUT

Since the 3-D comprehensive methodology is successfully applied to a single groove for performance evaluation and investigating the effect of various parameters such as groove geometry, this study can now be extended to multiple grooves by utilizing the findings of a single groove geometry. However, the implementation of these findings is not straightforward and requires additional calculations. In the first part of this chapter, modeling methodology of heat pipe with more than one channel is presented. In the second part of this section the dry out phenomenon is briefly explained which has a crucial effect on the performance of heat pipes. However, predicting the dry-out characteristics is a challenging task because even more complicated physical aspects are involved in the process, and their effects must be taken into account for accurate modeling.

Developing a mathematical model for the solution of a heat pipe is an important step, but the validation of that numerical model is another issue that needs to be handled properly. In the previous sections, the findings of the numerical model are compared with other numerical predictions in the literature. In the first part of this section, these findings are compared with the results of an experimental study, which was conducted in the scope of an MS thesis and TUBITAK project (Alijani et al., 2018) at Bilkent University. Implementation of the results of the single groove can be made by following two distinct approaches. First, the effective thermal conductivity based on the results of the single groove is calculated and a new material with an equivalent thermal conductivity is assigned to grooves and working fluid of a multichannel heat pipe. Second approach is more sophisticated, the amount of heat transfer via phase change is calculated for single groove and by defining equivalent phase-change heat transfer coefficient to the relevant boundaries, multichannel heat pipe is modeled.

### 4.1 Modeling of Multi-channel Heat Pipes

Alijani et al. (2018) investigated four different heat pipe geometries with distinct groove densities (number of grooves per unit width along the transverse direction of heat pipe) experimentally. Cross-sectional shape of the grooves was selected as a square (height of the grooves are equal to width values). Mentioned heat pipes were named according to their groove widths which are G-200, G-400, G-800 and G-1600. The number at the suffix indicated the dimensions of the groove cross-section (i.e. G-200 has a square groove cross-section whose dimensions are 200 $\mu$m $\times$ 200 $\mu$m). Thermocouples were placed at the bottom surface of the heat pipe. Locations of them ($TC_1$ – $TC_5$) are shown in the figure below. The geometric properties of the heat pipes such as groove width, groove height, pipe height, groove length and the dimensions of the heater and cooler sections are provided in Table 4.1.

Table 4.1: Geometric properties of heat pipes used in experiments (all units are given in $\mu$m)

| Heat Pipe | Groove Width ($w_g$) | Groove Height ($h_g$) | Pipe Height ($h_p$) |
|---|---|---|---|
| G-200 | 200 | 200 | 1500 |
| G-400 | 400 | 400 | 1500 |
| G-800 | 800 | 800 | 1500 |
| G-1600 | 1600 | 1600 | 2600 |

Heat pipes used in the experiments were manufactured from aluminium and isopropyl alcohol (IPA) was selected as working fluid. Since the type of the aluminium alloy was unknown (i.e. Al 6061-T6, Al 5083-O, etc.), thermal conductivity of the material has to be determined. Moreover, for cooling the pipes,

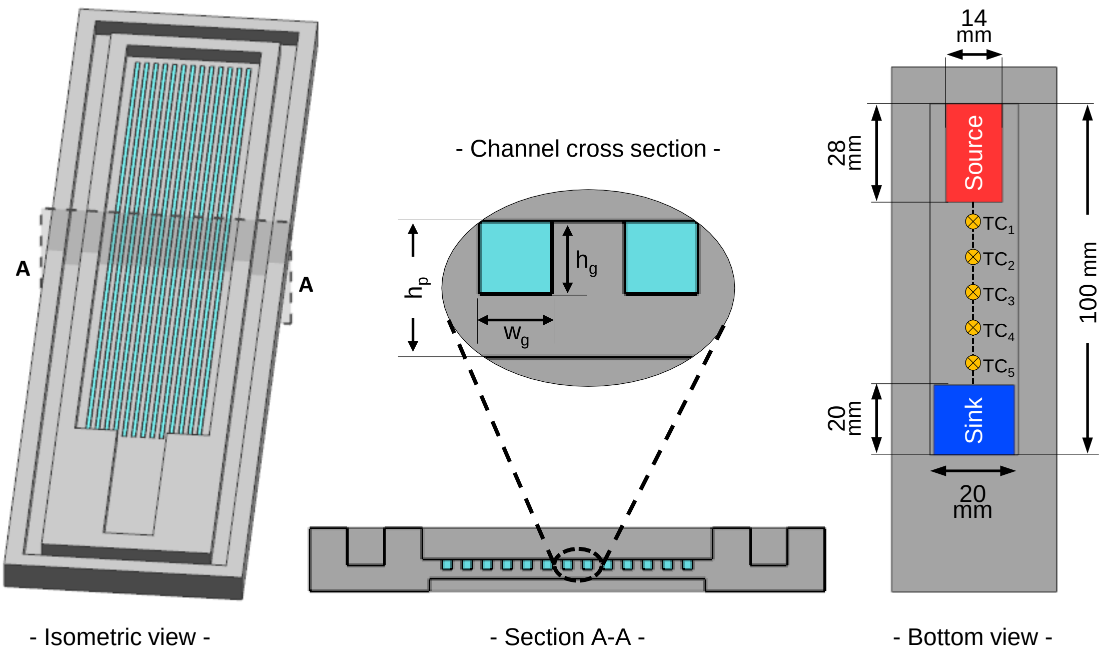


Figure 4.1: Multichannel heat pipe model

a rectangular copper bar (20mm × 20mm square cross-section and 100 mm height) was located to the bottom side of the aluminum base. 90 mm of the copper block was submerged into a water reservoir with continuous flow of water. Flow rate of the water was set between 1.6 to 1.8 L/min during the studies and water temperature was kept approximately 10°C. In order to model the physics appropriately, unknown heat transfer coefficient and ambient temperature (10 °C) boundary condition is assigned to the sink of the heat pipe.

Performing parametric analyses, unknown parameters is addressed. Alijani et al. (2018) conducted experiments without filling the grooves with working fluid (hereafter referred as a dry-case) for three distinct heat load values as 21 kW/m$^2$, 32 kW/m$^2$ and 42 kW/m$^2$. Heat is transferred only via conduction since no phase-change occurred during this operation. Using the temperature values measured by thermocouples, analysis model is built for all of the dry cases and conduction inside the heat pipe is investigated. There are two parameters whose values are determined through iterations: i) thermal conductivity of the material ii) sink heat transfer coefficient. Analyses are run for all groove geometries until the thermal conductivity of the solid and heat transfer coefficient values are found which satisfies the measured temperatures for all groove geometries. Temperature variations along the bottom surface where the thermocouples are located is plotted in the following figures.

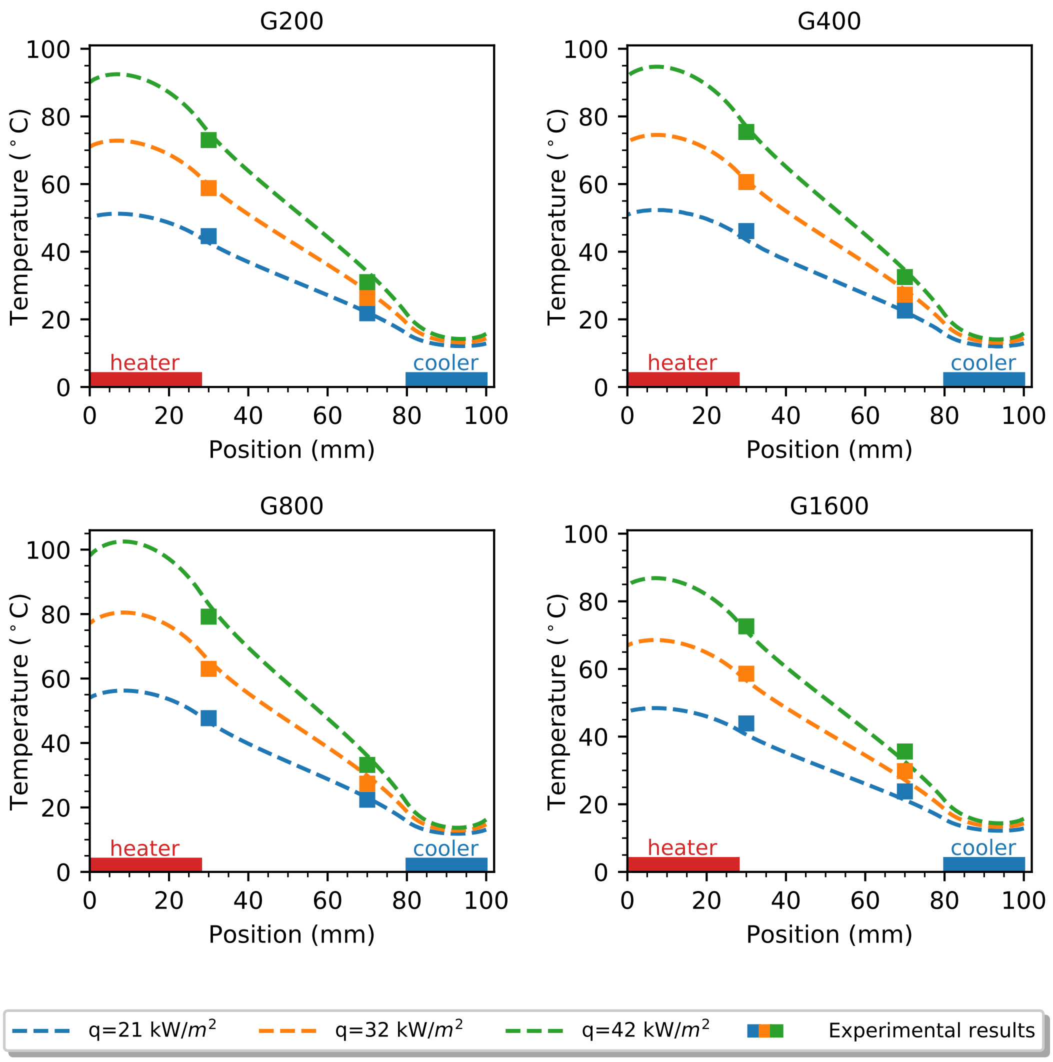


Figure 4.2: Temperature variation of the dry cases for different groove configurations

From the parametric analyses, thermal conductivity of the aluminum base and heat transfer coefficient of the sink are calculated as 162W/mK and 6000W/m$^2$K respectively.

Since all of the unknown parameters are calculated, results of the single groove can be employed to simulate the entire heat pipe. The first and simpler approach is calculating an equivalent thermal conductivity to include phase-change heat transfer. Analysis model of a single groove is built without the phase-change in which the heat pipe and working fluid materials are set as parametric and several analyses are performed by altering the equivalent thermal conductivity until the temperature variation on the groove is matched with the results obtained from the detailed and comprehensive modeling approach which is stated in Chapter-2.

Mentioned methodology is employed for four different groove models with distinct heat loads. After the performed analyses, temperature distributions at the bottom surface of the heat pipe for various heat pipe configurations are shown in Figure 4.3.

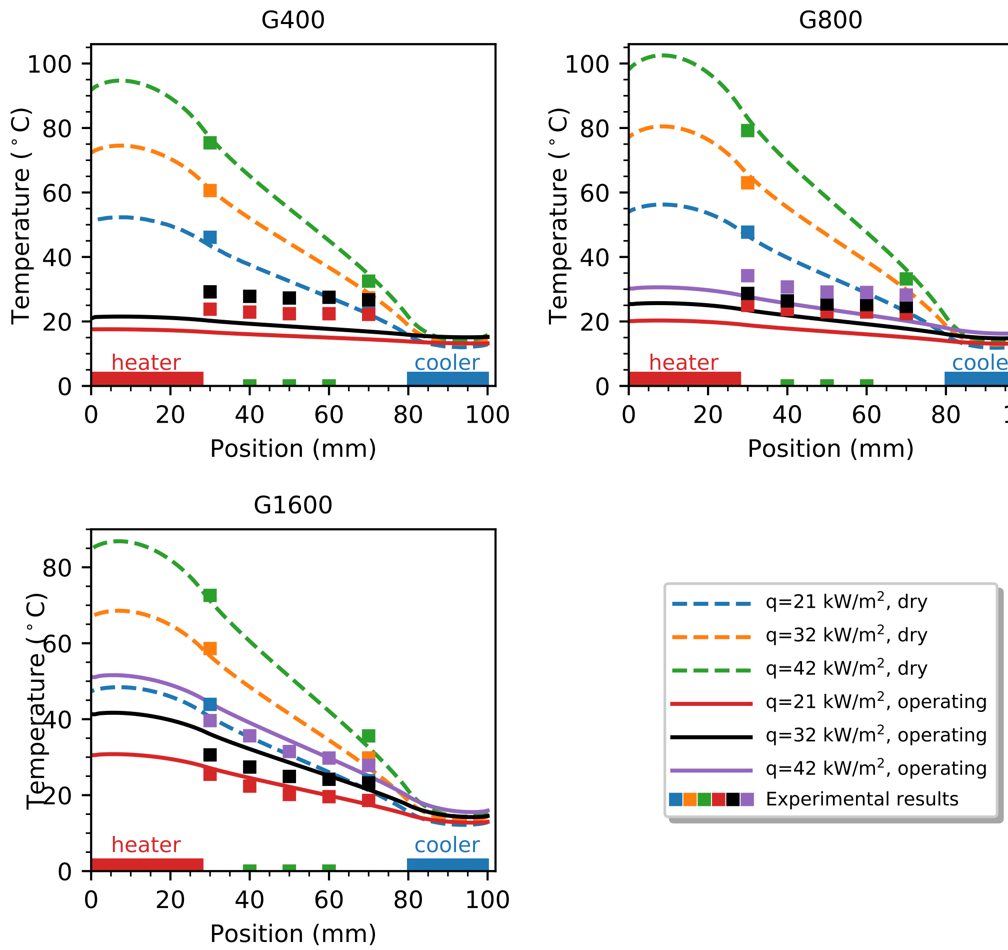


Figure 4.3: Temperature variation for studied groove models (equivalent thermal conductivity is defined)

Good agreement is obtained between the numerical approach and experimental results which is a clear indication of the validity of mathematical model developed to investigate thermal characteristics of flat grooved heat pipes.

The second approach to model entire heat pipe is more comprehensive and sophisticated. Similar to the first approach, phase-change heat transfer inside the single groove is investigated in detail by calculating the heat transfer rate via phase-change. Utilizing the results of the single groove such as the amount of heat transfer via phase change, analysis set up belongs to entire heat pipe is constructed. In this model, heat transfer from the fin top and liquid-vapor interface (heat transfer inside both micro and macro regions) is considered. Therefore, surfaces of the micro-region are split accordingly. The equivalent heat transfer coefficient obtained from the detailed model of single groove which is a function of space along the groove is set as a boundary condition on the entire heat pipe. The constant saturation temperature boundary condition is also assigned to the interface whose value is altered with the heat transfer coefficient variation in an iterative manner until; i) the heat transfer amount via phase-change satisfies the corresponding value which is obtained from the single channel. ii) the ratio of the evaporation-condensation heat transfer value converges to 1.

Three distinct heat pipe models with different groove densities as G-400, G-800 and G-1600 are investigated using the stated methodology. The temperature distribution on the G-1600 model under the 21kW/m$^2$ heat load is depicted in Figure 4.4

The temperature distributions along the line on the bottom surface where the thermocouples are located for various heat loads are also shown in Figure 4.5.

From the figures it is concluded that the results lie within the acceptable range of the corresponding experimental data. Therefore, the second approach can also be employed to model multi-channel heat pipes.

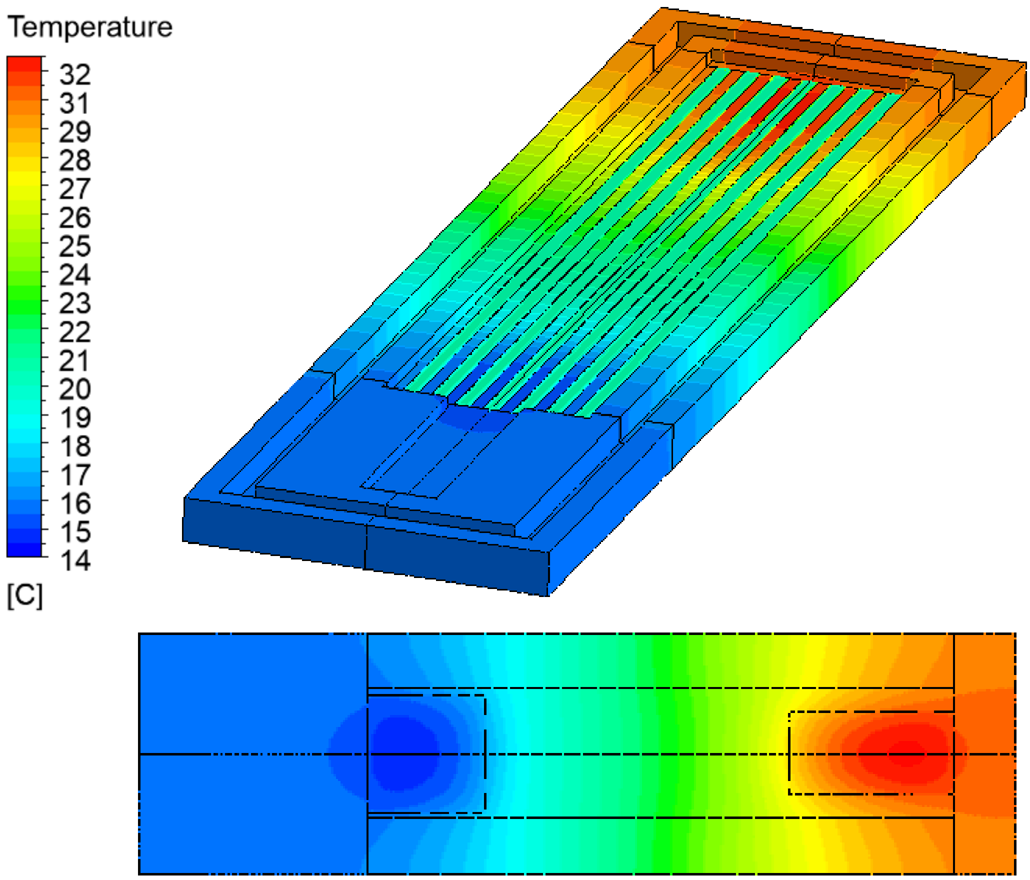


Figure 4.4: Temperature distribution on the G-1600 model for the 21kW/m$^2$ heat load

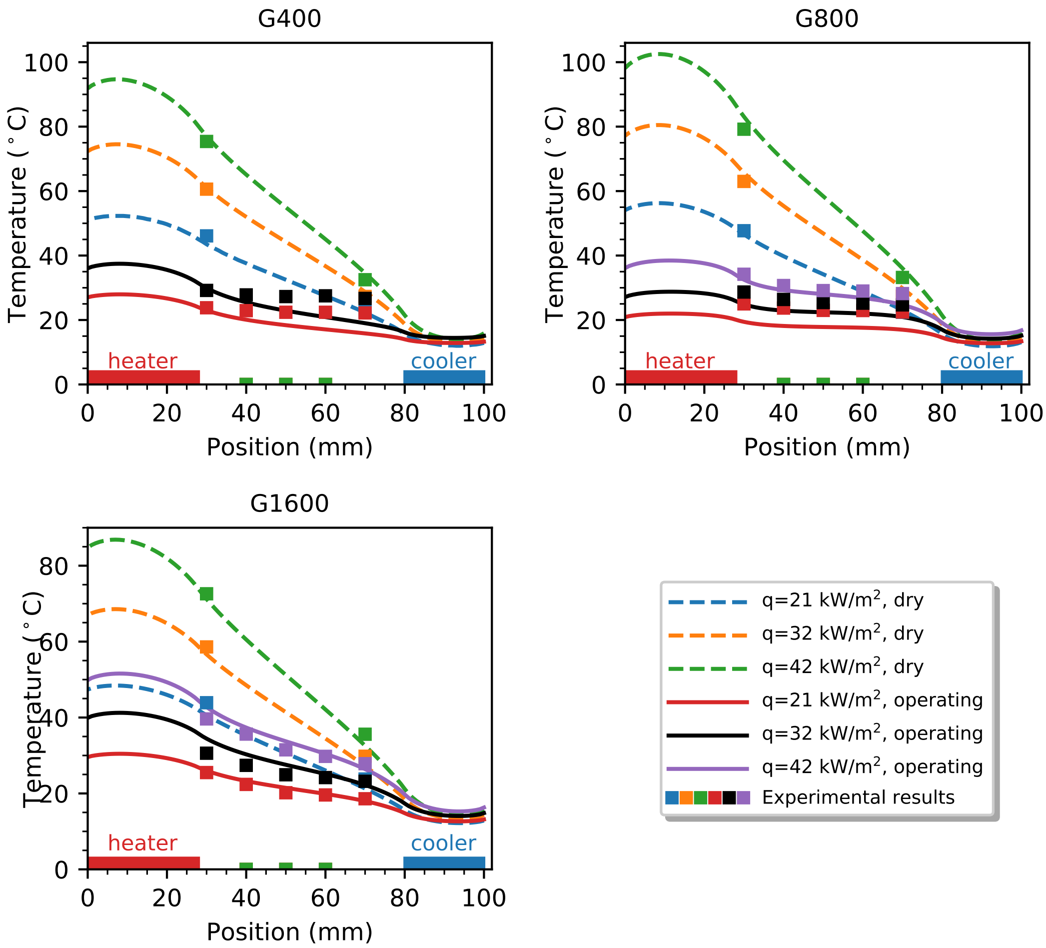


Figure 4.5: Temperature variation for studied groove models (equivalent phase change heat transfer coefficient is defined as boundary condition)

## 4.2 Prediction of Dry-out

Taking advantage of the phase-change heat transfer, heat pipes transport large quantities of heat but their performance is very sensitive to operating conditions therefore carefully selecting the heat pipe according to the application is crucial. At steady state, capillary pressure capacity and the flow resistance determines the maximum heat load capacity (capillary limit). Operating the heat pipe above the capillary limit may lead to dry-out in the evaporation zone. The dry-out must be avoided since it results elevated temperatures in the pipe. In the following figure, the dry-out phenomenon along the channel is shown. The angle between the walls of the container and liquid vapor interface is the meniscus angle. This angle can change due to the pressure inside the channel up to a critical point known as contact angle. If the heat load on the system is increased, the minimum value of meniscus angle cannot exceed the contact angle, instead the height of the liquid inside the channel decreases maintaining the contact angle. This phenomenon is the meniscus recession.

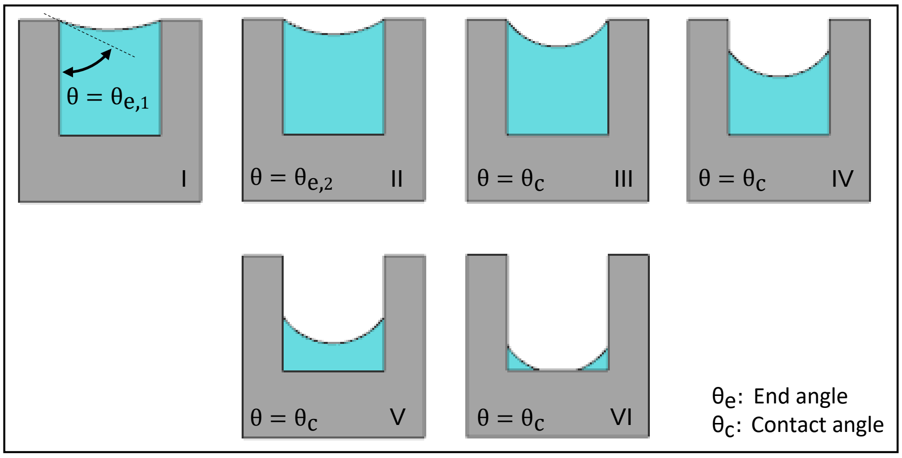


Figure 4.6: Meniscus recession during the dry-out

Predicting the dry-out characteristics of heat pipes is a challenging task because even more complicated physical aspects are involved in the process, and their effects must be taken into account for accurate modeling. Therefore using the methodology expressed in Chapter-2, dry-out characteristics of heat pipes can be predicted. However, the mentioned methodology cannot be applied directly and requires some minor revisions. First; the length of the dry-out zone is not known *a priori*. This problem can be handled with an iterative approach. At the beginning the length of the dry out zone is guessed and altered via secant method until the capillary limit is reached inside the channel. Second, after the dry-out, no phase-change occurs. For this reason, the boundary conditions defined in the original methodology must be changed accordingly. Since no fluid exists inside the zone where dry out occurs, the fluid (i.e. liquid-vapor interface) is not modeled in this region and all the boundaries inside are assumed to be isolated.

The setup, material properties and boundary conditions are kept the same with the validation case provided in Chapter-2 except the heat load. Heat load is increased 30% to trigger dry out. The temperature, meniscus curvature and mass flow variations for operating and dry out cases are plotted in Figure 4.7.

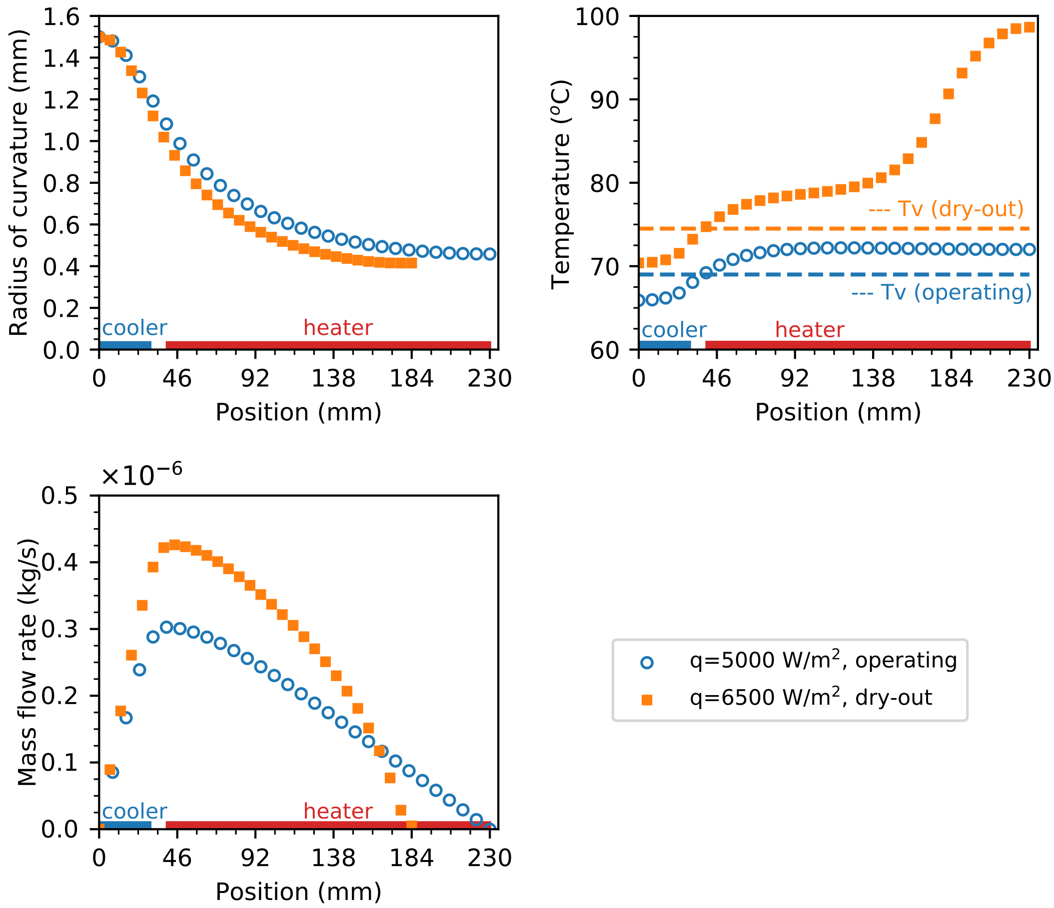


Figure 4.7: Temperature, meniscus curvature and mass flow variations for operating and dry out cases

From the plots, it is seen that for this load case dry-out occurs inside the heat pipe. After the dry-out temperatures increase in the evaporator. There is no chance to compare the results with experiments or other numerical approaches since none can be found in the literature. However, temperature and radius of curvature trends are aligned with expectations. During the modeling, the vapor flow was neither not modeled nor taken into account. More realistic model can be obtained by modeling the vapor flow inside the channel.

Single channel of G-1600 heat pipe is also investigated for different filling ratio values. In this study, filling ratio can be defined as the ratio of liquid volume inside the channel to total volume of the groove (volume of fluid which resides on the fin top is not taken into account). Starting from the fully flooded conditions (all groove volume is occupied by liquid), liquid volume inside the groove is gradually decreased to trigger the dry-out.

Temperature difference inside the heat pipe and vapor saturation temperature values are depicted in Figure 4.8. Trend of the results are compatible with the results of Alijani et al. (2018). From the results, it is seen that in specific filling ratio, optimum value of temperature difference inside the channel is obtained.

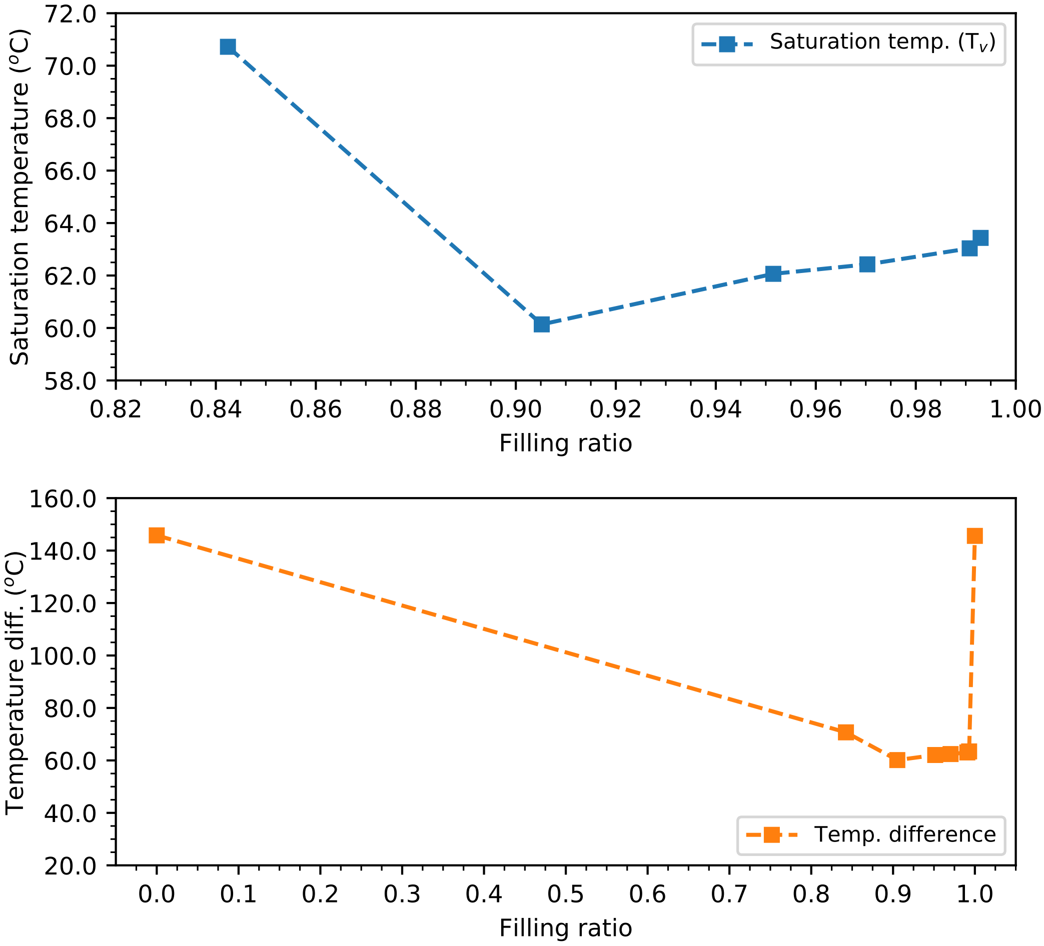


Figure 4.8: Saturation temperature and temperature difference values for distinct filling ratio values

# CHAPTER 5

# CONCLUSION AND RECOMMENDATIONS FOR FUTURE WORK

Heat pipes have been widely used in different applications in industry from space applications to thermal management of electronics owing to their superior ability to transfer significant amounts of heat with small temperature gradients. Nevertheless, modeling of heat pipes is still a challenging task due to their complicated nature and physical phenomena involved during their operation.

At first glance, although it seems the best results can be obtained with experimental methods, certain limitations and disadvantages emerges if experimental methods are employed. Experimental studies provide only external temperature measurements to characterize the system. It may not be feasible to investigate all parameters experimentally. It is essential to investigate the phenomena occurs in heat pipe in detail for the design point of view. Therefore, the need of empirically validated rigorous model of a heat pipe arises.

Although there are numerous studies both numerical and experimental in the literature, no comprehensive study about rigorous 3-D modeling of heat pipes has been reported yet. In this study, it is aimed to obtain flow and heat transfer characteristics inside the heat pipe to evaluate the parameters that effect performance of the heat pipes. Moreover, using the developed methodology, innovative channel geometries are put forward to increase heat carrying capacity with lower peak temperatures.

To address lacking of numerical studies, detailed mathematical model and analyses methodology is proposed. At the beginning, shape of the liquid-vapor interface and some of the input parameters are not known. Due to this reason it is not possible to solve the entire problem in a single step. Therefore the problem is divided into incremental sub-steps, namely the solution of phase change (to find evaporation and condensation mass flow rates), solution of the flow inside the groove (to find pressure distribution), and solution of heat transfer (to find temperature distribution). Incremental steps are dependent on each other in such a way that numerous output parameters of a particular incremental step would be input in following step. Since the incremental steps are dependent on each other, automated process is crucial to get a converged and unique solution. Since the manual implementation is impractical, computer code is written that runs the entire iterative loop in addition individual models that solve the phase change problem to compute the liquid-vapor interface shape and phase change mass fluxes is developed with using Python programming language.

Since the evaporation and condensation phase change models have significant importance on the accurate predictions of thermal performance of the heat pipe, detailed mathematical models are generated using the kinetic theory. The developed models are compared with the corresponding numerical results in the literature.

After validation of phase change models, parametric CAD and CFD models are generated using commercial software. The incremental steps are solved in an iterative manner. After obtaining the converged solution the results are compared with the corresponding values in the literature. It is stated that planned methodology and secant algorithm worked well for the simulation of a grooved heat pipe. Results show that methodology works successfully and can be implemented on new geometries to assess the thermal performance of heat pipes and design new groove geometries with superior performance.

After the modeling methodology is validated, the effect of various parameters is investigated using the developed approach. Various analyses are carried out to reveal the investigated effects. Geometric and operating parameters like groove height, groove width, filling ratio and length of the adiabatic section are changed and their effects on the heat pipe performance are investigated.

Having validated the developed methodology for the rectangular groove geometry and performing parametric studies, the methodology has been applied to various groove geometries to reveal the performance characteristics. Trapezoidal, reverse trapezoidal, wedge, Ω, circular and chamfered shapes are investigated. Two different modeling approaches are followed to enable a comparison between different geometries. First, fin top width and liquid cross-sectional area are kept constant by changing groove height. Second, channel height and liquid cross-sectional area are kept constant by changing the width of the fin top. After getting converged solutions, outputs are reviewed and groove shape effect on the heat pipe performance is given in detail. Furthermore, after assessment of the results, innovative groove shapes are introduced. Shape of the groove cross-section is altered along the groove while its cross-sectional area is kept constant e.g. condenser part is modeled as a trapezoidal shape whereas the evaporator part is modeled as a rectangular shape. No such model — which has a variable cross-section along the groove — has been presented in the literature before. With this unique design, improvement on the heat pipe performance is achieved.

Operating the heat pipe above the capillary limit may lead to dry-out in the evaporation zone. The dry-out must be avoided since it negatively affects the performance characteristics of an heat pipe and it is crucial to determine the parameters which may cause dry-out. Minor modifications have been made on the developed solution methodology and predictions about the dry-out phenomena inside the flat grooved heat pipe has been made in Chapter-4.

Finally, results obtained from single groove is implemented to a multi-channel rectangular flat grooved heat pipe. Vapor temperature and temperature variation of heat pipe are obtained as a result of analyzing the single channel. These results are utilized as an input to multi-channel heat pipes with different groove densities and various analyses are performed to find thermal performance of the heat pipes. These estimations are compared with the experimental results in the literature and found out that results are aligned with corresponding values obtained from the experiments.

Mathematical modeling of the heat pipes is not only limited with the studies stated in the previous chapters. More investigations related to various aspects about the heat pipes can be performed as an extension of outcomes of this thesis. Therefore, the following topics are recommended;

- Performance characteristics of a single channel are usually determined in 8 hours CPU time with the developed solution methodology using the computer whose specifications are given in Chapter 2. Review of the solution steps shows that most of the time is spent during the assignment of the boundary conditions to the CFD software because of the excessive number of data defined and stored in a discrete manner. Defining the boundary conditions as continuous functions would greatly reduce the number of stored and assigned data, hence the solution time. Therefore, by utilizing convenient methods (i.e. cubic splines interpolation) the boundary conditions can be defined as continuous functions and solution methodology can be revised to obtain the results faster.
- Temperature distribution on the heat pipe does not have to be periodic in lateral direction. The proposed methodology mentioned in the previous paragraph can be utilized for full simulation of the grooved heat pipe (not only a single channel). Since the number of parameters is reduced, it would be possible to employ the methodology to simulate more than one channel. Therefore, temperature change in lateral direction would be accounted for.
- In Chapter 2, several parametric studies are performed to investigate the effect of parameters on the heat pipe performance. However, in these studies only geometric properties of the heat pipe such as dimensions are investigated. In addition to investigated parameters, material properties such as thermal conductivity of the solid and liquid, surface tension, density or better effect of the Merit number can also be studied.
- Since the solution methodology is validated both with numerical and experimental studies, an optimization code can be used based on the defined operating conditions. Employing such an optimization program is also important from the design point of view because the program would allow the

users to investigate and understand the effect of other parameters of interest. Optimization code can also be utilized to obtain further novel groove geometries (e.g. the cross-sectional area can be changed along the groove to carry maximum heat load with minimum temperature difference).

- Interfacial shear stress was neglected during the modeling of the heat pipes based on the assumptions that volume occupied by vapor is sufficiently large. However, in some heat pipe designs, the volume of the vapor can be small which causes vapor velocities to increase and its effect on the thermal performance is no more negligible. Therefore, vapor flow can be modeled to investigate the effect of interfacial shear stress and this step can be implemented to the main driver.

- Condensation model is developed under the assumption that the liquid film on the fin top varies as a fourth-order polynomial. However, in the real case, a fourth-order profile may not be adequate to define the fluid film. Moreover, the transition from condensation to evaporation is not modeled in detail. In transition zones, a more complex physics may be in action. Therefore, issues related to phase-change phenomena can be addressed and phase-change models may be improved.

- The developed solution methodology is revised and utilized to predict the dry-out characteristics of heat pipes in Chapter 4. Dry-out inside the heat pipes usually occurs due to improper selection of heat pipe operating conditions, i.e. excessive heat load. During the development of mathematical model, some assumptions are employed such as the regions where dry-out occurs are assumed to be adiabatic and the effect of the vapor flow is not taken into account. But, the areas where dry-out occurs do not have to be insulated in real conditions. The trends of the results are aligned with the expectations, however, more detailed model should be prepared and validated with the experimental studies.

## REFERENCES


Akkuş, Y. and Dursunkaya, Z. (2016). "A new approach to thin film evaporation modeling". In: *International Journal of Heat and Mass Transfer* (101), pages 742–748. DOI: https://doi.org/10.1016/j.ijheatmasstransfer.2016.05.091.

Alijani, H., Çetin, B., Akkuş, Y., and Dursunkaya, Z. (2018). "Effect of design and operating parameters on the thermal performance of aluminum flat grooved heat pipes". In: *Applied Thermal Engineering* (132), pages 174–187. DOI: https://doi.org/10.1016/j.applthermaleng.2017.12.085.

ANSYS (2019). *Fluent Theory Guide*. Release 2019 R1.

Ayyaswamy, P. S., Catton, I., and Edwards, D. K. (June 1974). "Capillary Flow in Triangular Grooves". In: *Journal of Applied Mechanics* (41/2), pages 332–336. DOI: 10.1115/1.3423288.

Babin, B. R., Peterson, G. P., and Wu, D. (Aug. 1990). "Steady-State Modeling and Testing of a Micro Heat Pipe". In: *Journal of Heat Transfer* (112/3), pages 595–601. DOI: https://doi.org/10.1115/1.2910428.

Barari, B. (2012). "7th Congress of LACTRIMS". In: *Multiple Sclerosis* (18/12), pages 58–69. DOI: 10.9790/1684-1306055869.

Barba, M., Bruce, R., Bouchet, F., Bonelli, A., and Baudouy, B. (2019). "Thermal Study of a one-meter long Neon Cryogenic Pulsating Heat Pipe". In: *IOP Conference Series: Materials Science and Engineering* (502/1). DOI: 10.1088/1757-899X/502/1/012152.

Bejan A.and Kraus, A. (2003). *Chapter 16, Heat Pipes in Heat Transfer Handbook*. John Wiley & Sons Inc.

Cao, Y., Gao, M., Beam, J. E., and Donovan, B. (1997). "Experiments and analyses of flat miniature heat pipes". In: *Journal of Thermophysics and heat transfer* (11/2), pages 158–164.

Chen, X., Ye, H., Fan, X., Ren, T., and Zhang, G. (2016). "A review of small heat pipes for electronics". In: *Applied Thermal Engineering* (96), pages 1–17. DOI: http://dx.doi.org/10.1016/j.applthermaleng.2015.11.048.

Chi, S. W. (1976). *Heat Pipe Theory and Practice : A Sourcebook*.

*Cooler Master Co.* (2020). [Online]. URL: https://www.coolermastercorp.com/technology/design/heatpipe/. (Accessed: 07.08.2020).

Cotter, T. (1984). "Principles and prospects for micro heat pipes". In: ().

De Schampheleire, S., De Kerpel, K., Deruyter, T., De Jaeger, P., and De Paepe, M. (2015). "Experimental study of small diameter fibres as wick material for capillary-driven heat pipes". In: *Applied Thermal Engineering* (78), pages 258–267. DOI: 10.1016/j.applthermaleng.2014.12.027.

Deng, Y., Quan, Z., Zhao, Y., Wang, L., and Liu, Z. (2015). "Experimental research on the performance of household-type photovoltaic-thermal system based on micro-heat-pipe array in Beijing". In: *Energy Conversion and Management* (106), pages 1039–1047. DOI: 10.1016/j.enconman.2015.09.067.

Derjaguin, B. V. and Zorin, Z. M. (1992). "Optical study of the adsorption and surface condensation of vapours in the vicinity of saturation on a smooth surface". In: *Progress in Surface Science* (40/1), pages 83–117. DOI: https://doi.org/10.1016/0079-6816(92)90037-I.

Desai, A. N., Singh, V. K., and Patel, R. N. (Oct. 2019). "Effect of Geometrical Parameters on the Thermal Performance of Ammonia-Based Trapezoidal-Shaped Axial Grooved Heat Pipe". In: *Journal of Heat Transfer* (141/12). 121801. DOI: 10.1115/1.4044702.

Do, K. H., Kim, S. J., and Garimella, S. V. (2008). "A mathematical model for analyzing the thermal characteristics of a flat micro heat pipe with a grooved wick". In: *International Journal of Heat and Mass Transfer* (51/19), pages 4637–4650. DOI: https://doi.org/10.1016/j.ijheatmasstransfer.2008.02.039.

Faghri, A. (2014). “Heat Pipes: Review, Opportunities and Challenges”. In: *Frontiers in Heat Pipes* (5/1). DOI: http://dx.doi.org/10.5098/fhp.5.1.

Faghri, A. (1995). *Heat pipe science and technology*. Global Digital Press.

Faghri, A., Reynolds, D., and Faghri, P. (1989). “Heat pipes for hands”. In: *Mechanical Engineering-CIME* (111/6), pages 70–74.

Feenstra, J., Hofmeyer, H., Van Herpen, R., and Mahendran, M. (2018). “Automated two-way coupling of CFD fire simulations to thermomechanical FE analyses at the overall structural level”. In: *Fire Safety Journal* (96), pages 165–175. DOI: https://doi.org/10.1016/j.firesaf.2017.11.007.

Fernengel, J., Habla, F., and Hinrichsen, O. (2018). “Scripting as an Approach to Automated CFD Simulation for Packed Bed Catalytic Reactor Modeling”. In: *Chemie Ingenieur Technik* (90/5), pages 685–689. DOI: 10.1002/cite.201700153. eprint: https://onlinelibrary.wiley.com/doi/pdf/10.1002/cite.201700153.

Franchi, G. and Huang, X. (2008). “Development of composite wicks for heat pipe performance enhancement”. In: *Heat Transfer Engineering* (29/10). DOI: https://doi.org/10.1080/01457630802125740.

Galvan, R., F., Barranco, V., Galvan, J. C., Batlle, Sebastian FeliuFajardo, S., and García (2016). “We are IntechOpen , the world ’ s leading publisher of Open Access books Built by scientists , for scientists TOP 1 %”. In: *Intech* (i/tourism), page 13. DOI: http://dx.doi.org/10.5772/57353.

Gaugler, R. S. (1944). *“Heat Transfer Device”, U. S. Patent No. 2350348.*

Ghani, S., Gamaledin, S. M. A., Rashwan, M. M., and Atieh, M. A. (2018). “Experimental investigation of double-pipe heat exchangers in air conditioning applications”. In: *Energy and Buildings* (158), pages 801–811. DOI: 10.1016/j.enbuild.2017.10.051.

Gilchrist, S., Ewing, D., and Ching, C. Y. (2009). "On the design of an aero-engine nose cone anti-icing system using a rotating heat pipe". In: *Journal of Thermal Science and Engineering Applications* (1/2), pages 1–11. DOI: 10.1115/1.4000191.

Greco, A., Cao, D., Jiang, X., and Yang, H. (2014). "A theoretical and computational study of lithium-ion battery thermal management for electric vehicles using heat pipes". In: *Journal of Power Sources* (257), pages 344–355. DOI: 10.1016/j.jpowsour.2014.02.004.

Grover, G. M., Cotter, T. P., and Erickson, G. F. (1964). "Structures of very high thermal conductance". In: *Journal of Applied Physics* (35/6), pages 1990–1991. DOI: 10.1063/1.1713792.

Gu, X., Ciampa, P. D., and Nagel, B. (2017). "An automated CFD analysis workflow in overall aircraft design applications". In: *CEAS Aeronautical Journal* (3/13). DOI: https://doi.org/10.1007/s13272-017-0264-1.

Gully, P. (2014). "Long and high conductance helium heat pipe". In: *Cryogenics* (64), pages 255–259. DOI: 10.1016/j.cryogenics.2014.04.002.

Ha, J. M. and Peterson, G. P. (1996). "The Interline Heat Transfer of Evaporating Thin Films Along a Micro Grooved Surface". In: *Journal of Heat Transfer* (118/3), pages 747–755. DOI: https://doi.org/10.1115/1.2822695.

He, J., Guo, Y., Zhang, H., Miao, J., Wang, L., and Lin, G. (2017). "Design and experimental investigation of a neon cryogenic loop heat pipe". In: *Heat and Mass Transfer/Waerme- und Stoffuebertragung* (53/11), pages 3229–3239. DOI: 10.1007/s00231-017-2005-8.

Hirt, C. and Nichols, B. (1981). "Volume of fluid (VOF) method for the dynamics of free boundaries". In: *Journal of Computational Physics* (39/1), pages 201–225. DOI: https://doi.org/10.1016/0021-9991(81)90145-5.

Hu, M., Zheng, R., Pei, G., Wang, Y., Li, J., and Ji, J. (2016). "Experimental study of the effect of inclination angle on the thermal performance of heat pipe photovoltaic/thermal (PV/T) systems with wickless heat pipe and wiremeshed heat pipe". In: *Applied Thermal Engineering* (106), pages 651–660. DOI: 10.1016/j.applthermaleng.2016.06.003.

Jen, T. C., Gutierrez, G., Eapen, S., Barber, G., Zhao, H., Szuba, P. S., Labataille, J., and Manjunathaiah, J. (2002). "Investigation of heat pipe cooling in drilling applications. Part I: Preliminary numerical analysis and verification". In: *International Journal of Machine Tools and Manufacture* (42/5), pages 643–652. DOI: 10.1016/S0890-6955(01)00155-9.

Jiang, L., Ling, J., Jiang, L., Tang, Y., Li, Y., Zhou, W., and Gao, J. (2014). "Thermal performance of a novel porous crack composite wick heat pipe". In: *Energy Conversion and Management* (81), pages 10–18. DOI: 10.1016/j.enconman.2014.01.044.

Jiao, A. J., Riegler, R., Ma, H. B., and Peterson, G. P. (2005). "Thin film evaporation effect on heat transport capability in a grooved heat pipe". In: *Microfluidics and Nanofluidics* (1/3), pages 227–233.

Kamotani, Y. (1976). "Analysis of axially grooved heat pipe condensers". In: *14th Aerospace Sciences Meeting*, page 147.

Kang, S.-W., Tsai, S.-H., and Chen, H.-C. (2002). "Fabrication and test of radial grooved micro heat pipes". In: *Applied Thermal Engineering* (22/14), pages 1559–1568.

Khrustalev, D. and Faghri, A. (Nov. 1995). "Thermal Characteristics of Conventional and Flat Miniature Axially Grooved Heat Pipes". In: *Journal of Heat Transfer* (117/4), pages 1048–1054. DOI: 10.1115/1.2836280.

Khrustalev, D. and Faghri, A. (Feb. 1994a). "Thermal Analysis of a Micro Heat Pipe". In: *Journal of Heat Transfer* (116/1), pages 189–198. DOI: 10.1115/1.2910855.

Khrustalev, D. and Faghri, A. (1994b). "Heat transfer during evaporation and condensation on capillary-grooved structures of heat pipes". In: *ASME Winter Annual Meeting, Chicago* (287), pages 47–59.

Kim, R.-w., Hong, S.-w., Norton, T., Amon, T., Youssef, A., Berckmans, D., and Lee, I.-b. (2020). "Computational fluid dynamics for non-experts: Development of a user-friendly CFD simulator (HNVR-SYS) for natural ventilation design applications". In: *Biosystems Engineering* (193), pages 232–246. DOI: `https://doi.org/10.1016/j.biosystemseng.2020.03.005`.

Lee, J., Kim, D., Mun, J., and Kim, S. (2020). "Heat-transfer characteristics of a cryogenic loop heat pipe for space applications". In: *Energies* (13/7). DOI: `10.3390/en13071616`.

Lefèvre, F., Rullière, R., Pandraud, G., and Lallemand, M. (2008). "Prediction of the temperature field in flat plate heat pipes with micro-grooves – Experimental validation". In: *International Journal of Heat and Mass Transfer* (51/15), pages 4083–4094. DOI: `https://doi.org/10.1016/j.ijheatmasstransfer.2007.12.007`.

Lim, H., Kim, S., Im, H., Oh, K. H., and Jeong, S. (2008). "Fabrication and evaluation of a copper flat micro heat pipe working under adverse-gravity orientation". In: *Journal of Micromechanics and Microengineering* (18/10), page 105013.

Ling, W., Zhou, W., Liu, R., Qiu, Q., and Liu, J. (2016). "Thermal performance of loop heat pipe with porous copper fiber sintered sheet as wick structure". In: *Applied Thermal Engineering* (108), pages 251–260. DOI: `10.1016/j.applthermaleng.2016.07.121`.

Ling, Y. Z., Zhang, X. S., Wang, F., and She, X. H. (2020). "Performance study of phase change materials coupled with three-dimensional oscillating heat pipes with different structures for electronic cooling". In: *Renewable Energy* (154), pages 636–649. DOI: `10.1016/j.renene.2020.03.008`.

Lips, S. and Lefèvre, F. (2014). "A general analytical model for the design of conventional heat pipes". In: *International Journal of Heat and Mass Transfer* (72), pages 288–298. DOI: `10.1016/j.ijheatmasstransfer.2013.12.068`.

Liu, X., Zhang, R., Liang, Y., Tang, S., Wang, C., Tian, W., Zhang, Z., Qiu, S., and Su, G. (2020). "Core thermal-hydraulic evaluation of a heat pipe cooled nuclear reactor". In: *Annals of Nuclear Energy* (142), page 107412. DOI: https://doi.org/10.1016/j.anucene.2020.107412.

Longtin, J. P., Badran, B., and Gerner, F. M. (Aug. 1994). "A One-Dimensional Model of a Micro Heat Pipe During Steady-State Operation". In: *Journal of Heat Transfer* (116/3), pages 709–715. DOI: 10.1115/1.2910926.

Meisel, P., Jobst, M., Lippmann, W., and Hurtado, A. (2015). "Design and manufacture of ceramic heat pipes for high temperature applications". In: *Applied Thermal Engineering* (75), pages 692–699. DOI: http://dx.doi.org/10.1016/j.applthermaleng.2014.10.051.

Moon, S. H., Hwang, G., Ko, S. C., and Kim, Y. T. (2004). "Experimental study on the thermal performance of micro-heat pipe with cross-section of polygon". In: *Microelectronics Reliability* (44/2), pages 315–321.

Odabaşi, G. (2014). "Modeling of multidimensional heat transfer in a rectangular grooved heat pipe". PhD thesis. Middle East Technical University (METU).

Paiva, K. V. and Mantelli, M. B. H. (2015). "Wire-plate and sintered hybrid heat pipes: Model and experiments". In: *International Journal of Thermal Sciences* (93), pages 36–51. DOI: 10.1016/j.ijthermalsci.2015.01.037.

Peterson, G. P., Duncan, A. B., and Weichold, M. H. (1993). "Experimental investigation of micro heat pipes fabricated in silicon wafers". In: ().

Peterson, G. P. (1994). *An Introduction to Heat Pipes: Modeling, Testing, and Applications*. John Wiley & Sons Inc.

Poston, D. I., McClure, P. R., Dixon, D. D., Gibson, M. A., and Mason, L. S. (2014). "Experimental Demonstration of a Heat Pipe–Stirling Engine Nuclear Reactor". In: *Nuclear Technology* (188/3), pages 229–237. DOI: https://doi.org/10.13182/NT13-71.

Potash, M. and Wayner, P. (1972). "Evaporation from a two-dimensional extended meniscus". In: *International Journal of Heat and Mass Transfer* (15/10), pages 1851–1863. DOI: https://doi.org/10.1016/0017-9310(72)90058-0.

Reay, D. A., McGlen, R. J., and Kew, P. A. (2014). *Heat pipes: theory, design and applications*. 6th edition. Butterworth-Heinemann.

Reay, D. (1982). "The Perkins Tube—a noteworthy contribution to heat exchanger technology". In: *Journal of Heat Recovery Systems* (2/2), pages 173–187. DOI: `https://doi.org/10.1016/0198-7593(82)90045-5`.

Rullière, R., Lefèvre, F., and Lallemand, M. (2007). "Prediction of the maximum heat transfer capability of two-phase heat spreaders – Experimental validation". In: *International Journal of Heat and Mass Transfer* (50/7), pages 1255–1262. DOI: `https://doi.org/10.1016/j.ijheatmasstransfer.2006.09.015`.

Schneider, G., Yovanovich, M., and Wehrle, V. (1976). "Thermal analysis of trapezoidal grooved heat pipe evaporator walls". In: *11th Thermophysics Conference* (). DOI: `10.2514/6.1976-481`.

Schneider, G. and Devos, R. (1980). "Non-dimensional analysis for the heat transport capability of axially grooved heat pipes including liquid/vapor interaction". In: *AIAA, Aerospace Sciences Meeting*.

Schonberg, J. A. and Wayner Jr., P. C. (1992). "Analytical solution for the integral contact line evaporative heat sink". In: *Journal of thermophysics and heat transfer* (6/1), pages 128–134.

Schonberg, J., DasGupta, S., and Wayner, P. (1995). "An augmented Young-Laplace model of an evaporating meniscus in a microchannel with high heat flux". In: *Experimental Thermal and Fluid Science* (10/2). Aerospace Heat Exchanger Technology, pages 163–170. DOI: `https://doi.org/10.1016/0894-1777(94)00085-M`.

Stephan, P. and Busse, C. (1992). "Analysis of the heat transfer coefficient of grooved heat pipe evaporator walls". In: *International Journal of Heat and Mass Transfer* (35/2), pages 383–391. DOI: `https://doi.org/10.1016/0017-9310(92)90276-X`.

Suh, J.-S., Greif, R., and Grigoropoulos, C. P. (2001). “Friction in micro-channel flows of a liquid and vapor in trapezoidal and sinusoidal grooves”. In: *International Journal of Heat and Mass Transfer* (44/16), pages 3103–3109. DOI: `https://doi.org/10.1016/S0017-9310(00)00331-8`.

Sun, X., Li, S., Jiao, B., Gan, Z., and Pfotenhauer, J. (2019). “Experimental study on a hydrogen closed-loop pulsating heat pipe with two turns”. In: *Cryogenics* (97/October 2018), pages 63–69. DOI: `https://doi.org/10.1016/j.cryogenics.2018.10.010`.

Ternet, F., Louahlia, H., and Masson, S. (Jan. 2018). “Impact of Microgroove Shape on Flat Miniature Heat Pipe Efficiency”. In: *Entropy* (20), page 44. DOI: `10.3390/e20010044`.

Wang, C., Chen, J., Qiu, S., Tian, W., Zhang, D., and Su, G. H. (2017). “Performance analysis of heat pipe radiator unit for space nuclear power reactor”. In: *Annals of Nuclear Energy* (103), pages 74–84. DOI: `10.1016/j.anucene.2017.01.015`.

Wang, F., Li, G., Ma, W., Wu, Q., Serban, M., Vera, S., Alexandr, F., Jiang, N., and Wang, B. (2019). “Pipeline–permafrost interaction monitoring system along the China–Russia crude oil pipeline”. In: *Engineering Geology* (254/March), pages 113–125. DOI: `10.1016/j.enggeo.2019.03.013`.

Wang, H., Garimella, S. V., and Murthy, J. Y. (2007). “Characteristics of an evaporating thin film in a microchannel”. In: *International Journal of Heat and Mass Transfer* (50/19), pages 3933–3942. DOI: `https://doi.org/10.1016/j.ijheatmasstransfer.2007.01.052`.

Wayner, P. C., Kao, Y. K., and LaCroix, L. V. (1976). “The interline heat-transfer coefficient of an evaporating wetting film”. In: *International Journal of Heat and Mass Transfer* (19/5), pages 487–492. DOI: `https://doi.org/10.1016/0017-9310(76)90161-7`.

Xing, W., Ullmann, A., Brauner, N., Plawsky, J., and Peles, Y. (2018). “Advancing micro-scale cooling by utilizing liquid-liquid phase separation”. In: *Scien-*

*tific Reports* (8/1), pages 2–11. DOI: http://dx.doi.org/10.1038/s41598-018-30584-6.

Yang, L., Zhou, R., Jin, X., Ling, X., and Peng, H. (2016). "Experimental investigate on thermal properties of a novel high temperature flat heat pipe receiver in solar power tower plant". In: *Applied Thermal Engineering* (109), pages 610–618. DOI: 10.1016/j.applthermaleng.2016.07.075.

Zainal, N. A., Sulaiman, S. N., Shamsudin, M. A., and Waini, I. (2017). "Numerical Simulation of Different Models of Heat Pipe Heat Exchanger Using AcuSolve". In: *Engineering Technology International Conference 2016 (ETIC 2016)* (97/17). DOI: https://doi.org/10.1051/matecconf/20179701077.

Zhang, C., Chen, Y., Shi, M., and Peterson, G. (2009). "Optimization of heat pipe with axial "Ω"-shaped micro grooves based on a niched Pareto genetic algorithm (NPGA)". In: *Applied Thermal Engineering* (29/16), pages 3340–3345. DOI: https://doi.org/10.1016/j.applthermaleng.2009.05.008.

Zhang, H., Mi, M., Miao, J., Wang, L., Chen, Y., Ding, T., Ning, X., and Huo, Y. (2017). "Development and on-orbit operation of loop heat pipes on chinese circumlunar return and reentry spacecraft". In: *Journal of Mechanical Science and Technology* (31/6), pages 2597–2605. DOI: 10.1007/s12206-017-0501-x.

Zhang, Y. and Faghri, A. (2001). "Numerical simulation of condensation on a capillary grooved structure". In: *Numerical Heat Transfer: Part A: Applications* (39/3), pages 227–243.

Zhao, Y. nan, Yan, T., Liang, J., and Wang, N. (2019). "A new way of supercritical startup of a cryogenic loop heat pipe". In: *International Journal of Heat and Mass Transfer* (145), page 118793. DOI: 10.1016/j.ijheatmasstransfer.2019.118793.

Zohuri, B. (2020). "Chapter 1 - Heat pipe infrastructure". In: *Functionality, Advancements and Industrial Applications of Heat Pipes*. Edited by B. Zohuri. Academic Press, pages 1–45. DOI: https://doi.org/10.1016/B978-0-12-819819-3.00001-8.

# CURRICULUM VITAE

## PERSONAL INFORMATION

**Surname, Name:** Gökçe, Gökay
**Nationality:** Turkish (TC)
**Date and Place of Birth:** 07 December 1987, İzmir
**Marital Status:** Single
**Phone:** +90 536 325 5579
**Email** gokaygokce1@gmail.com

## EDUCATION

| Degree | Institution | Year of Graduation |
|---|---|---|
| M.S. | METU Mechanical Engineering | 2011 |
| B.S. | Gazi University | 2009 |
| High School | İzmir İnönü High School | 2004 |

## PROFESSIONAL EXPERIENCE

| Year | Place | Enrollment |
|---|---|---|
| 2012-Present | ASELSAN Inc., Ankara | Design Engineer |
| 2010-2012 | Punto Engineering, Ankara | CFD Specialist |